UCLouvain

FACULTE DES SCIENCES

Faculté des sciences

Functionalization of open-metal sites in stable MOFs through the use of small post-functionalized anchor molecules

Author: Séraphin Lacour

Supervisors: Prof. Sophie Hermans, Yaroslav Fillinchuk

Jury members: Prof. Tom Leyssens, Prof. Michael Singleton, Prof. Alexandru Vlad

Academic year 2019-2020

UCLouvain **Faculté des sciences**

Functionalization of open-metal sites in stable MOFs through the use of small post-functionalized anchor molecules

Author: Séraphin Lacour

Supervisors: Prof. Sophie Hermans, Yaroslav Fillinchuk

Jury members: Prof. Tom Leyssens, Prof. Michael Singleton, Prof. Alexandru Vlad

Academic year 2019-2020

Jury members:

Prof. Tom Leyssens – Université de catholique Louvain

Prof. Michael Singleton – Université de catholique Louvain

Prof. Alexandru Vlad – Université de catholique Louvain

Supervisors:

Prof. Sophie Hermans – Université de catholique Louvain

Prof. Yaroslav Filinchuk – Université de catholique Louvain

Mentor:

Timothy Steenhaut

Remerciements

Avant tout, je tiens à remercier les Professeurs Sophie Hermans et Yaroslav Filinchuk de m'avoir permis de réaliser mon mémoire dans leurs laboratoires. Leur disponibilité et précieux conseils m'ont beaucoup aidé à la réalisation de mon travail.

Je remercie les Professeurs Tom Leyssens, Michael Singleton, Alexandru Vlad, membres du jury, pour la lecture et leur présence lors de la défense de mon mémoire.

Ensuite, je remercie mon encadrant Timothy Steenhaut pour son partage de connaissances quotidien et sa disponibilité durant toute l'année.

Je remercie également le Dr. Koen Robeyns de m'avoir aidé lors des multiples analyses par diffraction de rayons X. Sa disponibilité fut également très appréciée.

Enfin, je remercie toutes les personnes que j'ai pu croiser lors de l'élaboration de mon mémoire, les membres du personnel et les autres étudiants pour leur accueil, leur aide et leur bonne humeur.

Summary

This project aims at synthesizing stable Ti, Al and Zr-based metal-organic frameworks (MOFs) with accessible open-metal sites, in order to functionalize them with ethylenediamine-like molecules, to obtain composite porous materials with $–NH_2$ functionalities. These materials are of interest in gas storage and catalysis.

After a general introduction, the present project is divided into four experimental parts. The first three cover the synthesis of stable MIL-100 and MIL-101 MOFs based on Al and/or Ti centres, as well as of UiO-66-Zr. The last part deals with the synthesis of a fluorescent probe that allows the detection of free amine groups.

In the first part, our attempts to synthesize MIL-100 MOFs structures based on Al and/or Ti as metal centres are described. The synthesis of pure MIL-100-Al was performed at a large scale, and the impact of the reagent concentrations, reaction time and temperature were evaluated. To produce MIL-100-Ti^{IV}, the $[Ti_6O_6(4\text{-tbbz})_6(O^iPr)_6]$ cluster and $Ti(O^iPr)_4$ compound were used as metal precursors. Solvothermal and mechanochemical methods were explored, as well as milder reaction conditions. However, none of those approaches allowed producing the target MIL-100-Ti^{IV}. Syntheses with a commercial mixed-metal Ti^{III}/Al source were also tried at different temperatures, with different reaction times, washing methods and concentrations of HCl as modulator. In this case, the syntheses only led to compounds with very poor crystallinity. The oxidation of the products by air was also evaluated and the structure seemed to withstand this treatment.

The second part deals with different attempts to synthesize MIL-101 structures. MIL-101-Ti^{III} was successfully produced from $TiCl_3$ by a procedure from the literature, but with a smaller surface area. However, we observed a complete collapse of the MOF's structure upon contact with air. Due to the small amounts of available $TiCl_3$, attempts were made to obtain mixed MIL-100-(Al)Ti^{III} from $(TiCl_3)_3{\cdot}AlCl_3$ instead. Unfortunately, those attempts only yielded amorphous samples.

The third part relates to the synthesis of UiO-66-Zr. This MOF was obtained at gram scale with high crystallinity. However, its functionalization could not be explored due to the Covid-19 lockdown.

The last part describes the synthesis of a BODIPY derivative. This fluorescent probe for the detection of $–NH_2$ functions was obtained in small amounts with satisfying purity and a qualitative test under UV irradiation confirmed its ability to detect free amines sites.

Conclusions and perspectives end up this thesis, putting forward the functionalization of MOFs with ethylenediamine and the capture of acidic gases such as CO_2 as the most interesting direction, as well as synthesis of mixed metal MIL-100-(Al)Ti.

Table of content

Abbreviations

4-tbbz-H	4-tert-butylbenzoic acid
ACN	Acetonitrile
BET	Branauer-Emmett-Teller
BTC	Benzene-1,3,5 tricarboxylate
DMF	Dimethylformamide
DEF	Diethylformamide
Eq.	Equivalent
EtOH	Ethanol
FTIR	Fourier-transform infrared spectroscopy
H_3BTC	Benzene-1,3,5 tricarboxylate acid, trimesic acid
$^{i}PrOH$	Isopropanol
LAG	Liquid-assisted grinding
TGA	Thermogravimetric analysis
THF	Tetrahydrofuran
MOF	Metal-organic framework
PSM	Post-synthetic modifications
PXRD	Powder X-ray diffraction
RT	Room temperature
SALE	Solvent-assisted linker exchange

I. Introduction

1. Metal-organic frameworks

1.1. Generalities

1.1.1. Classification of porous materials

Since the dawn of time, humankind has always tried to improve the efficiency of materials to overcome very particular problems depending on the context. Nowadays, the development of materials for applications such as gas separation and storage, heterogeneous catalysis or energy storage has become crucial.[1,2,3] Therefore, scientists have turned their interest to porous materials. Those can be classified into three main categories according to their nature and composition (Figure 1):

- ✓ ***Purely inorganic solids***, including zeolites which are *aluminosilicates* ($M_{x/n}[(AlO_2)_x(SiO_2)_y]\cdot mH_2O$), the related *aluminophosphates* ($AlPO_4$), *porous silica* (SiO_2) and other inorganic oxide as well as *carbon materials*, such as activated carbons;
- ✓ ***Organic materials***, which are divided in three main subsets: porous gels and polymers,[4] and *porous organic frameworks* (POFs) such as *covalent organic frameworks* (COFs) which are synthesized by assembling organic monomers through strong covalent bonds;[5]
- ✓ ***Hybrid materials***, which contain both organic and inorganic moieties, are found in between those two categories. Those hybrid materials include *metal-organic frameworks* (MOFs), which are the main subject of the present Master thesis.

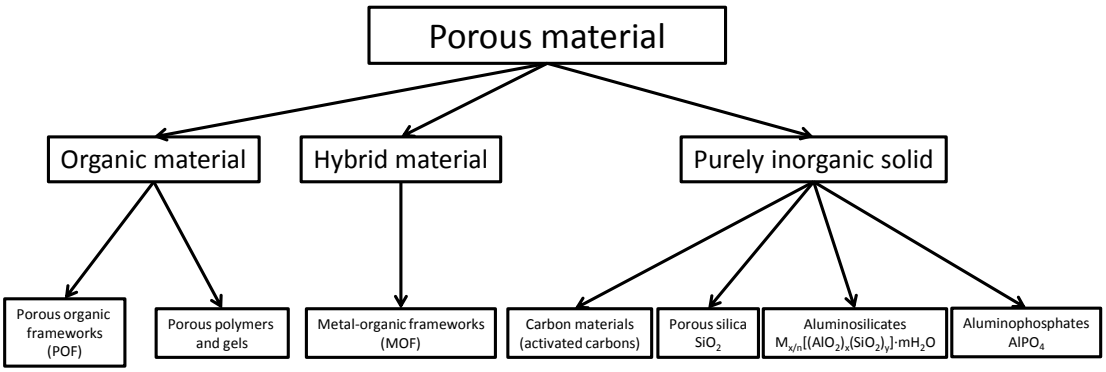

Figure 1. Main categories of porous materials.

1.1.2. MOFs: different generations of materials

MOFs are porous coordination polymers (sometimes referred to as "PCPs") made of metal atoms or clusters linked by bridging organic ligands. IUPAC defines metal-organic frameworks as being "a coordination network with organic ligands containing potential voids."[6] Indeed, not all MOFs possess intrinsic accessible porosity, but they all have structural cavities which are often occupied by guest molecules, most frequently residual solvents from their synthesis.

In some cases, those cavities can be emptied, but not always. The progress in MOF research over the years has brought the scientists to classify them into categories, or "*generations*", (see Figure 2).[7,8] MOFs of the first generation are characterized by collapsing of their potential voids after removal of the guest molecules. Improvement in structure stability has led to the discovery of a second generation of MOFs whose porosity is maintained even after guest removal. Later on, a third generation showing flexible and dynamic porosity upon applying chemical or physical stimuli was discovered. More recently, a fourth class, gathering MOFs that keep their topology and structure after post synthetic modifications, was added to this classification.[9]

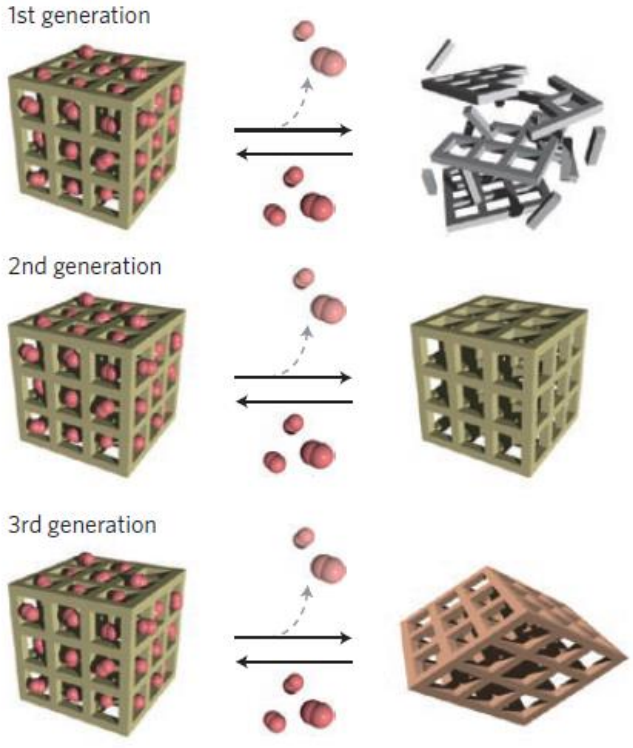

Figure 2. The three initial generations of porous coordination polymers (image taken from [8]).

Whether a given MOF will be from one generation or another depends on the building blocks composing it. For example, to produce a second generation MOF, the building blocks must be rigid and linked by strong chemical bonds. A dynamic structure of the third generation with "breathing" properties can be obtained by the assembling of flexible and / or stiff moieties. If flexible moieties compose the structure, their deformation induce the breathing properties, while for a structure only made of stiff moieties the breathing is due to the move of interpenetrated networks.[10] Another breathing type is the dynamic structure owing to host-guest interactions, leading to deformation of pores and even to a recoverable collapsing property in some cases. The strength of bonds also directly affects the stability of the MOF, and can be tuned by choosing appropriate building blocks. This aspect is discussed below in Section 1.2.2.

1.2. Physical properties

The main reason why the interest for metal-organic frameworks substantially grew over the past decades is probably due to their attractive physical properties. Their well-defined structure is responsible for interesting properties such as high porosity, low densities, and available active sites.

1.2.1. Textural properties

Even if other porous materials present interesting physical properties (e.g. zeolites), the in depth study of MOFs has revealed superior properties for certain features. Indeed, the BET surface area (see section 1.3.4) generally is between 200-500 m^2/g for zeolites, while the one of MOFs can go up to 10,000 m^2/g.[11] Moreover, the pore volume is higher in those coordination polymers than in zeolites. Pores can be classified according to their width: below 2 nm, they are termed *micropores*, beyond 50 nm they are called *macropores* and in between (2-50 nm) *mesopores*.[12]

All these aspects are important when considering the applications in catalysis or gas storage. The porosity allows the diffusion of the substrates to reactive sites, and higher pore size decreases diffusion limitations. The aperture of the pore, called the window, blocks the diffusion of larger molecules, thus giving rise to selectivity of gas adsorption.

1.2.2. Stability

Potential applications at industrial scale require stable compounds. This stability must be considered according to the desired application and can be stability with respect to water and/or acidic media and/or organic solvents, which we will call "*chemical stability*", as well as *mechanical* and/or *thermal* stabilities.

The *chemical stability* of MOFs is directly related to the strength of the metal to ligand bonds and this aspect can be predicted by the "Hard and Soft Acid and Bases" (HSAB) theory.[13] Indeed, when the MOF is composed of oxygenated ligands (e.g. hydroxyl or carboxylate type), the use of highly charged metal ions usually enhances the stability. This principle is often used in MOF design in order to guarantee the efficiency for particular applications.[13] MOFs based on the combination of carboxylate linkers with trivalent (e.g. Al^{3+}, Cr^{3+} and Fe^{3+}) and tetravalent metal ions (e.g. Zr^{4+} and Ti^{4+}) have therefore strongly attracted the attention in recent years. The stability towards water can also be increased by decorating MOFs with hydrophobic moieties. For example, a recent study reported such an enhancement of stability with respect to water after functionalization of the ligands with aliphatic chains of variable lengths.[14] Overall, chemical stability must be considered according to the system in which the MOF will be used (e.g. moist environment vs. organic solvent for example).

The *mechanical stability* of a given framework depends on the length of the ligands. In general, if the topology and nature of the cluster or metal centres is kept constant, the longer the ligand, the weaker the framework's stability. This aspect is illustrated in Figure 3 for three zirconium-based MOFs: UiO-66, UiO-67 and UiO-68.

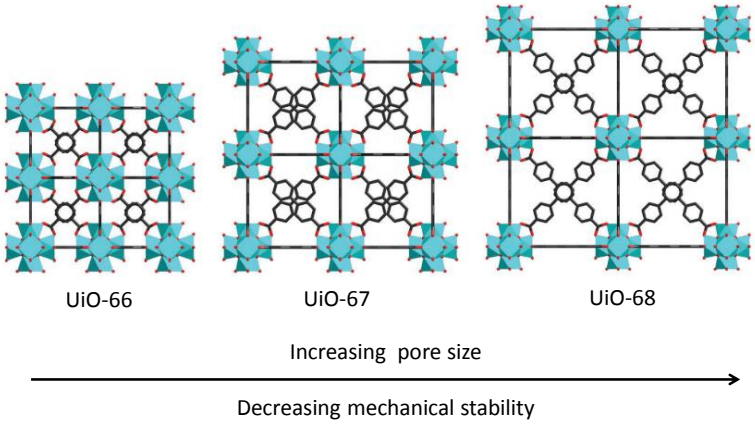

Figure 3. Influence of the ligand length on pore size and mechanical stability for UiO-66, UiO-67 and UiO-68, adapted from [13].

The number of ligands linked to each metal atom or cluster, which is called "connectivity", also plays an important role in the structural stability of MOFs. The higher the connectivity, the higher the chemical stability.[13] It should be noted that MOFs always contain structural defects such as metal atoms (or clusters) with not all expected sites occupied by the linkers. In the case of UiO-66 for example, 12 ligands are connected to the Zr-cluster in a defect-free structure. This means that even in a defect structure having one or two ligands missing for each cluster, the structure is still robust because 10 or 11 other linkers per cluster are keeping the framework together.

Finally, *thermal stability* is important because in order to make the reactive sites of MOFs accessible, the pores need to be emptied from all the molecules present in the structure, including coordinated solvents. This is performed by heating the MOF under vacuum, during a process called "activation". To withstand this treatment, the structure must be thermally stable. The intrinsic thermal stability of the organic linkers will always be a limitation in this respect. In the case of solvents with high boiling points, washing the solid with a solvent having a lower boiling point sometimes allows to decrease the activation temperature.

1.3. Characterization

MOFs are complex structures formed of both inorganic and organic building blocks. Therefore their characterization is not straightforward and several analytical techniques must often be combined to allow a complete understanding of the material.[9,13]

1.3.1. X-Ray diffraction (XRD)

In order to characterise the crystallinity of the product after a reaction, and hopefully determine its structure, XRD is performed. In case a MOF is obtained as well-defined single crystals, XRD analysis is rather straightforward. However, if only a powder can be obtained, powder X-ray diffraction (PXRD) must be used. Two common setups exist for doing this: the Bragg-Brentano (reflection) and the Debye-Scherrer (transmission in capillary) geometries. The first one is favoured for air stable compounds with high X-ray adsorption, and the sample preparation is more convenient. The second one is preferably used for sensitive powders since the sample can be handled in a glovebox where it is sealed in a glass capillary for analysis. In both cases, the obtained powder pattern is compared with structures from a database, for

which a simulation of the expected powder pattern is made by using an appropriate software (e.g. Mercury).

1.3.2. Infrared spectroscopy (FTIR)

Infrared spectroscopy is very useful to identify particular chemical functions thanks to the vibrations of bonds in the sample. For enabling the analysis of air sensitive samples, the equipment can be placed in a glovebox. Attenuated total reflection (ATR) can be used to make the measurement easier and more rapidly as well as avoiding mixing the sample with matrices like KBr.

1.3.3. Nuclear magnetic resonance spectroscopy (NMR)

Solid state NMR can be used to characterize MOFs. However, this method is highly specialized and not always available. An alternative is to dissolve the sample and perform liquid state NMR of the obtained solution. This allows to observe the ligand as well as residual solvents, or any other guest molecule, and to quantify them. For doing this, the MOF is typically treated in very acidic conditions (D_2SO_4 or DCl) in the presence of polar solvents able to dissolve the species formed under these conditions (d^6-DMSO or d^7-DMF).

1.3.4. Nitrogen physisorption

Information about the textural properties, such as the surface area and pore size, can be gained from nitrogen physisorption isotherms.[15] In practice, the analysis is conducted in two stages. The first one consists in heating the sample under vacuum to degas it. Then, calibrated quantities of nitrogen at 77K are adsorbed on the sample at low pressures and the exact pressure is monitored, yielding an isotherm of the quantity of nitrogen adsorbed in function of the equilibrium pressure. Useful information can be gained by the overall shape of the isotherm such as the porosity type (micro, meso or macro). The isotherms are divided into 6 types which are specific for particular systems. The obtained isotherm is then analysed using mathematical approaches, depending on the information one wants to obtain. For example, the Brunauer-Emmett-Teller (BET) theory and the Langmuir theory allow to determine the specific surface area. The pore volumes and size can be obtained by the Kelvin equation. The results are then compared to the literature.

1.3.5. Thermogravimetric analysis (TGA)

Thermogravimetric analysis gives the variation of the sample's mass while heating it under a flux of a given gas (typically air or nitrogen) following a well-defined temperature program. During the heating, the release of solvents or other guest molecules is highlighted with this method. Furthermore, TGA gives the decomposition temperature of the product. The measurement of the mass loss gives information about the stoichiometry between the metal and the ligands and about the amount of solvents molecules in a given compound.

1.3.6. Other characterization methods

Various other methods can be used for MOF analysis. For example, inductively coupled plasma (ICP) or atomic absorption spectroscopy (AAS) allow to quantify the ratio between two metals in the case of bimetallic MOFs. X-ray photoelectron spectroscopy (XPS) can be used to determine the oxidation state of the metal centres. Solid-state UV-visible spectrophotometry also gives information about oxidation states. Finally, scanning electron microscopy (SEM) can be used to assess the shape and the size of the particles.

1.4. Applications

The applications of the MOFs are directly linked to their physical properties (see section 1.2) and to the nature of the building blocks. Many applications exist but here we will mainly discuss catalysis and gas storage. However other important applications have been developed mainly in the sensing, electrochemical and biological fields.[13]

1.4.1. Catalysis

Catalysis is of crucial importance in modern industry, as many commodities are produced using catalysed processes (this is estimated at 80% of industrial chemical reactions). Many different types of reactions can be catalysed and therefore catalysis is often divided in several subsets: Lewis and Brønsted acid and base catalyses, redox catalysis and photocatalysis.[13]

With MOFs, catalysis of the Lewis acid type is possible thanks to the metal centres. The coordination sphere around the metal atoms often comprises solvent molecules that can be removed by heating under vacuum to create reactive "open-metal" sites which can interact with the substrate to be catalytically transformed.[13]

Brønsted acid catalysis with MOFs can also be achieved, for example by adding an acidic moiety on the ligands. Sulfonic acids can be used for this purpose, allowing a proton to be transferred from the ligand to the substrate to enable the reaction. Similarly, a basic moiety added on the ligands, such as an amine function, makes Brønsted base catalysis possible.

Redox catalysis can be achieved through the metals composing the nodes of the MOFs but also includes functionalization of the ligand with redox active catalysts or nanoparticles.[13,15] Examples of such modifications will be covered in Section 6.6.

Using photocatalysis for hydrogen generation or CO_2 reduction is currently studied.[13] This can be accomplished with oxo-clusters in MOFs made of photoactive metal centres such as Ti (e.g. MIL-100-Ti, see section 4.3 below).

1.4.2. Gas storage

Some porous compounds show reversible gas adsorption capabilities and this is an important property. There are several reasons to aim at storing gases and MOFs are particularly promising for such applications.

a. Capture of harmful gases

The possibility to purify the atmosphere or flue gases by removing the carbon dioxide or other harmful gases may be an interesting application in the context of air pollution. This requires selective sorption of the target gas. For this purpose, a great attention must be dedicated to the design of the MOF.

The first way to influence the selectivity is to play on the size of the pore windows (apertures). A judicious tuning of the size of those windows allows the selective adsorption of molecules that are small enough to enter the pores and exclusion of too large ones.

The second way to reach selectivity is by tuning the chemical nature of the adsorption sites. Acidic gases like CO_2 for example can be selectively adsorbed based on Brønsted acid-base type reactions. This can be achieved by decorating the internal surface with basic functions, such as $–NH_2$. It must be noted that “open metal sites” (which are Lewis acids) are also strong adsorption sites for CO_2 because the lone pairs of the oxygen atoms allow the frustrated metal to complete its coordination environment. However, this kind of adsorption is not very selective towards carbon dioxide (but can however be tuned by changing the nature

of the metal) and any other good complexing agent, such as moisture, will strongly compete with CO_2.

b. Storage of useful gases

Storage of energetic gases in MOFs for mobile applications like cars as well as in much larger industrial applications is widely studied and has already reached some real-life applications. For instance, Mercedes-Benz developed a hydrogen fuel tank based on MOFs and used it in a demonstration model of one of its cars (F125).[16] The storage of natural gas (methane) in a car is also feasible.

Another application appeared recently and consists in releasing 1-methylcyclopropene contained in MOFs.[17] This molecule has the property to interact with the surface of stored fruits and vegetables, preventing them from ripening. The MOF charged with the gas is contained in bags, and thus presents a convenient alternative to the use of gas cylinders (easier and less dangerous alternative). This product is currently sold by the company MOF Technologies under the name "Trupick".

1.5. General synthesis

Different synthesis strategies have been developed to obtain metal-organic frameworks.[18] The choice of the method will not only be decisive for obtaining the desired MOF structure but it will also have a huge impact on its properties. Indeed, the crystallinity and specific surface area are not governed only by the structure but also by the presence and amount of defects. Moreover, the potential applications of MOFs at industrial scale force the rationalization and optimisation of synthesis pathways.

1.5.1. Solvothermal synthesis

Solvothermal synthesis consists in heating a solution of the precursors in a sealed reactor under autogenous pressure for several hours to a few days. When water is used as solvent, this approach is called *hydrothermal* synthesis. The reaction temperature can be higher than the boiling point of the solvents under ambient conditions thanks to the use of high-pressure autoclaves. Increasing pressure and temperature directly affects the solubility and reactivity of the precursors and allows the synthesis of new compounds, unreachable under ambient conditions.[19] Dimethylformamide (DMF) and diethylformamide (DEF) are commonly used in the solvothermal synthesis of MOFs having carboxylate-type linkers, due

to the high boiling point of those solvents and their slow decomposition into amines that allow to deprotonate the carboxylic functions, facilitating the MOF synthesis. Alternatively, solution synthesis of MOFs can also be performed in classical flasks equipped with condensers. In this case, the boiling point of the solvents limits the temperature but the synthetic setup has the advantage of being much cheaper. In both cases, modulators can be used to slow down the crystal growth and prevent the rapid precipitation of amorphous phases.

1.5.2. Mechanochemical synthesis

Mechanochemical synthesis is an easy method to implement. It consists in grinding together precursors that are generally solids. In order to favour the reaction, some solvent can be added to the reactants, the procedure is then called *liquid-assisted grinding* (LAG). The simplicity, reliability, low cost, "green" aspect of the process (only small amounts of solvent are used) and possibility of large-scale production makes this approach a good synthetic method for obtaining MOFs. However, mechanosynthesis often induces the formation of defects in the materials.

1.5.3. Electrochemical synthesis

Electrochemical synthesis involves the application of a potential difference between two electrodes in a solution containing an electrolyte and the ligand. The potential difference allows the slow release of ions of the metal that will compose the MOF. In most cases, this is achieved by electrochemical dissolution of a (sacrificial) anode, which is made from the metal that will compose the nodes of the MOF. The slowly released metal cations then react with the solubilized linker to form the MOF.

2. Aluminium and Al-based MOFs

2.1. The chemistry of Al

Aluminium, which is the most abundant metal in the earth crust (~8.2% in mass), is mainly found as $Al_2O_3 \cdot xH_2O$ (bauxite).[20] The high bonding energy between aluminium and oxygen in the ore is due to the Lewis hardness of both the metal and oxygen.

Metallic aluminium is obtained through purification of alumina from Bauxite by dissolving the ore in NaOH (Bayer process), followed by dehydration of $[Al(OH)_4]^-$. Then, the obtained alumina is mixed with cryolithe (Na_3AlF_6) and the obtained eutectic mixture is melted and electrolyzed through the Hall-Héroult process to obtain aluminium on the cathode (eq. **1**). The obtained metallic aluminium can be used as reductive agent (see production of $TiCl_3 \cdot AlCl_3$, p.14).

$$\textit{Cathode}: Al^{3+}(Na_3AlF_6) + 3\ e^- \rightarrow Al \qquad \mathbf{1}$$

The Pourbaix diagram of aluminium (Figure 4), which allows to evaluate the thermodynamic stability of species in water as function of the pH and redox potential evolutions, shows that the only stable oxidation state in water is +III. Furthermore, aluminium is soluble at low and high pH, and insoluble near neutral conditions. The control of pH is thus essential in aqueous aluminium chemistry.

Because it is a hard Lewis acid, aluminium has the tendency to form clusters in aqueous solutions through olation and oxolation reactions. These processes account for the complexity of aluminium chemistry. Indeed, many different soluble oligomeric species, composed of aluminium metal centres linked through bridging oxygens and hydroxyls, are formed in water.[21] In all cases, aluminium has a coordination number of 6, because of its small ionic radius. Some examples of existing oligomeric clusters are represented in Figure 5.

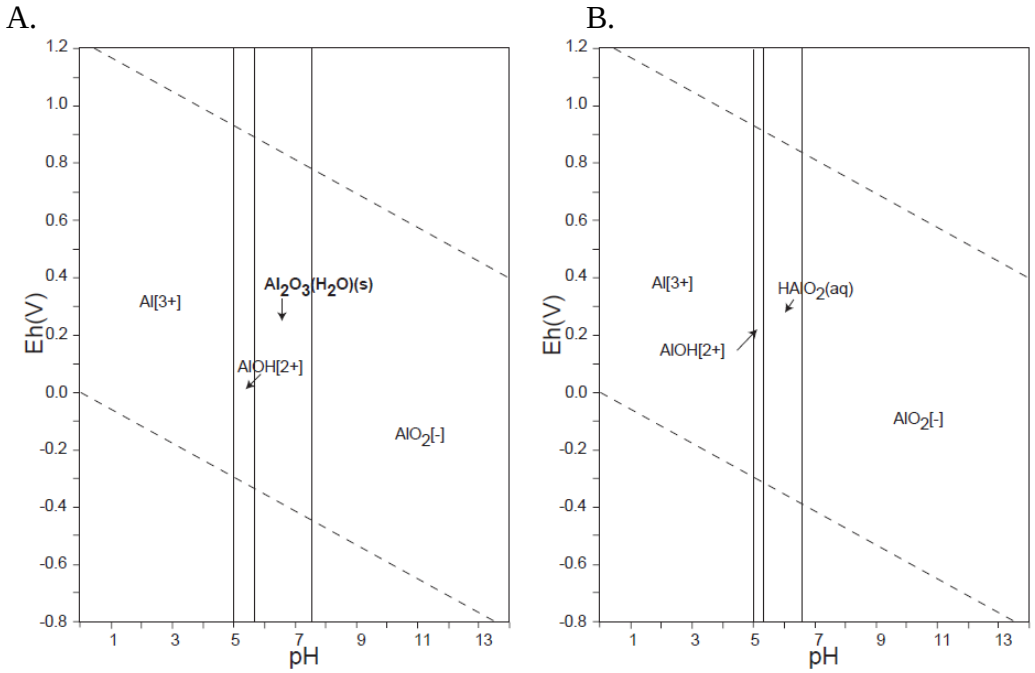

Figure 4. Pourbaix diagrams of the system Al-OH ($\Sigma = 10^{-10}$, 25°C). A. was drawn from a generic database in chemical engineering (FACT database) and B. was obtained through a database popular in geochemistry (SUPCRT). Taken from [22].

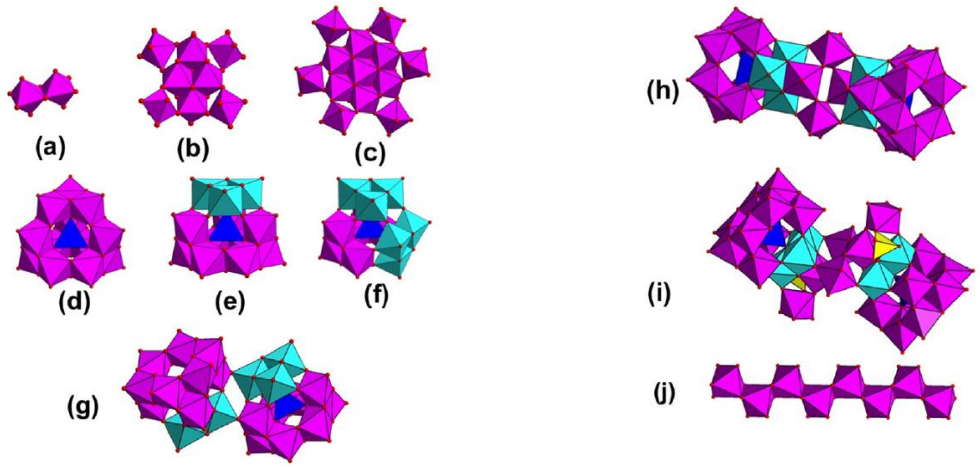

Figure 5. Examples of aluminium polycationic species crystallized from aqueous solutions. (a) Al_2J: $[Al_2(OH)_2(H_2O)_8]^{4+}$; (b) Al_8: $[Al_8(OH)_{14}(H_2O)_{16}]^{10+}$; (c) M-$Al_{13}$: $[Al_{13}(OH)_{24}(H_2O)_{24}]^{15+}$; (d) ε-$Al_{13}$: $[AlO_4Al_{12}(OH)_{24}(H_2O)_{12}]^{7+}$; (e) δ-$Al_{13}$: $[AlO_4Al_{12}(OH)_{24}(H_2O)_{12}]^{7+}$; (f) γ-$Al_{13}$: $[AlO_4Al_{12}(OH)_{25}(H_2O)_{11}]^{6+}$; (g) Al_{26}: $[Al_{26}O_8(OH)_{50}(H_2O)_{20}]^{12+}$; (h) Al_{30}: $[Al_{30}O_8(OH)_{56}(H_2O)_{24}]^{18+}$; (i) Al_{32}: $[Al_{32}O_8(OH)_{60}(H_2O)_{28}(SO_4)_2]^{16+}$; (j) Al_2-∞ $[Al_2(OH)_4(H_2O)_4]^{2+}$. Pink, light blue and dark blue are 6 coordinated Al, yellow is sulfate, red balls on the vertices are oxygens, taken from [21].

Aluminium chloride is a usual precursor for synthesis in the lab. It can be obtained in its anhydrous form from the reaction of metallic aluminium with Cl_2 or HCl (eqs. **2** and **3**). The reaction of Cl_2 occurs with molten aluminium and is highly exothermic, in practice the temperature is maintained between 670 and 850°C to form the dimeric Al_2Cl_6 solid.[23] $AlCl_3$ reacts exothermically with water due to its strong Lewis acidity. The reaction gives the

hydrated species $[Al(H_2O)_6]Cl_3$, which leads to the liberation of protons in water, thus making acidic solutions (eq. **4**).

$$2\ Al + 3\ Cl_2 \rightarrow 2\ AlCl_3 \qquad \mathbf{2}$$

$$2\ Al + 6\ HCl \rightarrow 2\ AlCl_3 + 3\ H_2 \qquad \mathbf{3}$$

$$AlCl_3 + 6\ H_2O \rightarrow [Al(H_2O)_6]Cl_3 \overset{H_2O}{\rightleftharpoons} [Al(OH)(H_2O)_5]Cl_2 + HCl \qquad \mathbf{4}$$

2.2. Al-based MOFs

The low density and low cost of aluminium make it a perfect candidate for creating MOF materials for large scale applications. Furthermore, Al^{III} is a hard Lewis acid according to the HSAB theory, as stated above, and therefore produces strong bonds with oxygenated ligands. This allows making robust MOFs by combining aluminium and linkers containing carboxylate functions. Such combinations are widely studied and allowed the synthesis of a plethora of interesting MOFs. The best known are those of the "MIL" family, among which we find MIL-53[24], MIL-96[25], MIL-110[26], MIL-100[27] and MIL-101[28] . The structures of the first three MOFs are given in Figure 6. The last two MOFs will be covered in more detail further in this Master thesis (see Section 4).

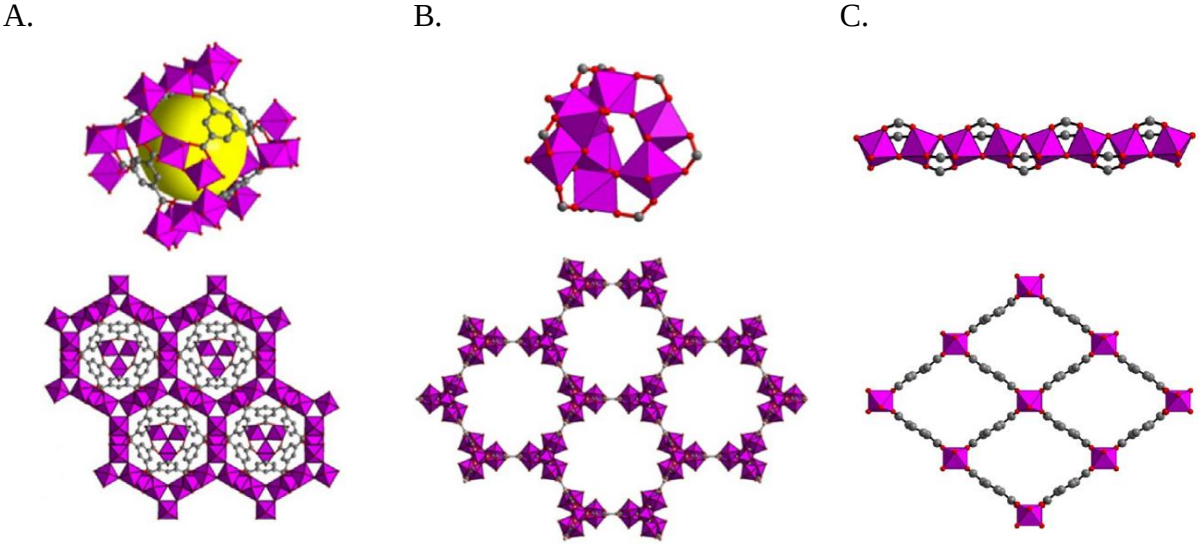

Figure 6. Oligomeric cluster and chain Al structures (upper images) and MOFs that they form (lower images) for (A.) MIL-96-Al, (B.) MIL-110(Al) and (C.) MIL-53-Al.

Those MOFs all contain six-coordinated Al atoms, either forming small clusters or long chains that are interconnected through the linkers to form microporous MOF networks. The presence of such clusters and chains in all those MOF structures is due to the propensity

of Al to form oligomers through olation and oxolation. Furthermore, MIL-96, MIL-100 and MIL-110 all contain the same linker and the formation of one structure instead of another is largely depending on the synthetic conditions (more information in section 4.2). Basically, Al-based MOFs are lightweight materials interesting for applications requiring low weight or low cost, such as gravimetric adsorption for applications in gas storage and separation.

3. Titanium, zirconium and Ti, Zr-based MOFs

3.1. The chemistry of Ti and Zr

Titanium and zirconium are transition metals in the fourth group of the periodic table. Their most stable oxidation state is +IV and therefore Ti^{IV} and Zr^{IV} are also hard Lewis acids according to the HSAB theory. This explains why they are found as oxygenated compounds in the earth crust.

3.1.1. Titanium

Titanium is the ninth most abundant element (~0.6% by mass), and the second most abundant transition metal (after iron), in the earth crust.[20] It is found in different minerals such as TiO_2 (rutile, anastase or brookite), $Fe^{II}TiO_3$ (ilmenite), $Fe_2Ti_3O_9$ (arizonite), $CaTiO_3$ (perovskite) and $CaTiSiO_5$ (sphene).[29] The reduction of rutile and ilmenite *via* a two-step chemical process is the basis of titanium industries. The first step, called *chloride process*, consists in the treatment of the mineral in the presence of carbon and chlorine at 800 or 900°C, depending on the mineral, to produce titanium tetrachloride (eqs. **5** and **6**).[30] Then, the obtained $TiCl_4$ is reduced by magnesium during the *Kroll process*, which is industrially applied since 1945, to produce metallic titanium (eq. **7**). The intermediate volatile air and water sensitive liquid $TiCl_4$ can be purified by distillation and is an attractive reagent for lab synthesis.

$$TiO_{2\,(s)} + 2\,Cl_{2\,(g)} + 2\,C_{\,(s)} \rightarrow TiCl_{4\,(g)} + 2\,CO_{\,(g)} \quad (800°C) \qquad \mathbf{5}$$

$$2\,FeTiO_{3\,(s)} + 6\,C_{\,(s)} + 7\,Cl_{2\,(g)} \rightarrow 2\,FeCl_{3\,(g)} + 2\,TiCl_{4\,(g)} + 6\,CO_{\,(g)} \quad (900°C) \qquad \mathbf{6}$$

$$TiCl_{4\,(g)} + 2\,Mg_{\,(l)} \rightarrow 2\,MgCl_{2\,(l)} + Ti_{(s)} \quad (900\text{-}950°C) \qquad \mathbf{7}$$

Titanium isopropoxide, a widely used precursor for making Ti^{IV} compounds, is obtained from $TiCl_4$ after reaction with isopropanol (eq. **8**).[31]

$$TiCl_4 + 4\,{}^{i}PrOH \rightarrow Ti(O^{i}Pr)_4 + 4\,HCl \qquad \mathbf{8}$$

Although the +IV oxidation state as well as the metal are most frequently encountered, titanium also exists in the +III oxidation state. $TiCl_3$ is a common Ti^{III} compound, which can be obtained through the reduction of $TiCl_4$ by aluminium (eq. **9**). This reaction produces $(TiCl_3)_3{\cdot}AlCl_3$, which can then be purified to obtain pure titanium (III) chloride. Alternatively, $TiCl_3$ can be obtained from high temperature reduction of $TiCl_4$ under a stream of hydrogen (eq. **10**).[32]

$$TiCl_4 + Al \rightarrow (TiCl_3)_3{\cdot}AlCl_3 \qquad \mathbf{9}$$

$$2\,TiCl_4 + H_2 \rightarrow 2\,TiCl_3 + 2\,HCl \qquad \mathbf{10}$$

A typical Pourbaix diagram of Ti, as well as one considering hydrated species of TiO_2 and Ti_2O_3, are presented in Figure 7. The analysis of the diagrams reveals that Ti^{III} is stable only in a very small window of strongly reducing and acidic conditions. Ti^{III} compounds are thus very sensitive to oxygen when present in water and must be handled and stored under inert atmosphere. Overall, the formation of TiO_2 is favoured over a wide range of conditions in water. For this reason, the synthesis of Ti^{IV} compounds is usually performed under inert and dry atmosphere to avoid the unwanted formation of TiO_2. Actually, the hydrolysis of Ti complexes is well known and allows the formation of TiO_2 nanoparticles, through the sol-gel method.[19] Due to its small size, and similarly to aluminium, titanium displays a coordination number of 6 in most compounds.

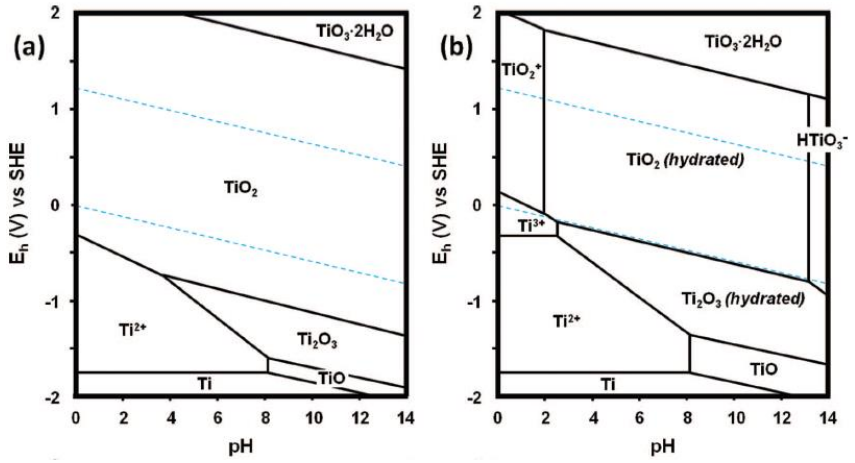

Figure 7. Pourbaix-type diagrams of Ti-H_2O system constructed considering a concentration of dissolved species equal to 10 µM, at 25°C. (a) Typical Ti-H_2O Pourbaix-type diagram, (b) considering hydrated species (TiO_2 and Ti_2O_3). The dashed lines represent the stability boundaries of water. Taken from [33].

3.1.2. Zirconium and Hafnium

Zirconium is a less abundant metal than titanium (~0.02% by mass).[20] It is found in the earth crust mainly in two types of minerals: zircon ($ZrSiO_4$) and baddeleyite (ZrO_2). Those ores also contain hafnium, with a Hf/Zr ratio approximately equal to 2/98. This is due to the nearly identical ionic radius of Zr and Hf, which is caused by the lanthanide contraction, as well as their common oxidation state (+IV). Zirconium and hafnium have a larger ionic radius than Ti and their coordination number can therefore exceed 6. Coordination numbers of 7 and even 8 are quite frequent in Zr and Hf compounds. The high reticular energy of the silicate and oxide leads to costly transformation processes. As for titanium, the transformation of the mineral into the metal involves the use of the chloride process to obtain $Zr(Hf)Cl_4$ (eqs. **11-13**) followed by reduction *via* the Kroll process (**14**).[34] Contrary to $TiCl_4$, zirconium tetrachloride is a polymeric solid with a high melting point.[30] Obtaining pure $ZrCl_4$ requires an additional distillation to separate it from $HfCl_4$, explaining the high cost of pure zirconium.

$$ZrSiO_{4\,(s)} + 4\,C_{(s)} + 4\,Cl_{2\,(g)} \rightarrow ZrCl_{4\,(s)} + SiCl_{4\,(l)} + 4\,CO_{(g)} \quad \textbf{11}$$

$$ZrSiO_{4\,(s)} + 2\,C_{(s)} + 4\,Cl_{2\,(g)} \rightarrow ZrCl_{4\,(s)} + SiCl_{4\,(l)} + 2\,CO_{2\,(g)} \quad \textbf{12}$$

$$ZrO_{2\,(g)} + 2C_{(s)} + 2\,Cl_{2\,(g)} \rightarrow ZrCl_{4\,(s)} + 2\,CO_{(g)} \quad \textbf{13}$$

$$ZrCl_4 + 2\,Mg \rightarrow Zr + 2\,MgCl_2 \quad \textbf{14}$$

Zirconyl chloride ($ZrOCl_2 \cdot 8H_2O$) is an interesting water soluble zirconium compound. It can be obtained from hydrolysis of zirconium tetrachloride, or by reaction of ZrO_2 with hydrochloric acid.[35]

Pourbaix diagrams of Zr, obtained using different software and databases, are presented in Figure 8. By opposition to Ti, zirconium shows no stable species in the +III oxidation state in water. Despite the differences observed between the diagrams, which reflects the difficulty of controlling Zr chemistry in water, the common observation is that only +IV species are stable in water.

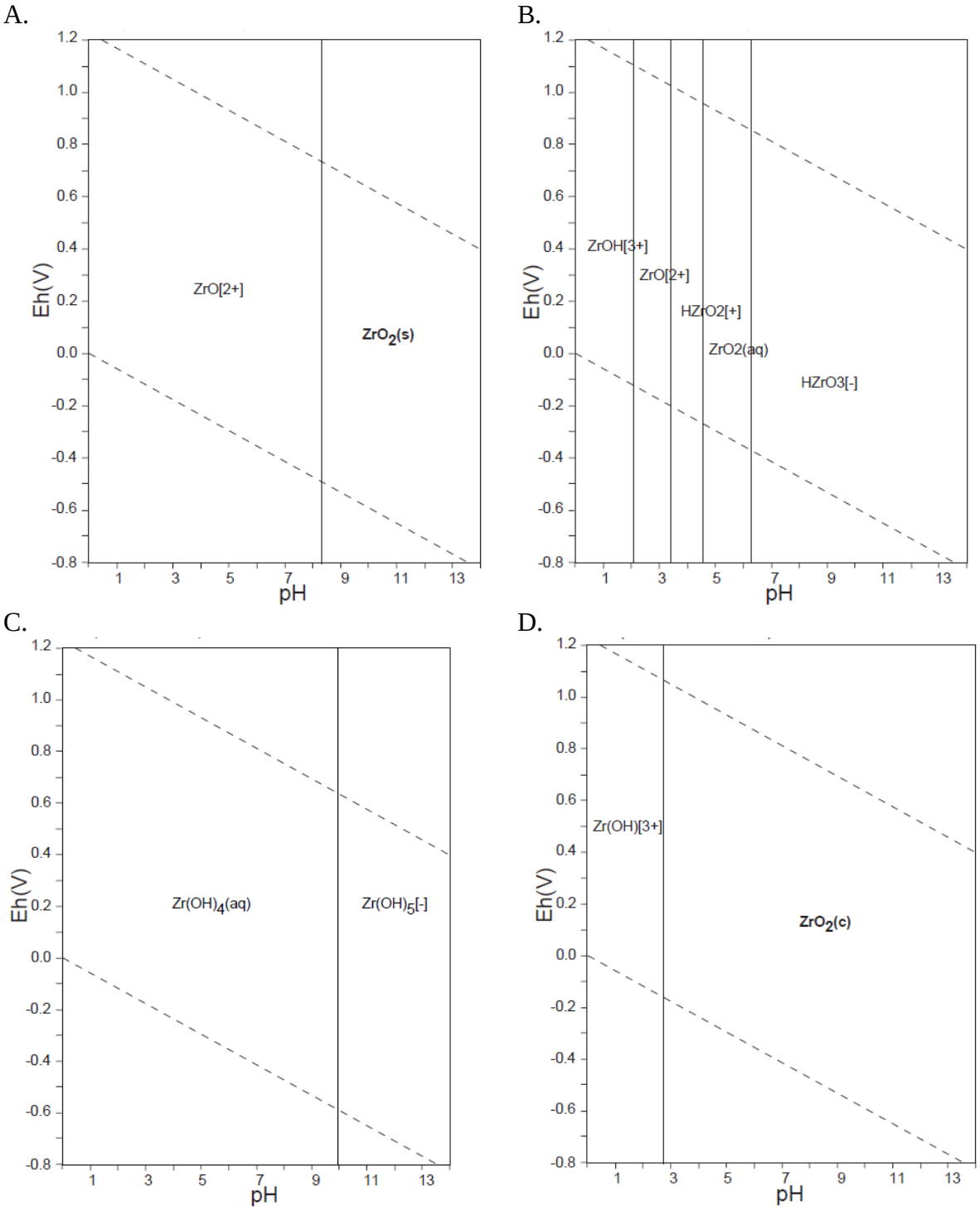

Figure 8. Pourbaix diagrams of the Zr-OH system ($\Sigma = 10^{-10}$, 25°C). A was drawn from a generic database in chemical engineering (FACT database). B was obtained through a database popular in geochemistry (SUPCRT). C and D are taken from a safety assessment database for radioactive wastes (JNC-TDB and HATCHES)[22].

3.2. Ti and Zr-based MOFs

The high positive charge of tetravalent titanium and zirconium and their resulting oxophilicity has attracted researchers to develop stable MOFs with oxygenated ligands, and

especially with carboxylate-containing linkers. Although the resulting frameworks possess high thermal and chemical stabilities, their synthesis requires specific synthetic conditions due to the strength of the linker-to-metal bonds, which often leads to precipitation of amorphous compounds instead of the desired porous crystalline materials.

Only few examples of Ti-based MOFs are described in the literature because of the complexity of titanium chemistry.[13,36] Nevertheless, the field has recently gained much attention, in particular with the motivation to develop photoactive materials.[7] Investigation of the possibility to obtain Ti-MOFs was first of all performed by using $TiCl_4$ or $Ti(O^iPr)_4$ as metal sources as they are obtained at large scale industrially and are thus readily available. However, the high reactivity of those titanium sources often leads to the formation of amorphous products. To overcome this problem, researchers have focussed their attention on the use of preformed Ti-clusters with lower three dimensional organization as precursors to form MOFs by ligand exchange.[15,36] Another way to obtain Ti-MOFs is to prepare the framework with another metal and perform post-synthetic exchange to introduce titanium in the structure (see Section 6.2 for an example).

Photoactivity of Ti-based MOFs can be achieved through ligand-to-metal charge transfer (LMCT). This phenomenon is responsible for the ability of MIL-100-Ti^{IV}, a MOF which will be covered in more detail in Section 4.3, to generate hydrogen from water by action of light (water splitting).[37] When a photon excites the aromatic linker of the MOF, it transfers an electron to a Ti^{IV} centre which is reduced into Ti^{III} (Figure 9). The Ti^{III} in turn reduces water to H_2 while the titanium is re-oxidized to Ti^{IV}. In summary, Ti-MOFs are of interest because they are stable, lightweight materials with potential photoactivity.

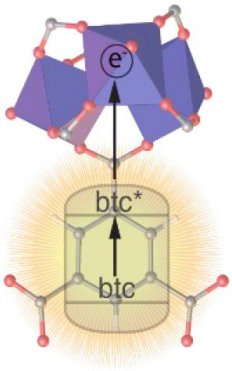

Figure 9. Representation of the ligand-to-metal charge transfer in MIL-100-Ti, from the aromatic linker to the Ti metal centre at the origin of its photoactivity. Taken from[37].

Ti-based MOFs, as well as Al-based ones, usually possess metal centres with a coordination number of 6. The higher coordination numbers of Zr, which can easily go up to 8, leads to higher connectivity of the metal centres in Zr-based MOFs, thus further increasing the mechanical stability of the structures. The synthesis of zirconium-based MOFs is usually based on the use of $ZrCl_4$ or $ZrOCl_2 \cdot 8H_2O$ as metal sources. The best-known example of a Zr-MOF is probably UiO-66, which will be described in detail in Section 5.

4. MIL-100 and MIL-101

MIL-100 and MIL-101 are two interesting highly porous MOF structures (Langmuir surface areas up to 3100 m^2/g and 5900 m^2/g respectively) that were discovered in France by the group of Gérard Férey. "MIL" stands for "Material of Institute Lavoisier", named after the research institute where those MOFs were discovered.[38,39]

4.1. Structural organisation

MIL-100 and MIL-101 are isotopological MOFs having a cubic crystal lattice with the $Fd\bar{3}m$ space group, that are both made of M_3-μ_3-oxo clusters interconnected with carboxylate-type linkers (see Figure 10). The clusters are composed of three octahedral metal centres (M_1, M_2 and M_3) linked through a central μ_3 bridging oxygen atom. The carboxylates of the linkers connect two adjacent metal centres together in the equatorial position. Coordinated solvent molecules and/or anions (L_1, L_2 and L_3 = H_2O, EtOH, F^-, Cl^-, OH^-, EtO^-, O^{2-}, etc.) occupy the apical positions. The nature of those ligands depends on the synthesis conditions and the charge that needs to be compensated. Indeed, the metal centres can have several oxidation states (+II, +III and/or +IV), which have a direct influence on the stability of the framework.

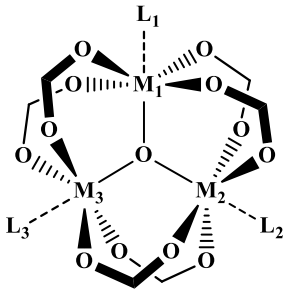

Figure 10. Structure of the cluster in MIL-100 and MIL-101 structures. M_1, M_2 and M_3 are metallic centres at +II, +III and/or +IV oxidation states, L_1, L_2 and L_3 are either solvents or anions molecules to compensate the global charge of the cluster.

What differentiates both MOFs is the linker, which is benzene-1,3,5-tricarboxylate (BTC^{3-}, also called trimesate), for MIL-100 and terephthalate (benzene 1,4-dicarboxylate, BDC^{2-}) for MIL-101. The linkers interconnect the clusters to form large (or super) tetrahedra, of which the ligands form either the triangular faces, for MIL-100, or the edges, for MIL-101. The clusters compose the vertices of those tetrahedra (Figure 11, A).

A.

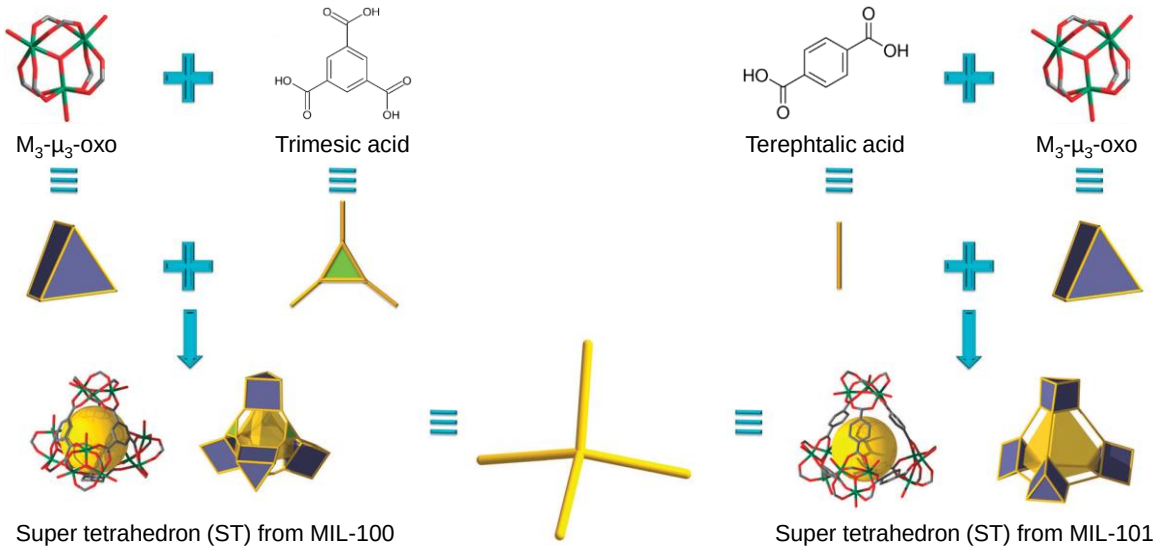

B.

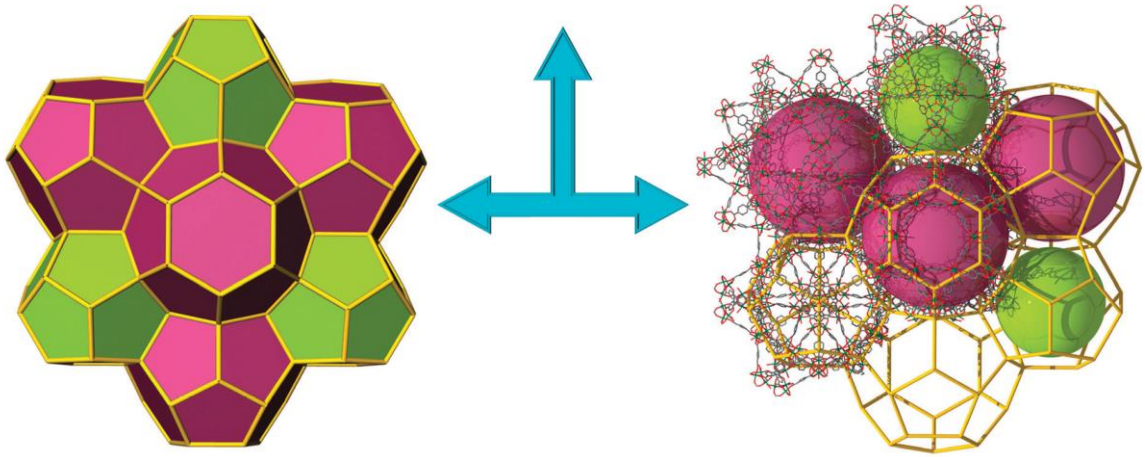

Figure 11. Three-dimensional structures of MIL-100 and MIL-101, modified from [39].

The assembly of those tetrahedral building blocks leads to the formation of two types of interconnected cages (25 Å and 29 Å diameter for MIL-100, 29 Å and 34 Å diameter for MIL-101) (Figure 11, B). The pores of those MOFs have "small" pentagonal and "large" hexagonal apertures. Those have a diameter of approximately 4.8 Å and 8.6 Å for MIL-100, and 12 Å and 16 Å for MIL-101, respectively. The particular structural characteristics allow an easy diffusion of the substrates to accessible actives sites, making these MOFs among the

most promising metal-organic frameworks especially for applications in catalysis and storage of large molecules.

Due to the huge size of the unit cells, some difficulties occur for characterization by X-ray diffraction. Indeed, both MOFs are difficult to obtain as single crystals and must most of the time be characterized by PXRD. Furthermore, the main diffraction peaks are located at low angles, because of the huge cell volumes (Table 1). The identical topology of both MOFs is responsible for similarities between their powder patterns. However, the larger lattice of MIL-101 shifts the diffraction peaks to lower angles than for MIL-100 (Figure 12).

Table 1. Comparison of crystallographic data of cubic MIL-100-Cr and MIL-101-Cr[40,41].

	MIL-100-Cr	MIL-101-Cr
Cell parameter (Å)	71.26	88.87
Cell volume (Å^3)	361 774	701 860

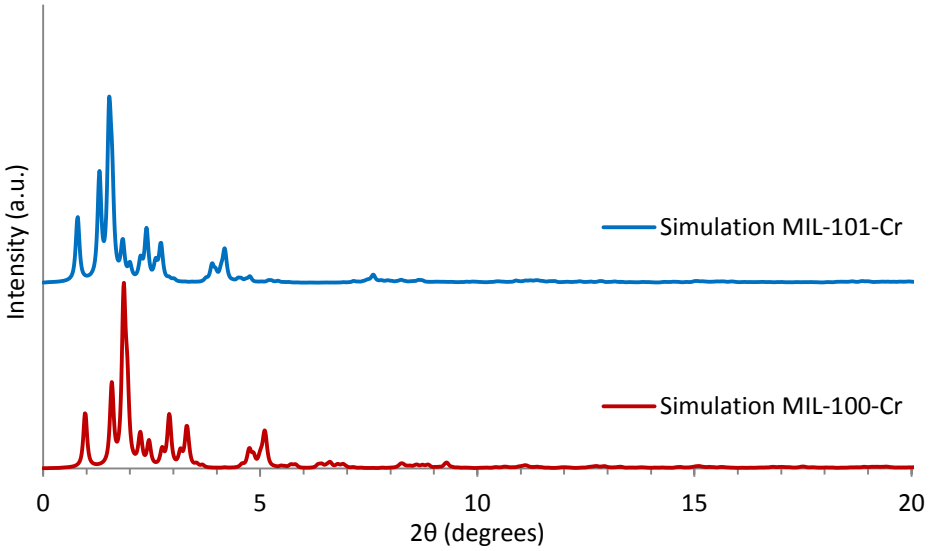

Figure 12. Comparison of X-ray diffraction powder pattern simulation for MIL-100-Cr[42] and MIL-101-Cr[41] ($Mo_{K\alpha}$ radiation, 0.71073 Å).

MIL-100 and MIL-101 both exist as monometallic and bimetallic MOFs. In the monometallic case, the frameworks with Cr and Fe as metal centres are the most widely studied. Both MOFs also exist with Sc[43], V[44,45] and Mn[46,47] and monometallic MIL-100 exists with Al[27]. Bimetallic MIL-100 and MIL-101 were synthesized with a wide range of metal combinations, mainly based on Cr or Fe as principal element. Only few examples of bimetallic MIL-100 containing aluminium or titanium are described in the literature, and to the best of our knowledge no such MIL-101 structures exists.

The structure of MIL-100 was first reported with chromium (MIL-100-Cr) in 2004 by Férey and co-workers.[40] Because no single crystal could be obtained, its structure was solved by using powder X-ray diffraction data. Because of the complexity of the framework and of the resulting powder pattern, the structure could only be solved through combination of computational predictions and Rietveld refinement on synchrotron data. For this, the authors simulated different possible hybrid building blocks with various metal/ligand ratios based on Cr-based trimers, as previous experiments suggested that those were present in the structure. The computationally simulated arrangement of those hybrid building blocks gave them three potential structures, from which powder patterns were simulated and compared with the experimental one. A perfect match was highlighted for one of those candidate structures. The same method was used for MIL-101-Cr in 2005.[48]

Later on, the structures of MIL-100 and MIL-101 composed of other metals were solved through Rietveld refinement based on the models developed for the chromium containing MOFs. For some MIL-100 structures, single crystals could even be obtained, allowing to get a better insight into the structure at the atomic level, this is for example the case of MIL-100-Al, which will be discussed in the next section.

4.2. Synthesis and properties of MIL-100-Al and MIL-101-Al

MIL-100-Al is the third compound of the MIL-100 family that was discovered, after MIL-100-Cr and MIL-100-Fe, and was first reported in 2009.[27] Single crystals were isolated from the reaction of aluminium nitrate with H_3BTC in water at low pH (0.5-0.7) under solvothermal conditions (210°C, 3.5h). The obtained framework had a BET surface area of 2152 m^2/g.

Pure MIL-101-Al has not yet been reported in the literature. However, the structure built from 2-amino terephthalate instead of terephthalate as linker was synthesized by reaction of 2-amino terephthalic acid with $AlCl_3$ in DMF under solvothermal conditions.[28] Surprisingly, the same reaction performed with terephthalic acid as linker source did not yield MIL-101-Al but formed MIL-53-Al instead (see section 2.2). The researchers also tried the synthesis of NH_2-MIL-101-Al starting from $Al(NO_3)_3$ instead of the chloride reactant. However, the reaction led to the formation of NH_2-MIL-53-Al. The same happens when the solvent is changed from DMF to H_2O. The differences are explained by the fact that MIL-53 is a thermodynamic product, while MIL-101 is a kinetic one, and the reaction conditions play an important role in the control of kinetics.

Such synthetic issues have also been evidenced for MIL-100-Al, which is not the most thermodynamically stable MOF composed of aluminium and the BTC^{3-} linker. Indeed, this MOF can be transformed into MIL-110 and MIL-96 (see Figure 6), the latter being the most thermodynamically stable MOF.[49,50] Recently in our lab, we optimized a method for obtaining MIL-100-Al form $AlCl_3$ and H_3BTC in a H_2O/EtOH mixture in the presence of some DMF and HCl that were added as modulators. The mixture was left to react at 60°C and the quality of the obtained MOF was assessed after different reaction times, showing that the crystallinity and porosity of MIL-100-Al increased for 6 days of reaction, but thereafter the surface area decreased and MIL-96-Al was formed as a secondary phase (see Figure 13).

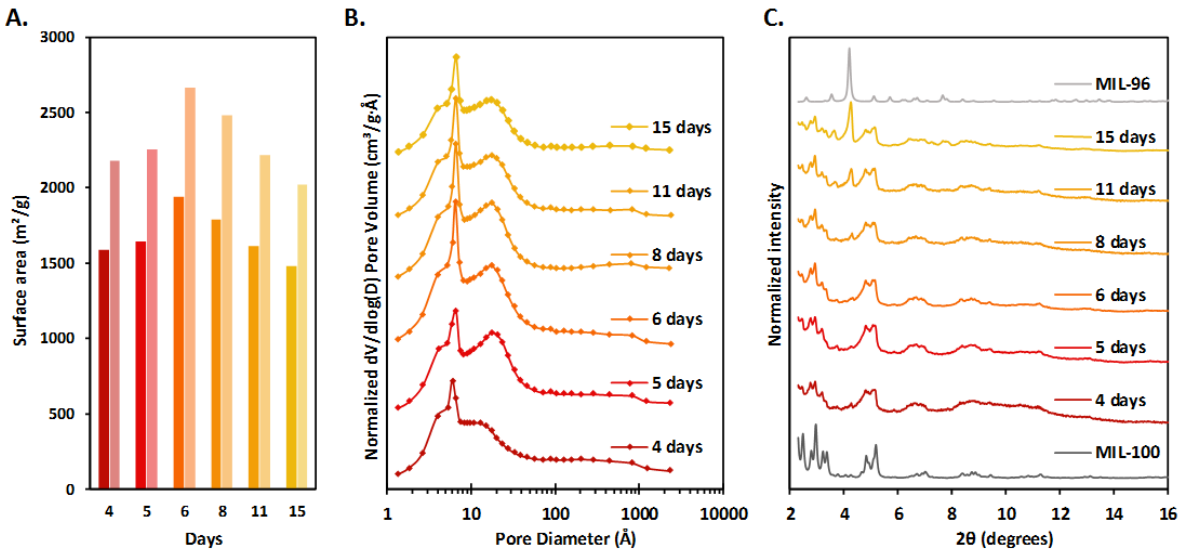

Figure 13. A. Evolution of the Brunauer-Emmett-Teller (dark colours) and Langmuir (light colours) surface areas of Al-BTC MOF samples obtained after different reaction times. B. Evolution of the Barrett-Joyner-Halenda pore size distribution of Al-BTC MOF samples obtained after different reaction times. C. PXRD patterns of Al-BTC MOF samples obtained after different reaction times.

Concerning the bimetallic MOFs, none example with aluminium as principal metal has been reported yet. However, MIL-100-Fe doped with Al is described two times in the literature.[51,52]

4.3. Synthesis and properties of MIL-100-Ti and MIL-101-Ti

The stability and interesting properties of Ti-MOFs (see sections 1.2.2 and 3.2) make titanium-based MIL-100 and MIL-101 very promising. However, because of the complexity of titanium chemistry (see section 3.1.1), the synthesis of those compounds was only succeeded recently. The examples below cover all the literature about MIL-100 and MIL-101 containing titanium as principal metal.

The synthesis of MIL-101-Ti^{III} was the first published, in 2015.[53] This MOF was obtained by heating terephthalic acid and $TiCl_3$ in a mixture of DMF and ethanol at 120°C for 18h. The product was recovered by filtration as a dark purple solid. Because Ti^{III} is very sensitive to oxidation, all those manipulations were performed under N_2 atmosphere. The composition of the cluster (Figure 14) was experimentally determined by solution NMR (digestion) experiments, which revealed that the counter anion balancing the residual positive charge of one of the Ti^{III} centres is ethanolate. The coordination spheres of the two other Ti^{III} atoms are completed by solvent molecules (DMF).

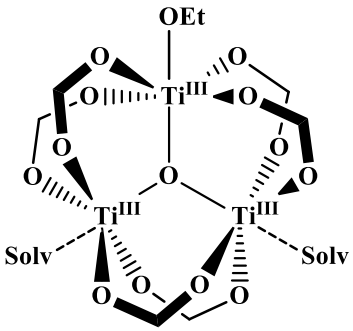

Figure 14. Composition of the Ti_3-μ_3-oxo cluster in MIL-101-Ti^{III}, determined by NMR digestion experiments (Solv = DMF). Reproduced from[53].

The specific surface area of the reported compound is among the highest of all titanium-based porous materials: 4440 m²/g (Langmuir) and 2970 m²/g (BET). The authors of the study also performed O_2 adsorption experiments after previous activation of the MOF, which removes only one out of the two solvent molecules of the clusters, and observed that oxygen irreversibly binds to the MOF. According to the study, the open metal site resulting from the removal of one of the coordinated solvent molecules reacts with oxygen to form superoxide O_2^- (Figure 15, A) or peroxide O_2^{2-} (Figure 15, B) moieties.

A. B.

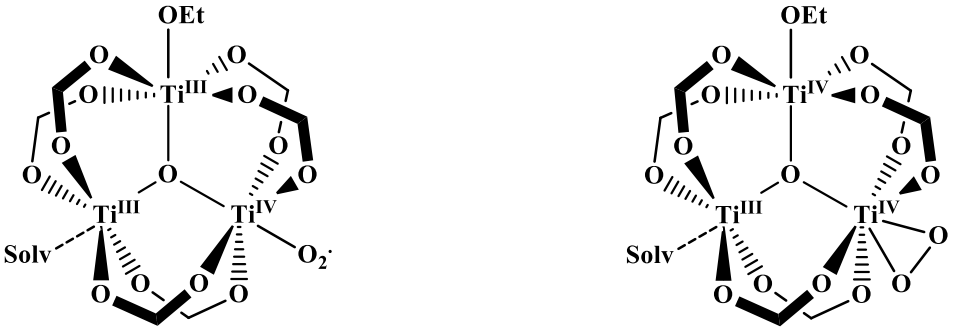

Figure 15. Proposed compositions of the Ti_3-μ_3-oxo cluster in MIL-101-Ti after exposition to O_2, (A.) with the formation of a superoxide anion and (B.) with the formation of a peroxide anion. Reproduced from[53].

It is only in 2019 that the first monometallic MIL-100-Ti^{IV} was reported by Castells-Gil *et al.*[37] It was obtained through reaction of a preformed $[Ti_6O_6(4\text{-tbbz})_6(O^iPr)_6]$ cluster (Ti_6 cluster) (see Figure 16) with H_3BTC in a CH_3CN/THF solvent system under solvothermal conditions (160°C for 48h). Acetic acid was added to the mixture as modulator to obtain a highly crystalline MOF. During the reaction, the Ti_6 cluster is rearranged to form the Ti_3-μ_3-oxo cluster of the MOF. The solvothermal process changes the solubility and the reactivity of the reagent.[19]

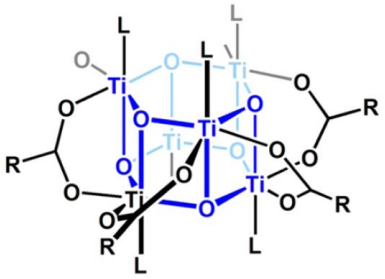

Figure 16. Structure of $[Ti_6O_6(4\text{-tbbz})_6(O^iPr)_6]$, or Ti_6, cluster. $^-$OOR = 4-tbbz (4-*tert*butylbenzoate), L = $^-O^iPr$. Taken from[54].

The obtained compound has a BET surface area of 1321 m²/g. The +IV oxidation state of Ti makes the MOF highly stable. Indeed, the authors showed that MIL-100-Ti^{IV} resists to a large range of pH values, between pH = 2 and 12, without loss of crystallinity. They also showed that the solid remains stable up to 450°C.

In order to determine the composition of the cluster, the authors performed DFT calculations and found two plausible compositions of the Ti_3-μ_3-oxo cluster having OH^- and/or O^{2-} as counter anions and/or H_2O to complete the coordination sphere of Ti (see Figure 17). The small energy difference between the two proposed structures does not clearly favour one over the other. In both clusters, four negative charges on the apical ligands are needed to obtain neutral entities. The cluster on the left (Figure 17, A.) possesses a water molecule, which could potentially be removed upon activation, possibly generating an open metal site.

A. B.

Figure 17. Proposed compositions of Ti_3-μ_3-oxo cluster in MIL-100-Ti^{IV}, reproduced from[37].

More recently, a synthesis of monometallic MIL-100-Ti^{III} *via* a combination of electrochemical and solvothermal methods was discovered.[55] The synthesis starts from the electrochemical reduction of a solution of terephthalic acid and $TiCl_4$ in an EtOH/DMF mixture to generate $TiCl_3$ (and hydrogen) *in situ* (Figure 18). The obtained solution is then heated solvothermally to yield a highly porous MOF having a BET surface area of 1736 m^2/g. The authors compared their electrochemical approach with the use of commercial $TiCl_3$ as Ti(III) source, and skipping the electrochemical reduction step. The BET surface area of the MOF obtained by this way was much lower (1304 m^2/g).

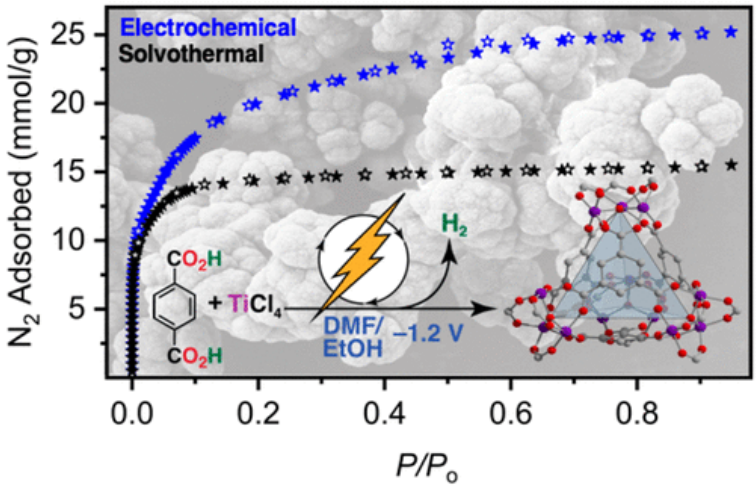

Figure 18. Scheme of the electrochemically-mediated synthesis of MIL-100-Ti^{III} and comparison of the N_2 adsorption isotherms of the MOFs obtained through the two different synthesis approaches (electrochemical-solvothermal and purely solvothermal). Taken from[55].

The authors used the same approach to synthesize MIL-101-Ti^{III}. In this case, they also observed that the surface area of the MOF obtained through their new synthetic approach (3285 m^2/g, BET) was higher than the one reported from conventional solvothermal synthesis (2970 m^2/g).

Surprisingly, the authors found that the positive charge of the cluster was counterbalanced by a fluoride anion in the case of electrochemical synthesis (Figure 19, A.), which was explained by the presence of NBu_4PF_6 that was used as electrolyte, and a chloride anion for the synthesis performed with commercial $TiCl_3$ (Figure 19, B.). The coordination sphere of the two other Ti atoms is completed by solvent molecules.

A. B.

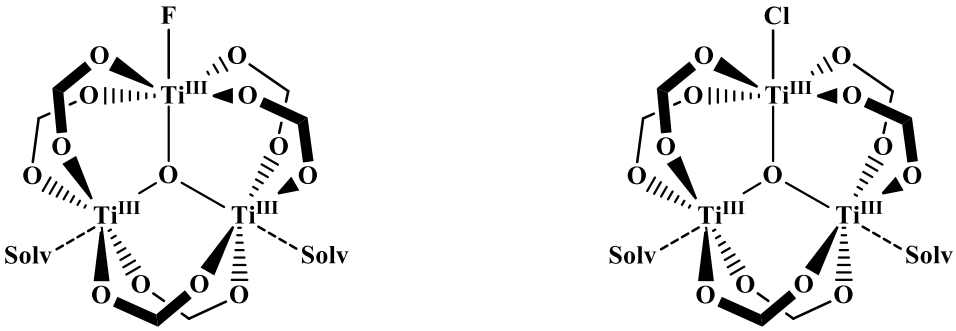

Figure 19. Proposed compositions of Ti_3-μ_3-oxo cluster in MIL-100-Ti^{III}, Solv = coordinated solvent molecule. Reproduced from[55].

Very recently (March 2020), a synthesis of bimetallic MIL-100-(M)Ti^{IV} (M being a doping metal) was described by Castells-Gil *et al.* This synthesis starts from a preformed mixed metal MOF containing Ti and Ca interconnected by BTC^{3-} ligands but having a different structure from MIL-100. This MOF, named MUV-10(Ca), undergoes a post-synthetic metal exchange with a first-row transition metal in the +II oxidation state (M = Fe^{2+}, Co^{2+}, Ni^{2+} or Zn^{2+}). During the metal exchange, Ca is replaced by the transition metal and a new MOF structure, which the authors called MUV-101(M), is formed. This MOF is isostructural to MIL-100 and the obtained compound is in fact MIL-100-(M)Ti^{IV} (see Figure 20).[56]

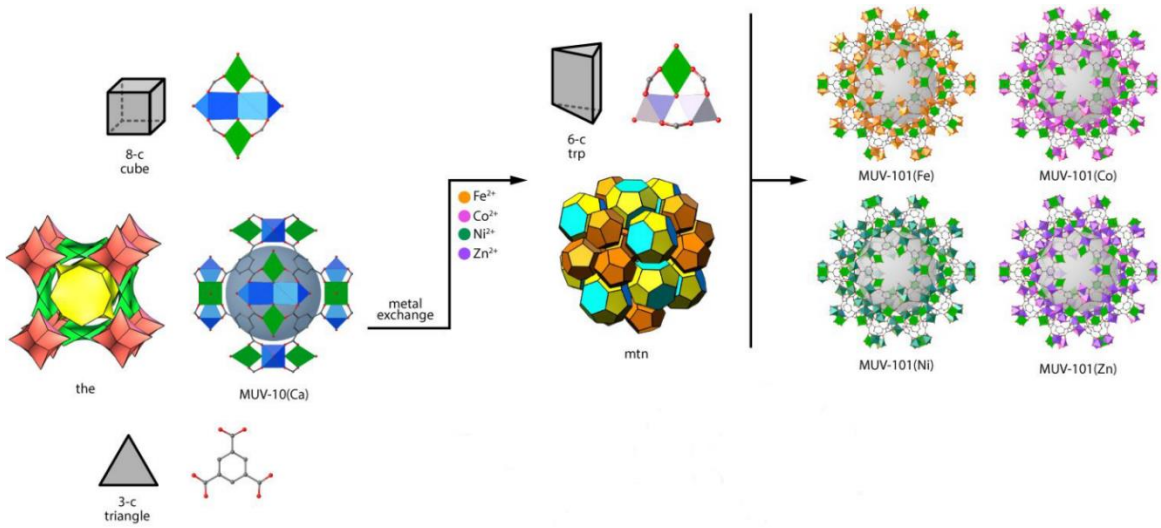

Figure 20. Synthesis scheme of MUV-101, a MOF isostructural to MIL-100, prepared from a bimetallic Ti and Ca MOF (MUV-10(Ca)). Modified from[56].

5. UiO-66

UiO-66 is currently one of the most studied MOFs. The name "UiO" is related to the University of Oslo (*Universitetet i Oslo*), where it was discovered by Lillerud and co-workers. This microporous zirconium-based MOF possesses an important surface area (S_{BET} = 1160 m^2/g) as well as high thermal and chemical stability, making this MOF very attractive for a lot of applications.[57]

5.1. Structural organization

The three-dimensional structure of UiO-66 is built from metal clusters connected through terephthalate linkers. Each cluster is composed of six eight-coordinated zirconium atoms which form the vertices of an octahedron. Those zirconium atoms are linked together by μ_3-O^{2-} and μ_3-OH^- groups in an alternate fashion (Figure 21, a).[58] Each cluster is connected to twelve carboxylate groups of the terephthalate linkers that interconnect the clusters to form the MOF's structure (see Figure 22). The assembly of the clusters and ligands leads to the formation of tetrahedral and octahedral cages with sizes of 8 Å and 11 Å respectively, having pore apertures of 6 Å.

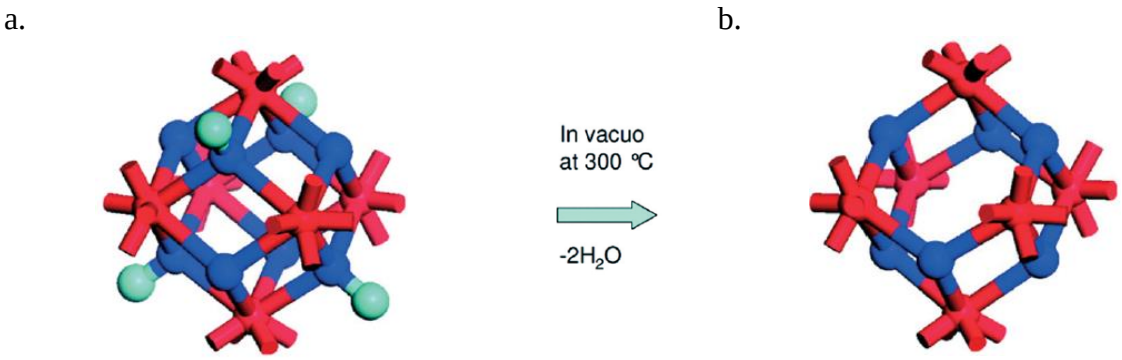

Figure 21. Structure of the Zirconium-based cluster of UiO-66 (a.) before and (b.) after activation (red = Zr, blue = O, cyan = H). The incomplete red bonds represent the bonds with carboxylates linkers, the linkers being omitted for clarity. Modified from[58].

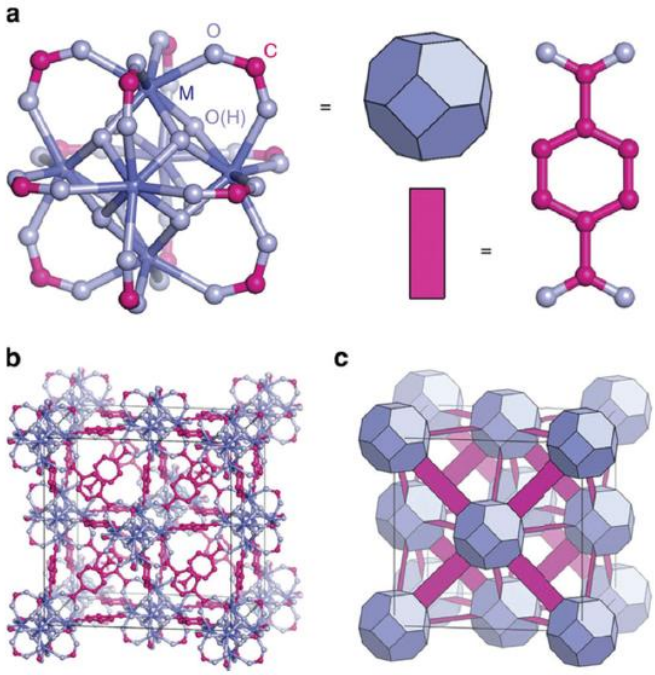

Figure 22. Three-dimensional structure of UiO-66: (a.) Zr_6 cluster and (b. and c.) crystal lattice. Carbon atoms are represented in pink, oxygen atoms in light blue and zirconium atoms in dark blue. Hydrogen atoms are omitted for clarity. Taken from[53].

UiO-66 can be activated at high temperature (~300°C) under vacuum. During this process, two μ_3-OH^- groups and the hydrogens of two other μ_3-OH^- ligands are removed. The remaining oxygen atoms of those two last OH groups are then converted into μ_3-O^{2-}. The activation results in a net loss of two H_2O molecules per cluster and the Zr atoms become seven coordinated after this fully reversible process (Figure 21, b).

The space group of UiO-66, like MIL-100 and MIL-101, is $Fm\bar{3}m$.[57] However, its cell length, of 20.75 Å, is about three to four times smaller than for the two described MOFs of the MIL series. The smaller cell volume allows to easily crystallize UiO-66 and allowed to solve its structure from single crystal data.[19] Those features also make the powder pattern of this MOF less complex. Diffraction peaks appear at higher angles than for MIL-100 and MIL-101, facilitating the analysis of this compound (Figure 23).

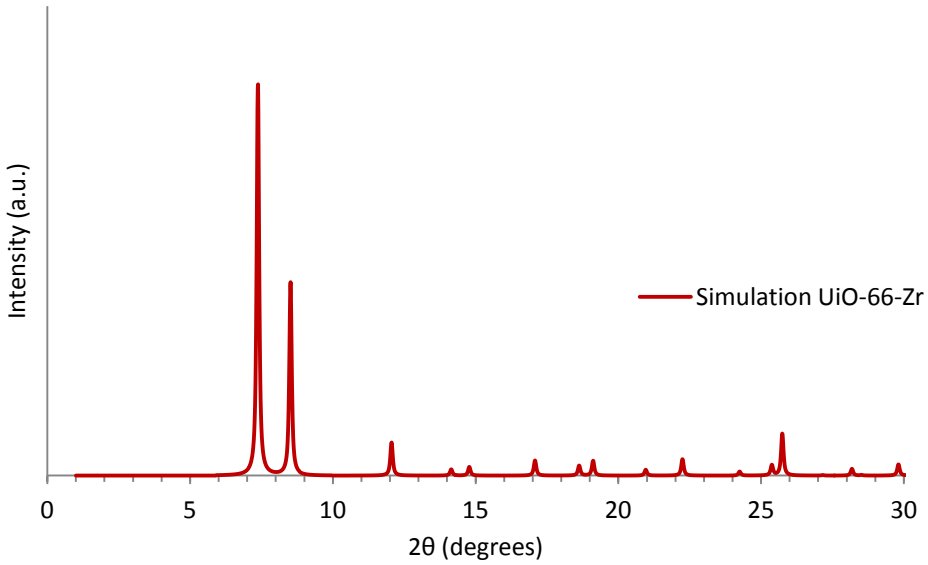

Figure 23. X-ray diffraction powder pattern of UiO-66-Zr simulated from the structure solved by single-crystal XRD data ($Cu_{K\alpha}$ radiation of 1.54056 Å)[59].

5.2. Synthesis and properties of UiO-66-Zr

The synthesis of UiO-66 generally involves the use of $ZrCl_4$ or $ZrOCl_2{\cdot}8H_2O$ as zirconium source and terephthalic acid as linker source. Those are usually mixed in a solution of a solvent of the amide type (e.g. DMF or DEF) and the mixture is then heated under solvothermal conditions. Addition of modulators and using appropriate concentrations, temperatures and reaction times allows the formation of single crystals.

UiO-66 studies are concentrated on the framework containing zirconium as metal centres, but the structure also exists with hafnium, cerium and, more exotically, several types of actinides (uranium[60], thorium[61], neptunium[62] and plutonium[63]).[58] Several bimetallic structures were also reported, with a mix of Zr/Hf, Zr/Ti and Zr/Ce.[64,65,66] UiO-66(M)Zr doped with other lanthanides or transition metals were also reported.[67]

UiO-66-Zr is thermally stable up to 400-540°C and possesses high chemical stability toward acid and base solutions as well as on exposure to solvents (DMF, ethanol and water, among others).[58] The incorporation of Ce in the clusters of UiO-66 decreases the thermal and mechanical stability.[64] By contrast, the substitution of Zr by Hf in the clusters does not have a huge influence on the stability of the framework.

6. Functionalization

6.1. Generalities

Post-synthetic modifications (PSM) allow adding new functionalities to MOFs that cannot always be incorporated to the structure by direct synthesis. This allows improving their efficiency for several applications (see 1.4). PSM regroup post-synthetic exchange (PSE) of metal and linker as well as functionalization of the linker and/or the metal centres.

6.2. Post-synthetic metal exchange

Post-synthetic metal exchange is widely used to introduce different metals in MOFs in which they cannot be incorporated through direct synthesis. This can be either because of the propensity of the metal to adopt coordination modes different from the one in the target structure or because of too high reactivity between the metal source and the linker, which leads to the precipitation of amorphous compounds by direct synthesis. The method consists in immersing a preformed MOF containing a given metal in a solution containing metal ions of a different nature, which are used for the exchange. This process can result in the formation of a bimetallic MOF in case of partial exchange or of a monometallic MOF in case of total exchange. The ratio of metals in the MOF can be controlled by the reaction conditions.

For example, Lau *et al.* published the synthesis of UiO-66-(Ti)Zr, which is performed through immersing preformed UiO-66-Zr in a mixture containing a source of Ti.[66] The authors synthesized a series of UiO-66(Ti)Zr MOFs having different Ti/Zr ratios and showed that there was an optimal ratio for CO_2 uptake in the structure. This improvement is explained by the smaller size of Ti compared to Zr, resulting in a shorter Ti-O bond which decreases the pore size and approximates the ideal pore size for CO_2 adsorption.[68]

During post-synthesis metal exchange, the structure of the initial MOF can also completely change. This is for example the case of the transformation of MUV-10(Ca) into MIL-100(M)Ti (see above, Section 4.3).

6.3. Post-synthetic linker exchange

Solvent-assisted linker exchange (also called SALE), is the most frequently method used to achieve post synthetic linker exchange. It consists of reacting the MOF in a solution containing the linker that one wants to incorporate into the framework.[69] This exchange

allows the introduction of functionalized ligands while keeping the initial topology of the MOF. This strategy is often used to incorporate functions that are incompatible with the direct synthesis of the MOF because their presence would interfere with the crystallization process.

This strategy was used to insert a catechol group on the terephthalate linker of UiO-66 (see Figure 24).[70] The adjacent alcohol functions were subsequently metalated by Cr, and the resulting compound was revealed to have catalytic activity in the oxidation of secondary alcohols to ketones, with a high recyclability.

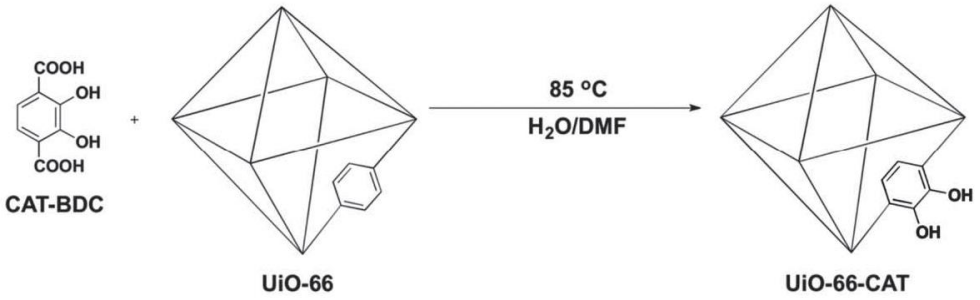

Figure 24. Reaction scheme of post-synthetic modification by linker exchange in UiO-66. Taken from[71].

6.4. Functionalization of the linker

New functionalities that cannot be added through direct synthesis of the MOF can also be introduced by chemical post-modification of the linker that is already present in the framework. An example is the functionalization of MIL-101-Cr with nitro functions by exploiting the chemistry of the aromatic ligand. Those functions can then be reduced to $–NH_2$ and the chemistry of amines can be used to graft, for example, an active ruthenium-based homogeneous catalyst through click-chemistry (see Figure 25).[72] The generated catalyst possesses a higher activity in oxidation of alcohols into aldehydes than $RuCl_3 \cdot 3H_2O$ under the same reaction conditions.

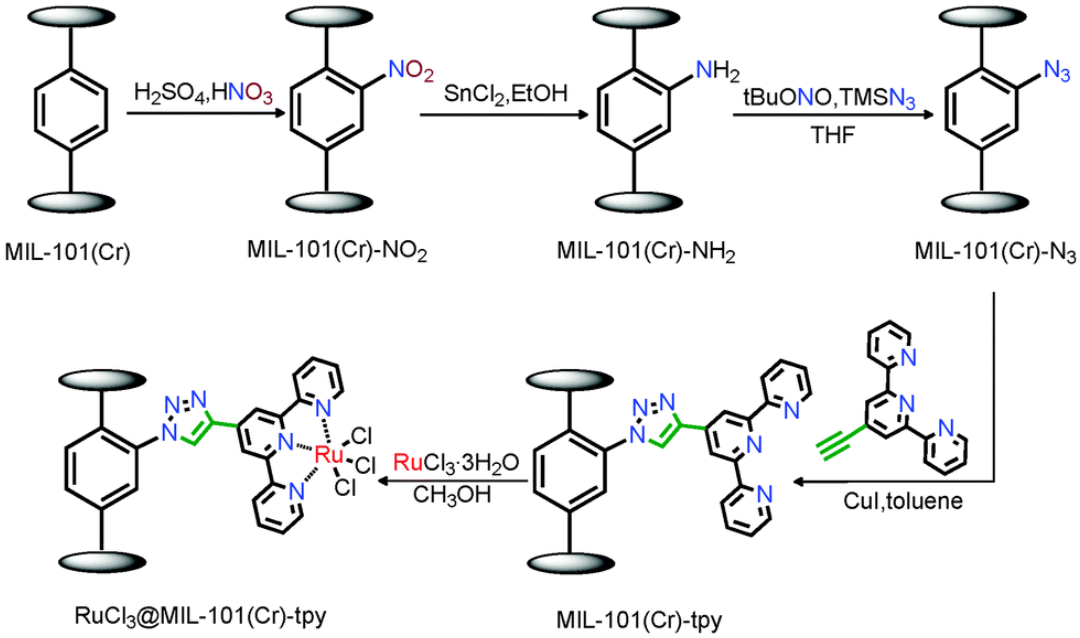

Figure 25. Reaction scheme for the grafting of a Ru-based catalyst within MIL-101-Cr by post-synthetic modification of the linkers. Taken from[72].

6.5. Functionalization of the metal

The metal centres of MOFs can also be used for grafting functions of interest. This is generally possible through the open metal sites of the MOF and is performed by coordinating a molecule of interest to the sites usually occupied by solvent molecules after synthesis.

For example, the functionalization of MIL-101-Cr was performed by first removing the two coordinated water molecules present on the Cr_3-μ_3-oxo clusters allowing to create two open metal sites. Those were then reacted with dopamine, which possesses an amine function that can bind to the frustrated Cr atoms (Figure 26).[73] The catechol function of the grafted dopamine was then metalated with vanadium (IV), and the obtained functionalized MOF was used as catalyst for the oxidation of thioanisole to sulfoxide in the presence of tert-butyl hydroperoxide.

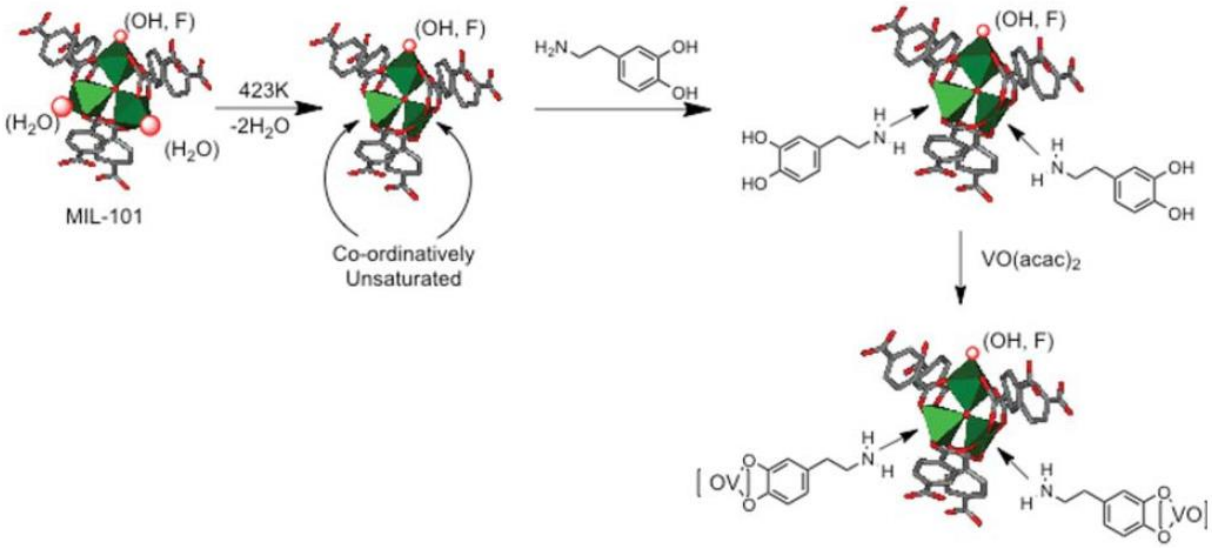

Figure 26. Reaction scheme to functionalize MIL-101-Cr with dopamine, followed by the metalation of the catechol function with vanadium (IV). Taken from[73]

6.6. Functionalization with ethylenediamine: state of the art

Molecules of choice for the post-functionalization of the metal are ethylenediamine and its derivatives. Ethylenediamine is a cheap commercial molecule that possesses two amines moieties. It can be anchored to MOFs by reacting one $–NH_2$ extremity to their open-metal sites. The second amine remains pendant in the MOF's pores. This procedure allows grafting free amine functions in an easy and cheap fashion, unlocking tons of possibilities. Similarly, ethanolamine and cysteamine can be regarded as derivatives of ethylenediamine for which one of the extremities is replaced by an alcohol or thiol function, respectively.

In the literature, only few examples of ethylenediamine grafting in MOFs were reported. Férey *et al.* demonstrated the first example of this type of functionalization in 2008 in MIL-101-Cr. They showed the possibility to functionalize the open metal sites with either ethylenediamine or diethylenetriamine, and demonstrated that the free amine functions are available as base catalysts for performing Knoevenagel condensation reactions.[74] They also showed that the obtained ethylenediamine-grafted MOF could be used for the synthesis of MOF-encapsulated noble metal nanoparticles.

MIL-101-Cr is since then the most studied MOF for ethylenediamine grafting and the obtained compounds were used to remove methyl orange from solutions,[75] to remove Pb(II) from aqueous solutions,[76] to adsorb rare earth elements[77] or for the photoreduction of CO_2

into CO.[78] Ethylenediamine-grafted MIL-101-Cr was also post-functionalized with salicylaldehyde to form grafted salen ligands. The resulting compound was reacted with chloroauric acid to form a catalytically active composite material containing both Au^{3+} coordinated salen complexes and metallic gold nanoparticles (see Figure 27).[79] The functionalization of MIL-101-Cr with ethanolamine was also studied and the obtained compound demonstrated activity to remove phenol from fuels thanks to hydrogen bonding.[80]

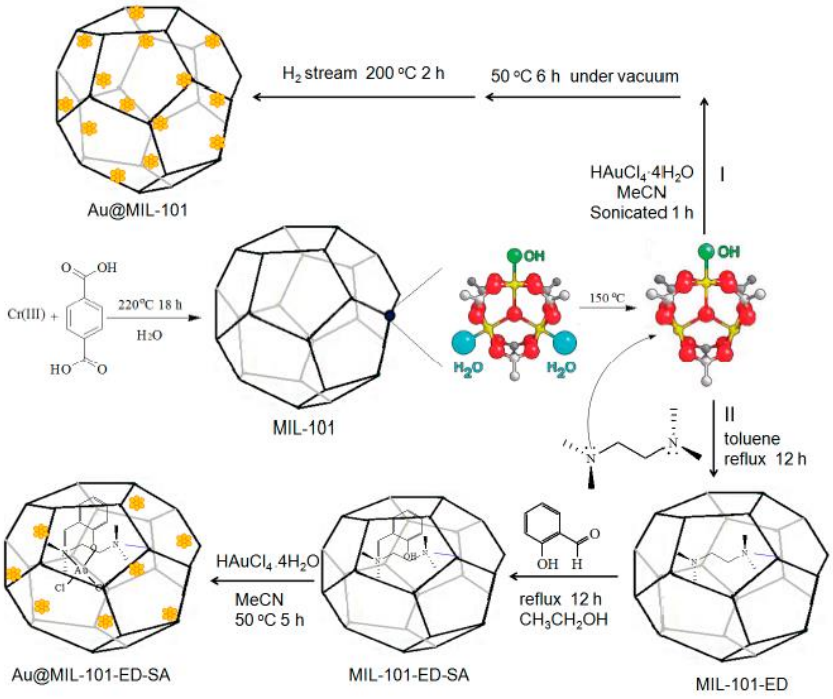

Figure 27. Reaction scheme of the functionalization of MIL-101-Cr with ethylenediamine on the open-metal sites, followed by a post-functionalization with gold nanoparticles and a salen ligand. Taken from[79].

Only few other MOF structures were studied for their ability to be functionalized with ethylenediamine. Those mainly include derivatives of MOF-74 and scarce examples with UiO-66, HKUST-1, MOF-5 and ZIF-67. Studies of those compounds were mainly oriented towards CO_2 capture, detection or separation from other gases. A complete list of all the examples and applications of the functionalization of MOFs with ethylenediamine and its derivatives is given in Table 2. Overall, the functionalization of MOFs with amine functions leads to many applications in gas storage due to the high affinity with CO_2, or in catalysis due to its basic nature and to the rich chemistry of amines for post-synthetic modifications.[81]

Table 2. List of MOFs that were functionalized with ethylenediamine derivatives and their applications.

MOF	Application	Reference
Ethylenediamine – used *without post-functionalization*		
MIL-101(Cr)	Removal of methyl orange from solutions	75
MIL-101(Cr)[1]	Adsorption of Naproxen and clofibric acid	82
MIL-100(Cr)*	Denitrogenation of model fuels with MOFs (effect of acidity and basicity)	83
Mg_2(dobpdc): dobpdc = 4,4'-dihydroxy-(1,1'-biphenyl)-3,3'-dicarboxylic acid	CO_2 uptake from air and flue gas	84
Mg-MOF-74	H_2/CO_2 separation using a MOF membrane	85
MIL-101(Cr)	Removal of Pb(II) from aqueous solutions	76
Mg_2(dondc : dondc = 1,5-dioxido-2,6-naphthalenedicarboxylic acid	Selectivity of CO_2 over N_2	86
Mg/DOBDC : DOBDC = dioxybenzenedicarboxylate	CO_2 capture and enhancing stability in humid conditions	87
M-MOF-74 (M = Mg, Ni, Co, Zn)	CO_2 detection	88
Mg_2(dobpdc): 4,4'-dihydroxy-(1,1'-biphenyl)-3,3'-dicarboxylic acid	CO_2 capture	89
MIL-101(Cr)	Adsorption of rare earth elements	77
HKUST-1	CO_2/CO separation	90
Mg-MOF-74 (DOBDC = 2,5-dioxido-1,4-benzenedicarboxylate)	Thin films on chips for the detection of CO_2 (and benzene)	91
UiO-66	(ethylenediamine grafted on a free carboxylic acid, in the form of an amide), adsorption of Gd^{3+}	92
MIL-101(Cr)	CO_2 photoreduction (to CO)	78
ZIF-67	Permselective membrane for H_2/CO_2 separation	93
Mn-DOBDC: DOBDC = 2,5-dihydroxyterephthalic acid	CO_2 uptake and water resistant	94
MOF-5-Zn	Drug delivery of piroxicam	95
MOF-74-Zn: 2,5-Dihydroxyterephtalic acid	Fluorescent probe to detect tetrabromobisphenol A (pollutant)	96
UiO-66-Zr	Ethylenediamine grafted on the ligand, adsorption removal of anti-cancer drugs	97
Ethylenediamine – with *nanoparticles*		
MIL-101(Cr)	Au-Pd nanoparticles for dehydrogenation of formic acid (hydrogen storage)	98
MIL-101(Cr)	Pd nanoparticles, catalysis in aerobic oxidation of alcohols	99
MIL-101(Cr?)	Pd nanoparticles for dynamic kinetic resolution of amines (with enzymes)	100
MIL-101-Cr	Pd nanoparticles, catalysis for dehydrogenation of formic acid and H_2 generation at room temperature	101
Ethylenediamine derivatives		
M_2(dobpdc), M = Zn, Mg, dobdc = 4,4'-dioxido-3,3'-biphenyldicarboxylate	CO_2 capture from air and flue gas	102
M_2(dobpdc) (M = Mg, Sc → Zn (first transition metal serie)	CO_2 adsorption, by grafting of 1,1-dimethyl-1,2-ethylenediamine	103

[1] Functionalization also done with aminomethanosulfonic acid

Ethylenediamine – *with post-functionalization*		
MIL-101(Cr)	Au^{3+}/Au^{0} catalyst for three-component coupling synthesis of propargylamines (NH_2 functionalized by salicylaldehyde)	[79]
MIL-100(Cr)	Transformation of -NH_2 into –$N(CH_2PO_3H_2)_2$, catalytic synthesis of N-heterocyclic pyrimido[4,5-b] quinolines	[104]
Ethanolamine – used *without post-functionalization*		
MIL-101(Cr)	Adding hydroxyls to enhance phenol adsorption	[80]
Cysteamine – used *without post-functionalization*		
UiO-66	Removal of Hg^{2+} from water	[105]
Cysteamine – *with post-functionalization*		
MIL-101(Cr)	Catalytic production of acetals (transformation into sulfonic acids)	[106]

7. Aim of the project

The goal of the present project is to synthesize various stable MOFs with potential open-metal sites and functionalize them with ethylenediamine and ethanolamine and evaluate the possibility of using the resulting pendant functions (-OH or –NH_2) for post-functionalization and further applications.

For this purpose, MIL-100, MIL-101 and UiO-66 were selected as candidate MOF structures because they possess potentially accessible open-metal sites. The possibility to obtain MIL-100 and MIL-101 MOFs with Ti and Al as metal centres and UiO-66 with Zr atoms will be evaluated as we expect that those metals will enable to make frameworks that are stable enough to withstand the treatment with the reactive ethylenediamine. A particular attention will be paid to assessing the possibility to yield those MOFs on a large scale (several grams), by adapting existing procedures of the literature if necessary in order to perform all the functionalization tests on a unique batch of each MOF.

Once the MOFs will be obtained, they will be heated under vacuum to remove the coordinated solvent molecules in order to free the open-metal sites. The MOF will then be ready for the functionalization with amine derivatives. To assess whether the functionalisation with amines and/or alcohols is efficient, the reaction will first be tried with fluorinated derivatives of ethylenediamine and ethanolamine (see Figure 28). This should enable easy analysis of the grafting efficiency by detection of the fluorine by XPS and of the C-F bonds through FTIR. Then, the same reaction will be performed with ethylenediamine and ethanolamine.

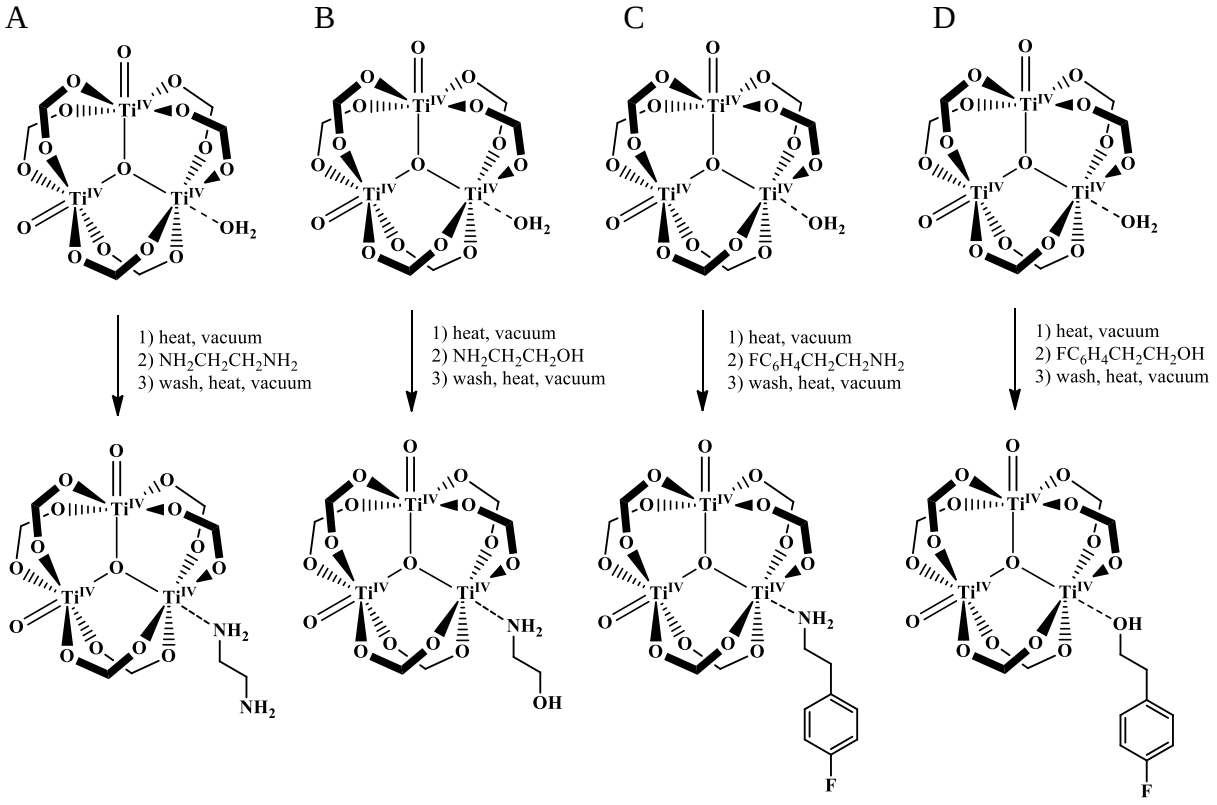

Figure 28. Reaction schemes of the functionalisation of Ti_3-μ_3-oxo cluster with (A.) ethylenediamine. (B.) ethanolamine, (C.) a fluorinated ethylenediamine derivative, and (D.) a fluorinated ethanolamine derivative.

The availability of the resulting amine functions for further post-functionalization will also be evaluated. For this purpose, we intend to take advantage of the absence of absorption bands of the Al^{III}, Ti^{IV} and Zr^{IV} MOFs in the visible region of the spectrum and use a fluorescent probe. This probe consists of a BODIPY molecule having a thiomethyl function, which is known to react with primary amines in a covalent way. The free BODIPY probe gives off a green fluorescence, but after reaction with amines, the fluorescence becomes blue. If an amine site of the grafted ethylenediamine (or ethanolamine) if available for post-functionalization, the functionalised MOF should demonstrate blue fluorescence after reaction with the probe (see Figure 29).

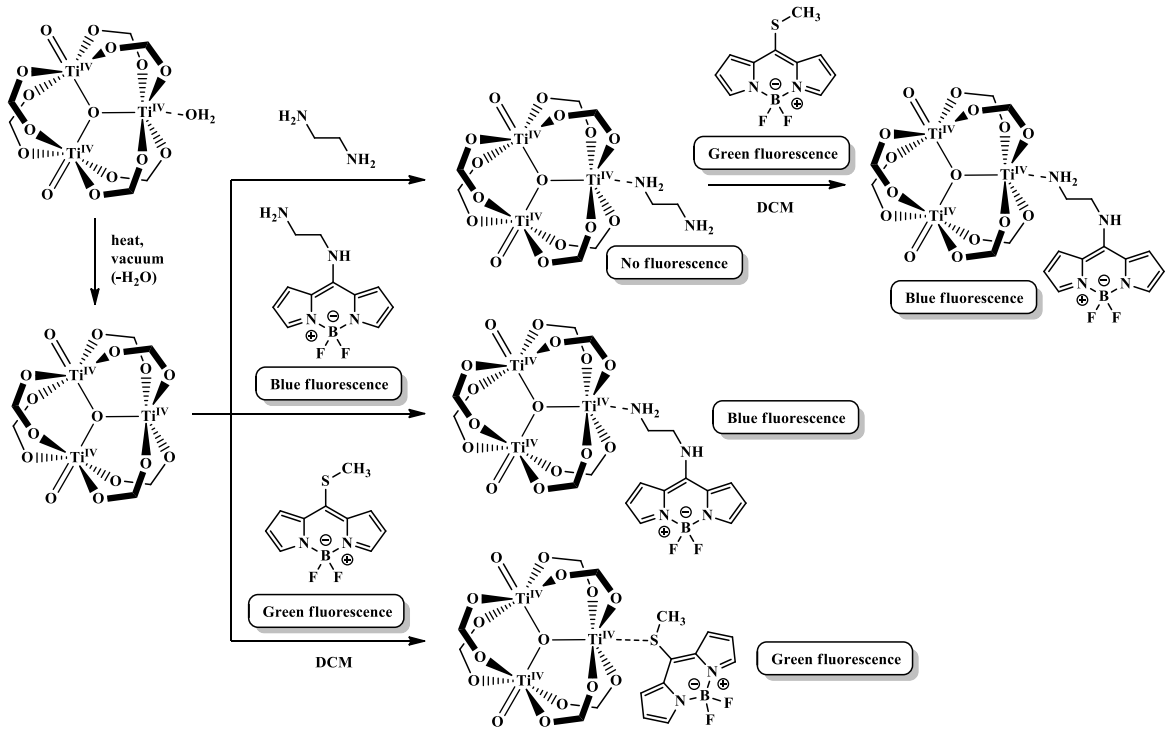

Figure 29. Reaction scheme of the BODIPY probe with Ti_3-μ_3-oxo cluster to demonstrate the presence of free amine functions

In the case of ethanolamine grafting, both OH-linking and NH_2-linking are possible in theory (see Figure 30). A test with the fluorescent probe should allow to discriminate between both possibilities.

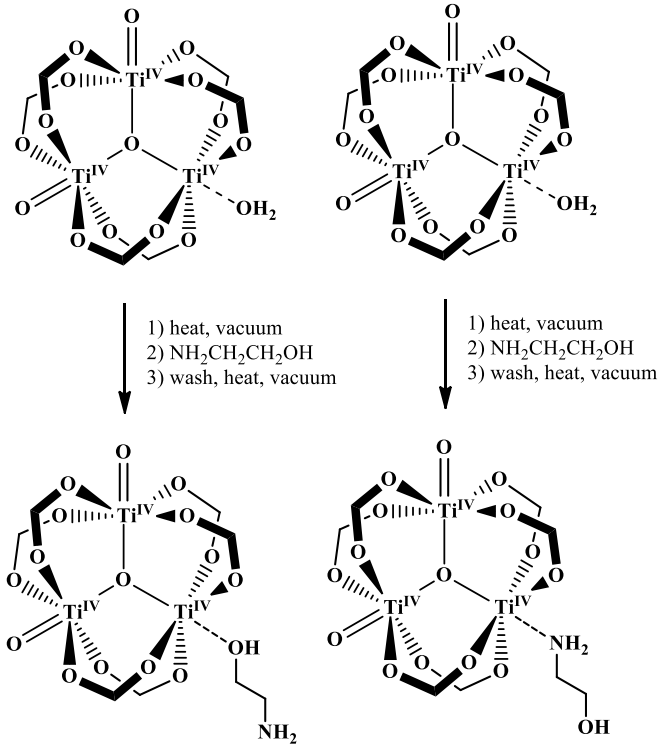

Figure 30. Two possibilities of O-link or N-link of ethanolamine on Ti_3-μ_3-oxo cluster

Besides producing MOF materials with new interesting properties, this project also aims at getting some clues about the exact composition and chemical properties of the clusters composing the frameworks through NMR experiments by measuring the ethylenediamine/ligand ratio to determine the ethylenediamine/metal atom ratio or by diffraction on single crystals. Indeed, up to now it is not clear if all the metals sites occupied by solvent molecules can be activated and functionalized. This is especially the case of MIL-100-Ti^{IV}, in which it is not clear whether the cluster indeed contains a removable water molecule or if the sites are all occupied by oxide and hydroxide functions that are not removable upon heating (see Figure 17).

After a short section about notations (II.1), the chapters II.2 and II.3 of this work will cover the attempts to synthesize MIL-100 and MIL-101, respectively, with Al and Ti as metal centres, both as monometallic and bimetallic MOFs. Then the synthesis of UiO-66-Zr will be discussed in chapter II. 4. Finally, chapter II.5 will cover the synthesis of the BODIPY derivative as fluorescent probe and the evaluation of its ability to be used to detect free amines.

II. Results

1. Notation

To facilitate the understanding of the present work, some specific notations were used to describe the target MOFs. The notation that is used throughout this work is **MOF-(M$_2$)M$_1^x$**, were "MOF" is the common name of the MOF structure (i.e. MIL-100, MIL-101 or UiO-66) and M_1 and M_2 are the main and doping (when present) metals composing the structure. X is the oxidation state of the main metal and is indicated only in the case of Ti, which can be in its +III or +IV state. According to this notation, MIL-100-(Al)Ti^{IV} is a MOF having the MIL-100 structure with clusters mainly composed of Ti atoms at the +IV oxidation state doped by aluminium.

2. MIL-100

2.1. MIL-100-Al

2.1.1. Large scale synthesis based on known procedure (6 L scale)

A procedure to obtain MIL-100-Al was previously developed in our lab. Large amounts of this MOF were needed for a collaborative project in our lab and this procedure was therefore scaled up. The large-scale synthesis was carried out by heating $AlCl_3$ with H_3BTC in a water:ethanol (1:1) mixture with small amounts of HCl and DMF at 80°C for 6 days. The mixture was then poured in various screw-capped glass bottles of 2.5 L (1 bottle) and 500 ml (10 bottles) capacity. The solid products were recovered and washed by centrifugation and their purity was assessed by PXRD (Figure 31). The positions of the diffraction peaks correlate nicely with the ones of the simulation, showing that MIL-100-Al was successfully obtained. Differences in relative peak intensities can be noticed and those can be explained by the presence of solvent molecules in the pores.

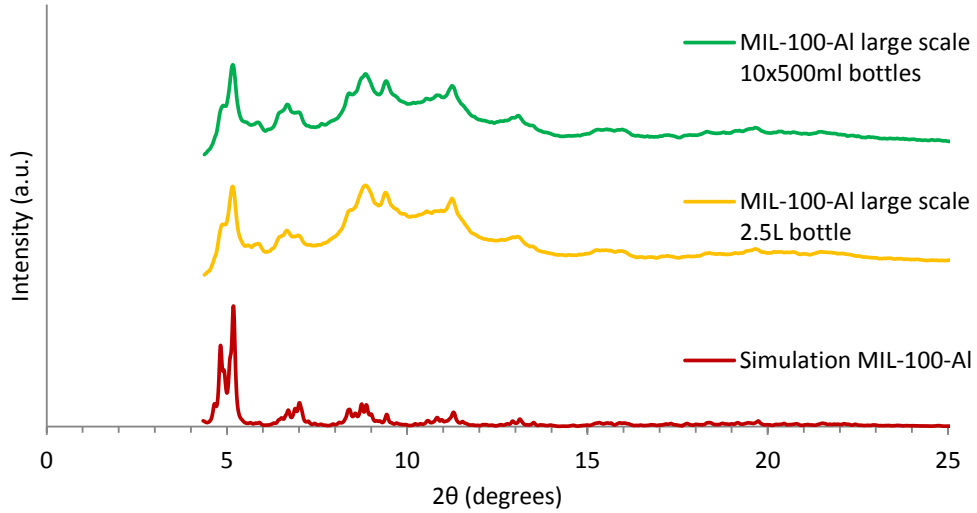

Figure 31. X-ray powder patterns of the products obtained by using $AlCl_3$ and H_3BTC as reagents at 80°C for 6 days, for the scale-up experiment of MIL-100-Al, compared with a simulated pattern (cif file[27]).

2.1.2. Small-scale synthesis without HCl

A small-scale synthesis was performed by using exactly the same parameters as previous experiments in our lab but without adding HCl with the motivation to evaluate the necessity of HCl for the synthesis, as well as to evaluate whether its absence would allow increasing the yield. Figure 32 shows a powder pattern of the obtained compound, which shows low crystallinity. The experiment demonstrates the importance of adding HCl in our synthesis.[49,50]

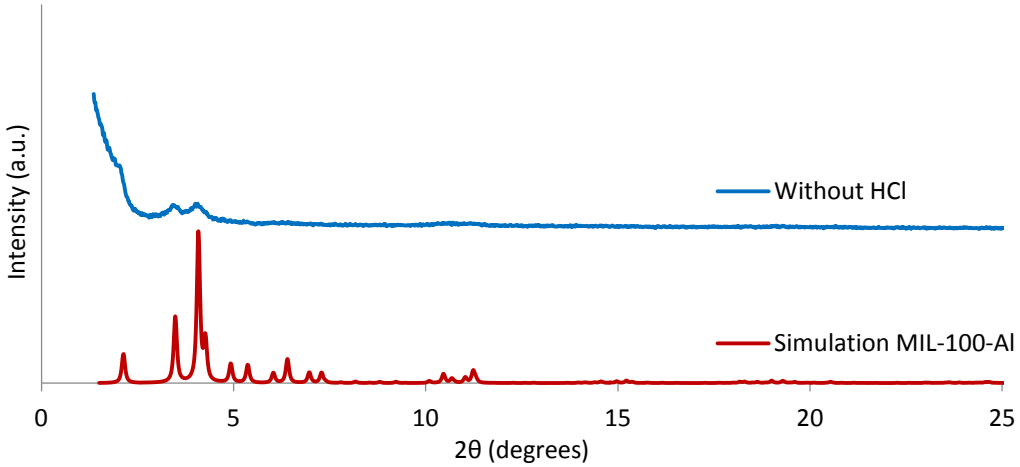

Figure 32. X-ray powder pattern of the product obtained when performing the synthesis of MIL-100-Al without adding HCl, compared with a simulation of MIL-100-Al (cif file[27]).

2.1.3. Variating the $AlCl_3$ and H_3BTC concentrations

Since the repeated centrifugation and washing steps take a lot of time for performing large-scale syntheses, we decided to increase the concentrations of the precursors in the reaction mixture to evaluate if we can obtain more product in less solvent. The previous large-scale synthesis was done with concentrations of 0.022 mol/l and 0.025 mol/l of $AlCl_3$ and H_3BTC, respectively. In this experiment, the concentrations ratios were kept constant but each individual concentration was multiplied by four to reach 0.086 mol/l ($AlCl_3$) and 0.1 mol/l (H_3BTC). PXRD analysis showed that the synthesis yields a product with poor crystallinity, as shown in Figure 33. Changing the concentrations of the reagents modified the concentration ratios with both modulators HCl and DMF (ratio divided by four), and had a deleterious an impact on the reaction. These ratios should be kept constant in future experiments.

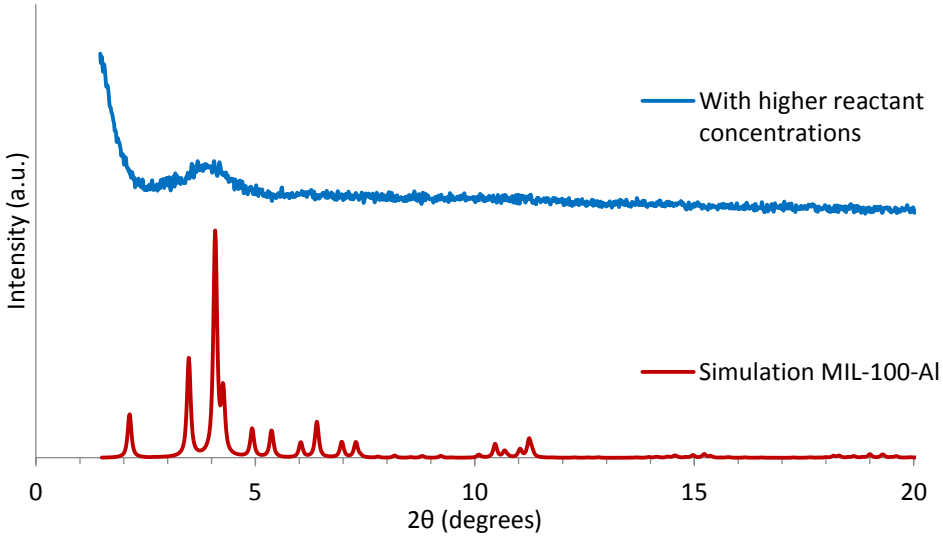

Figure 33. X-ray powder pattern of the product obtained by multiplying $AlCl_3$ and H_3BTC concentrations by four for the synthesis of MIL-100-Al, compared with a simulation of MIL-100-Al (cif file[27]).

2.1.4. Increased reaction temperature (100°C) and reduced reaction time (41h)

Since the time needed for the synthesis is very long, a test at a higher temperature was performed to accelerate the rate of the reaction. The same concentrations of reactants as for the first MIL-100-Al synthesis were used, but the temperature was set at 100°C. The reaction time was simultaneously decreased to 41h. We approximate that the reaction rate is multiplied by two with ten additional degrees, and calculated a reaction time four times lower at 100°C. Analysis by PXRD confirms the formation of MIL-100-Al, but a second crystalline phase,

MIL-96-Al, is also present in the product, as demonstrated by its typical peaks at 7.7 and 9.1 degrees on the diffraction pattern (see Figure 34). The presence of MIL-96, which is the thermodynamic product, indicates that the reaction time should be reduced even further to obtain pure MIL-100. However, it was demonstrated in previous work of our lab that the porosity of the product increases with reaction time at the beginning of the synthesis and reaches a maximum after a certain time (when the reaction is performed at 80°C) (see section 4.2 and Figure 13). A time consuming screening at 100°C with variable durations should be carried out to identify an optimum reaction time to obtain the highest possible porosity while avoiding the formation of the MIL-96-Al phase.

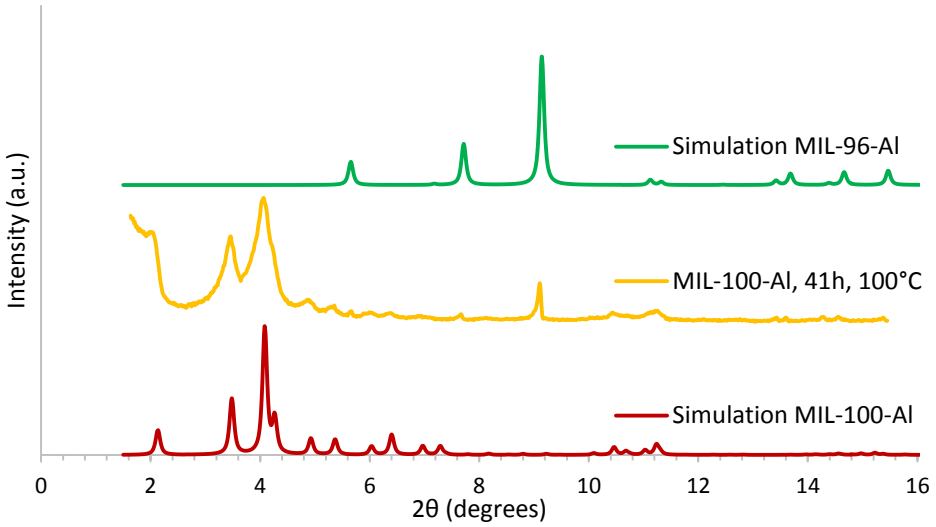

Figure 34. X-ray powder pattern of the products obtained when performing the synthesis of MIL-100-Al at 100°C for 41h, compared with simulations of MIL-100-Al (cif file[27]) and MIL-96-Al (cif file[25]).

2.2. MIL-100-Ti^{IV}

The synthesis of MIL-100-Ti^{IV} was carried out along a modified protocol reported by Castells-Gil *et al.*.[37] This procedure involves the use of the $[Ti_6O_6(4\text{-tbbz})_6(O^iPr)_6]$ cluster (denoted as Ti_6) as precursor. The crystallographic structure of this cluster is given in Figure 35. This compound is stable in air and in aqueous solutions.[54]

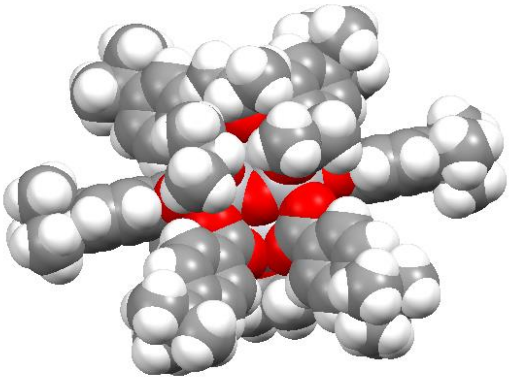

Figure 35. Crystallographic structure of $[Ti_6O_6(4\text{-tbbz})_6(O^iPr)_6]$, taken from the .cif file from[54]

2.2.1. Synthesis of a Ti_6 cluster as precursor

Before attempting the synthesis of the MOF, the Ti_6 precursor must thus be synthetically obtained. We tried to obtain several grams of this Ti_6 precursor before attempting the synthesis of the MOF, which must be realized at large scale, according to the aim of the project.

The synthesis of the cluster consists in reacting $Ti(O^iPr)_4$ with 4-*tert*-butylbenzoic acid (4-tbbz-H) in an ^{i}PrOH:THF mixture at 60°C for 24h under air atmosphere, and then further at 70°C for another 24h to obtain yellow crystals. For more convenience, we decided to perform the reaction in an open Erlenmeyer flask instead of using solvothermal conditions in a closed vial, as described in the original report.[54] Several reaction conditions were tested in order to find a suitable way for producing a single large batch for further experiments. Different precursor concentrations and volumes were tested (see Table 3).

Figure 36 summarizes the obtained powder patterns. The simulation (red curve) was performed through the Mercury software from the .cif file of the compound.[54] The analysis reveals that all the samples are highly crystalline and the positions of the diffraction peaks of all the obtained samples nicely correspond to the simulation, indicating that the desired compound was successfully obtained. The change in the intensity of the low angle peaks come from different occupation of large voids by solvent molecules.

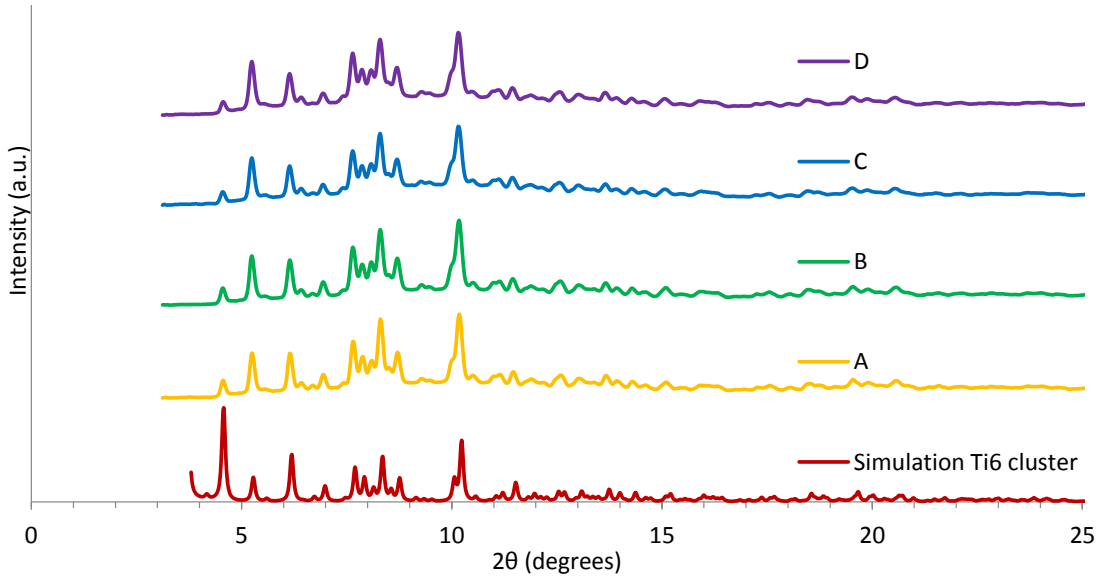

Figure 36. X-ray powder diffraction patterns of the Ti_6 cluster samples obtained using different synthesis conditions and simulated powder pattern for comparison (cif file[54]). Table 3 gives details of experimental conditions.

We observed that the synthesis is easy to perform, scalable and leads to high yields (Table 3). Moreover, the yields that we obtained are 86% or higher while the reported yield is only of 64%.[54] We hypothesize that this could be due to the facilitated formation of the cluster in the presence of water, which is continuously introduced in the Erlenmeyer flask by the moisture of the air, if one assumes the following formation reaction (eq. **15**) :

$$6\ Ti(O^iPr)_4 + 6\ \mathbf{H_2O} + 6\ \text{4-tbbz} \rightarrow [Ti_6O_6(\text{4-tbbz})_6(O^iPr)_6] + 18\ {}^iPrOH \qquad \mathbf{15}$$

Figure 37 presents the FTIR spectra of the different obtained Ti_6 samples. The comparison of the spectra shows no difference with the spectrum of the literature (see Figure 70 in the annexes), confirming that the product Ti_6 was obtained with high purity in each case.

TGA analysis reveals that the cluster starts its decomposition around 275°C (see Figure 38 and Figure 71 in the annexes for more details), which is in line with the observations made in the literature (Figure 72 in the annexes). The experimental weight loss (starting at 100%) is 77%, which correlates with the calculated value of 73%, assuming a residue of TiO_2.

Table 3. Reaction conditions used and yields obtained for the synthesis of $[Ti_6O_6(4\text{-tbbz})_6(O^iPr)_6]$.

Conditions	A	B	C	D
Reactant				
$Ti(O^iPr)_4$	0.04 mol/l	0.04 mol/l	0.04 mol/l	0.16 mol/l
4-tbbz-H	0.32 mol/l	0.32 mol/l	0.32 mol/l	1.28 mol/l
^{i}PrOH:THF (3:1)	30 ml	150 ml	150 ml	75 ml
Yield (%)	86	97	Quantitative	Quantitative

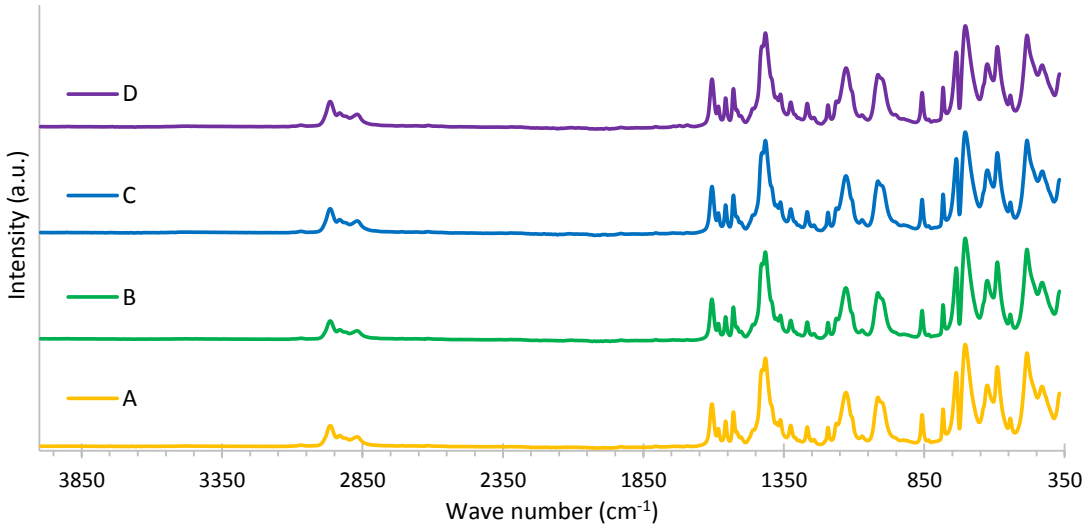

Figure 37. FTIR spectra of the Ti_6 cluster samples obtained using different synthesis conditions.

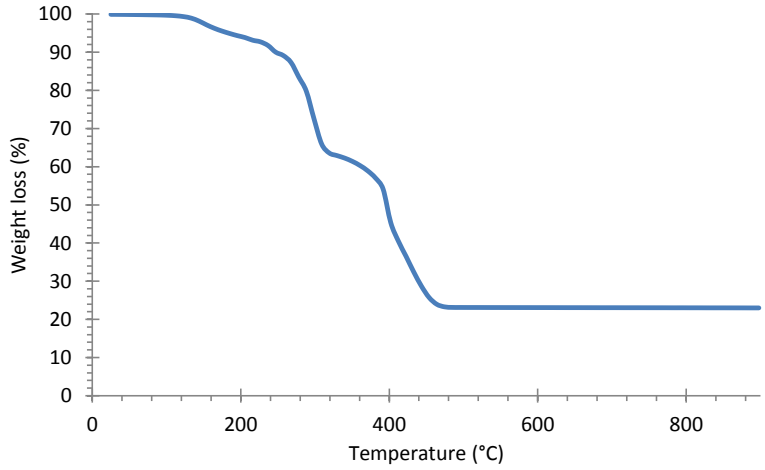

Figure 38. TGA of $[Ti_6O_6(4\text{-tbbz})_6(O^iPr)_6]$ cluster under air, sample D.

2.2.2. Synthesis of MIL-100-Ti^{IV} according to published procedure

The procedure published by Castells-Gil *et al.* involves the reaction of Ti_6 with H_3BTC in an ACN:THF mixture in the presence of acetic acid as modulator under solvothermal conditions.[37] The authors performed the synthesis of MIL-100-Ti^{IV} in glass vials (the volume is not given). However, we wanted to perform our grafting experiments on MOF samples resulting from one single batch to ensure that the results would be comparable. Therefore, we tried to obtain MIL-100-Ti^{IV} on a much larger scale.

A first trial was done in a Teflon bomb (250 ml) at 160°C for 40h starting from 0.145 g (80.5 µmol) of Ti_6, which corresponds to quantities 20 times higher than reported. However, when opening the bomb, it appeared that all the solvent was evaporated. PXRD revealed that the obtained solid was amorphous (see Figure 39, A). Because of the evaporation of the solvent, the solvothermal conditions for the synthesis were not fulfilled anymore. From this, it was concluded that the Teflon bomb was not a suitable reactor for this synthesis.

Because the Teflon bomb was not able to contain the solvents due to excessive pressure caused by the high temperature, we performed the experiment in a stainless steel autoclave with 0.433 g (0.24 mmol) of Ti_6, which corresponds to quantities 60 times higher than reported. This time the solvents were contained by the reactor and a solid deposit formed at the bottom of the container. However, PXRD analysis revealed that this product was also amorphous (see Figure 39, B).

The results of the two above experiments indicate that the synthesis is not scalable in our conditions. We however decided to test the synthesis with the quantities given in the published procedure in similar conditions to see whether we were able to reproduce the experiment.

We thus attempted the synthesis in a screw capped glass vial (4 ml) with 7.4 mg (4.11 µmol) of Ti_6, the same quantities as in the article. However, in this case, the solvent has also evaporated and a dry solid was obtained. PXRD analysis shows that in this case, a crystalline product was obtained; but unfortunately, the positions of the diffraction peaks did not correspond to the ones expected for MIL-100-Ti (see Figure 39, C). Comparison with experimental powder patterns of Ti_6 and H_3BTC (Figure 40) revealed that the cluster is no

longer present (absence of peak at 6.15 degrees): it decomposed during the course of the reaction. All the peaks of the sample C show a concordance with the peaks of trimesic acid, therefore the product still contains unreacted H_3BTC. However, the product was washed with ethanol, which should have removed remaining H_3BTC since it is highly soluble in this solvent.

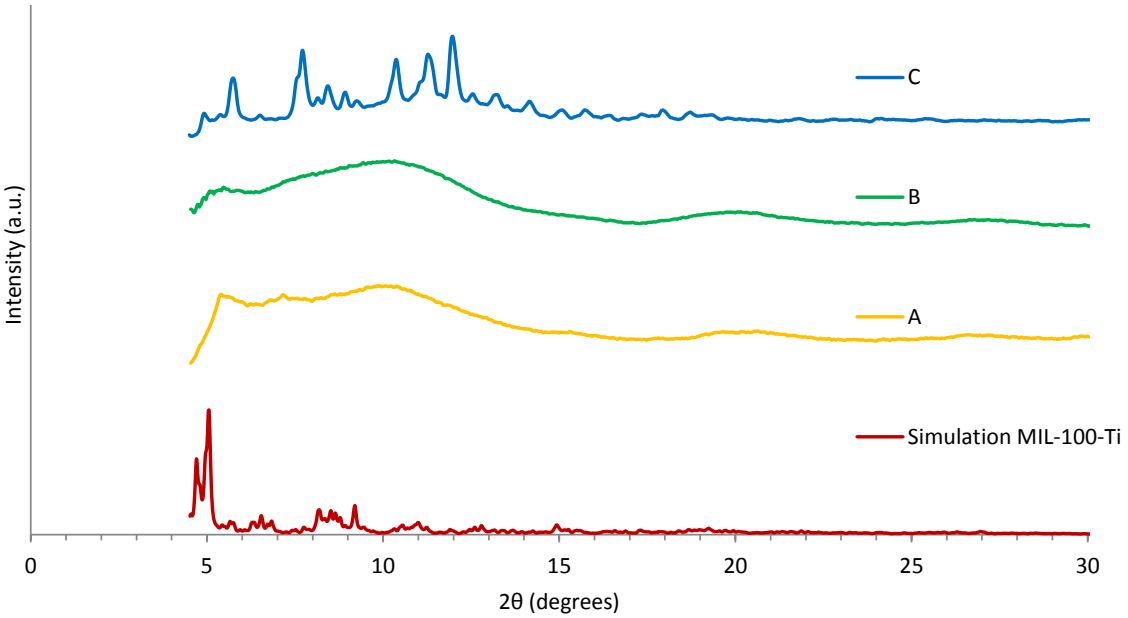

Figure 39. X-Ray powder diffraction pattern of the products obtained from the reaction of Ti_6 with H_3BTC in different reactors, compared with a simulation of MIL-100-Ti (cif file[37]) (A) Reaction in Teflon bomb; (B) reaction in stainless steel autoclave and (C) reaction in glass vial.

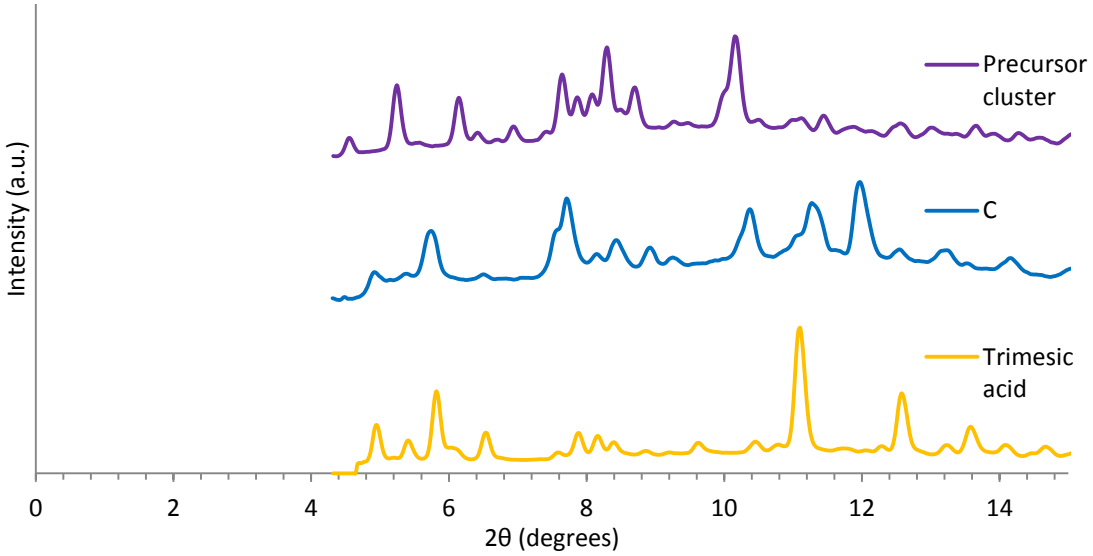

Figure 40. X-Ray powder diffraction pattern of the product obtained from the reaction in a glass vial (C) compared with the reagents (Ti_6 cluster and H_3BTC, both are experimental measurements).

The volume of the reactor in the reported procedure is not specified. Therefore, the fact that the reaction was not performed with the same filling rate may explain the failure, as this parameter is critic for solvothermal synthesis.

2.2.3. Attempts of synthesis in water

Because syntheses performed under solvothermal conditions are often difficult to scale-up, we tried to obtain MIL-100-Ti^{IV} under milder conditions. For this reason, we selected water as solvent and decided to perform the syntheses at ambient pressure, keeping the reaction temperature well below the boiling point of water. The Ti_6 cluster is a good candidate titanium source for such experiments because it presents resistance to hydrolysis, as mentioned in the article of K. Hong, W. Bak and H. Chun,[54] thus avoiding the immediate formation of TiO_2 that would occur if other Ti sources such as $TiCl_4$ or $Ti(^iOPr)_4$ would be used.[54] As source of ligand, we selected $Na_3BTC{\cdot}3H_2O$ because of its solubility in water and because previous reports, among which one from our lab, demonstrated that it is a good source of BTC^{3-} for aqueous synthesis of some MOFs.[51,69] The hope behind this idea was that BTC^{3-} would exchange with the 4-$tbbz^-$ ligand of the Ti_6 cluster, followed by a rearrangement to Ti_3-μ_3-oxo clusters, allowing the self-assembly of the MOF.

In the first attempt, the Ti_6 cluster was stirred in an aqueous solution of $Na_3BTC{\cdot}3H_2O$ for 24h at room temperature. The solid that was recovered from this mixture by centrifugation was analysed by PXRD (see Figure 41). The analysis and comparison with the PXRD pattern of the initial cluster revealed that the powder was in fact unreacted Ti_6, demonstrating that even in the presence of BTC^{3-} anions the cluster did not react in water at room temperature.

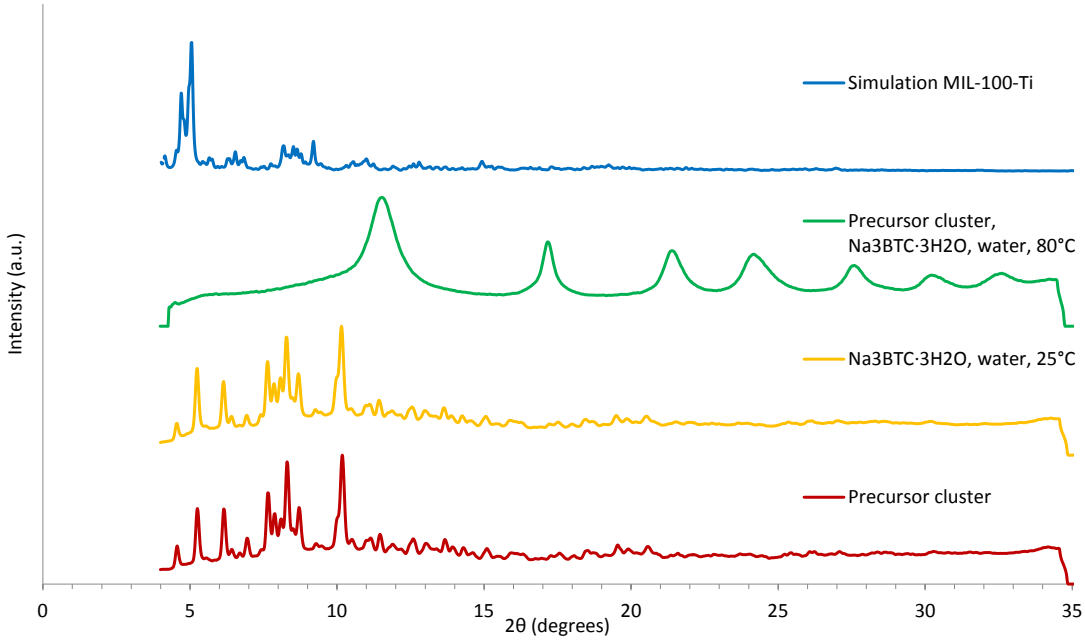

Figure 41. X-ray powder pattern of the products obtained from the Ti_6 cluster and $Na_3BTC{\cdot}3H_2O$ as reagents in water at 25°C and 80°C, compared with experimental measurement of Ti_6 and simulation of MIL-100-Ti (cif file[37]).

A second attempt was performed at 80°C for 63h, to increase the probability of the cluster to react. In this case, a solid could also be recovered by centrifugation. PXRD analysis revealed that the obtained compound was neither the desired MOF nor the starting cluster as no peaks of those compounds are present in the experimental powder pattern (see Figure 41).

The powder pattern was compared to a simulated pattern of anatase (TiO_2) (Figure 42). The position of the peaks of both simulated and experimental patterns matched well, indicating that the obtained product is unfortunately anatase. This shows that the Ti_6 cluster was hydrolysed at the higher temperature tested in the presence of BTC^{3-}. The large width of the diffraction signals is indicative of the fact that the crystallites are nanoparticles. FTIR analysis showed a broad signal from 850 cm^{-1} to the lower limit of the spectrometer (370 cm^{-1}), corresponds to the spectrum expected for TiO_2 (see Figure 43 and Figure 73 in annexe for the reference).[107] Additional peaks, compared to the spectrum of pure TiO_2, are present between 1400 to 1550 cm^{-1}. One could hypothesize that those could be due to the presence of ligands (4-tbbz and/or H_3BTC) that are capping the nanoparticles. However, those peaks are located in the fingerprint region and thus no precise information about the nature of those entities can be gained from FTIR analysis only.

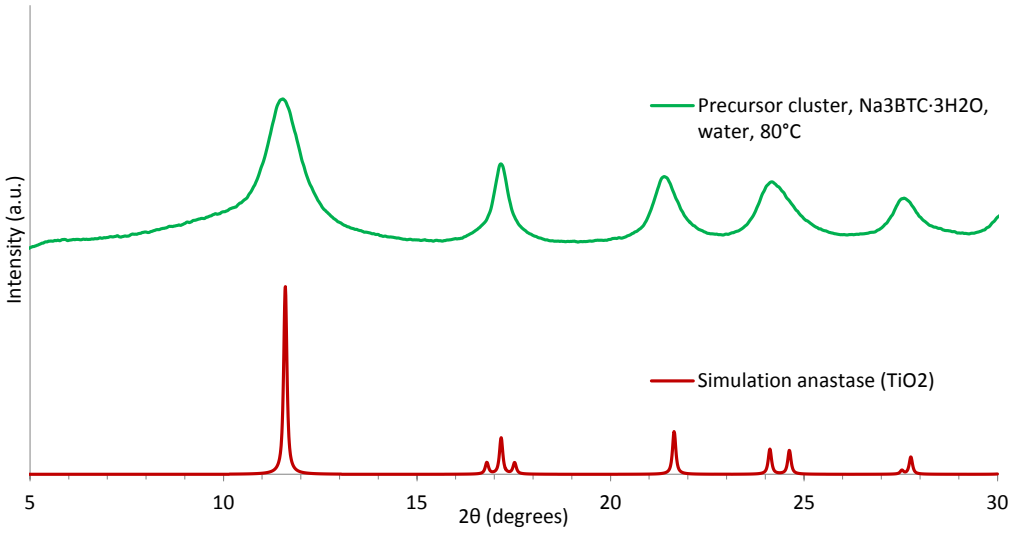

Figure 42. X-ray powder pattern of the product obtained from the Ti_6 cluster and $Na_3BTC{\cdot}3H_2O$ as reagents in water at 80°C, compared with a simulation of anastase (TiO_2) (cif file[108])

In conclusion, the reactions of the Ti_6 cluster in water to produce MIL-100-Ti were not successful. No reaction seems to occur at room temperature, and complete hydrolysis occurs when the reaction is performed at higher temperature.

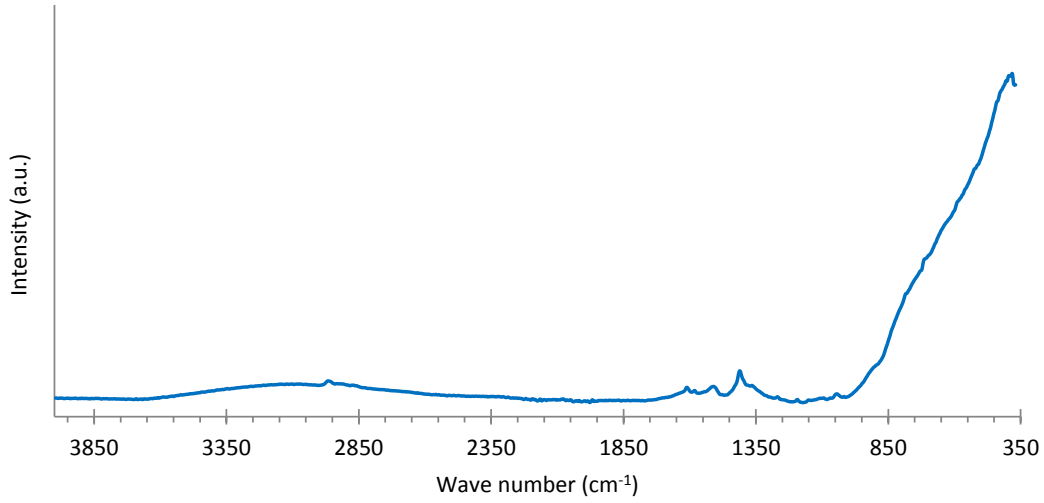

Figure 43. FTIR spectrum of the product obtained from the Ti_6 cluster and $Na_3BTC{\cdot}3H_2O$ as reagents in water at 80°C

2.2.4. Synthesis through post-synthetic metal exchange

In our lab, we previously developed an easy, green and scalable synthesis of MIL-100-Fe.[51] We hypothesized that this MOF could serve as template to obtain MIL-100-Ti through post-synthetic exchange of the metal, by reaction with a commercial Ti precursor.

To perform this exchange, we first activated MIL-100-Fe to remove any coordinated solvent molecules from the synthesis. Then THF was added, followed by $TiCl_4$ and the obtained solution was refluxed for 63h under argon atmosphere. The addition of titanium(IV) chloride immediately formed a yellow precipitate, probably due to the formation of $TiCl_4(THF)_2$.[109] However, the presence of this titanium complex was not considered as an issue because it was previously used for post-synthetic metal exchange of zirconium by Ti in UiO-66.[65,66] After cooling down the mixture, a solid was collected by centrifugation and analyzed by PXRD. Figure 44 shows that a product with poor crystallinity was obtained. The large bump of the pattern's background between roughly 5 and 15 degrees indicates the presence of an amorphous phase. Some neat peaks are also present on the pattern, indicating the presence of a second, more crystalline, phase. However, the powder pattern of this phase did not match the simulations of MIL-100 and we were unable to determine its nature.

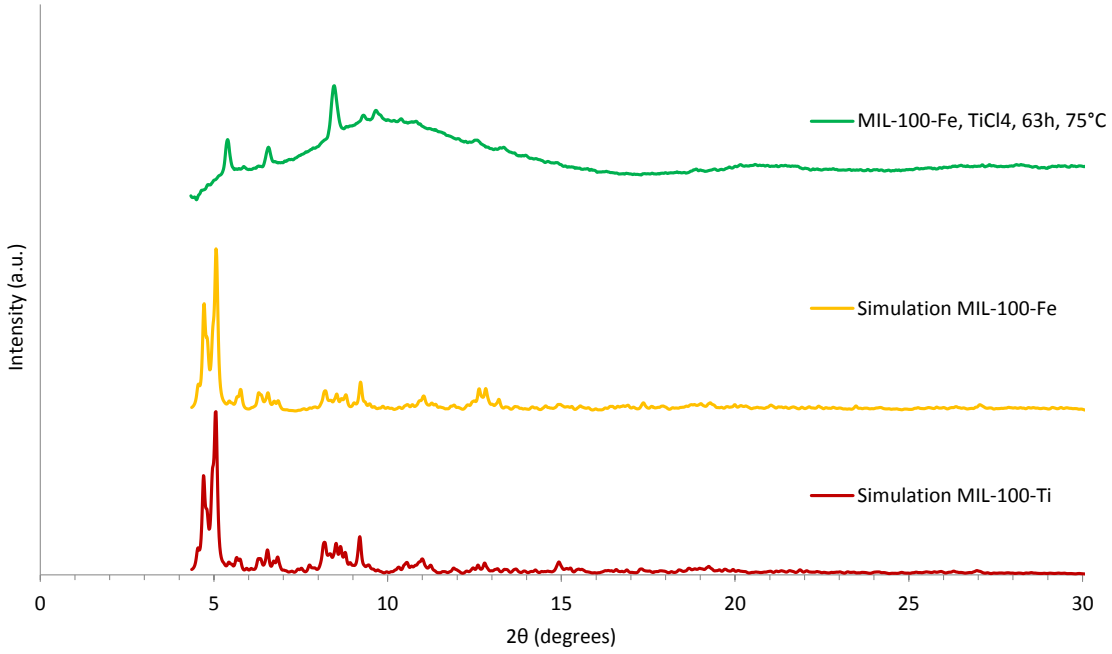

Figure 44. X-ray powder pattern of the product obtained from MIL-100-Fe and $TiCl_4$ as reagents in THF, compared with simulations of MIL-100-Ti (cif file[37]) and MIL-100-Fe (cif file[110]).

2.2.5. Synthesis using $Ti(O^iPr)_4$ as metal source

We performed some trials to obtain MIL-100-Ti^{IV} by using $Ti(O^iPr)_4$ as metal source, because it is commercial and easier to handle than $TiCl_4$. We explored several approaches under mild conditions that would be easy to reproduce at larger scale, if the experimental conditions used allow to obtain the desired MOF.

We first tried to react the selected Ti source with H_3BTC at low temperature to slow down the rate of the process in order to facilitate the formation of a crystalline product. Ethanol was chosen as solvent because it easily dissolves both reagents. The reaction was performed by adding an ethanol solution of $Ti(O^iPr)_4$ to an ethanol/H_3BTC solution at -78°C under air, in a dropwise fashion. Then, the solution was allowed to reach room temperature and a white gel was obtained. A solid was recovered by centrifugation and drying under vacuum. However, PXRD analysis of the product indicated that an amorphous product was formed (see Figure 45).

Because of the too high reactivity of trimesic acid with $Ti(O^iPr)_4$, we decided to use an ester of H_3BTC instead. Indeed, complexation with Ti is then only possible after decomposition of the ester functions to slowly form carboxylates on the linker precursor. A first test was done by adding $Ti(O^iPr)_4$ to a mixture of trimethyl 1,3,5-benzenetricarboxylate in formic acid under air, and subsequently heating at 70°C for 16h. Formic acid was chosen as solvent to facilitate the slow decomposition of the ligand into carboxylates (according to eq. **16**). A solid was obtained after centrifugation and PXRD analysis revealed that again the obtained compound was amorphous and that the target product was not obtained (see Figure 45).

$$BTC(Me)_3 + HCOOH \rightarrow HBTC(Et)_2 + HCOOEt \qquad \textbf{16}$$

The last experiment was performed by adding $Ti(O^iPr)_4$ to a solution of the less reactive triisopropyl 1,3,5-benzenetricarboxylate in ethanol under air, followed by stirring and heating for 12h at 80°C, and a solid was recovered after centrifugation. PXRD analysis showed that the product is crystalline (Figure 45). However, the position of the diffraction peaks did not correspond to MIL-100. The pattern was compared to those of the triisopropyl ester and the one of H_3BTC (see Figure 46). However, the powder patterns did not match as a there is no diffraction peak at ~10° neither at 5°, 6.5° or 11.5° on the pattern of the product, excluding the presence of the triisopropyl ester, for the peak around 10°, and of H_3BTC, for the three last peaks. However, this analysis cannot exclude that a polymorphic structure or solvate of those compounds is present in the product.

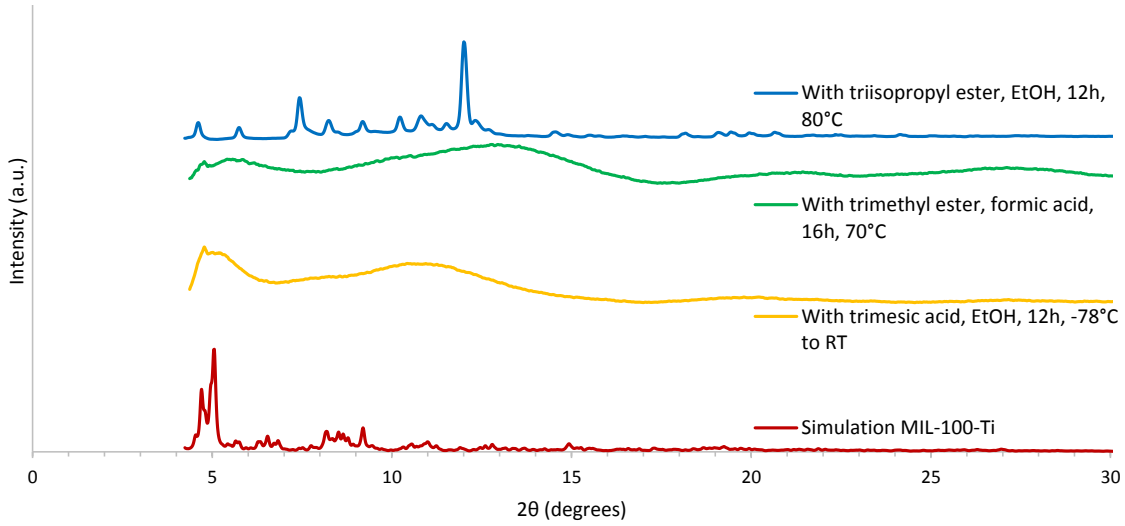

Figure 45. X-ray powder pattern of the products obtained by using $Ti(O^iPr)_4$ as reagent, compared with a simulation of MIL-100-Ti (cif file[37]).

A FTIR analysis was performed on the compound to complement PXRD, and signals are present in the aromatic region around 1360 and 1473 cm^{-1} and in the C=O region at 1718 cm^{-1} (see Figure 47). The presence of ketones, aldehydes and carboxylic acids can be excluded (absence of clear signals around 2500-3200 cm^{-1}). Overall, the spectrum showed many similarities with a reference spectrum of the triisopropyl ester, with only differences in the fingerprint region. Those observations made us think that the product was not a MOF, but probably a simple derivative of the ligand. TGA analysis confirmed that no MOF was obtained, as there was no residual mass after heating under air (annexes Figure 74). This confirmed that the product did not contain Ti, as TiO_2 would have formed upon calcination if this had been the case, leading to a non-null residual mass in TGA.

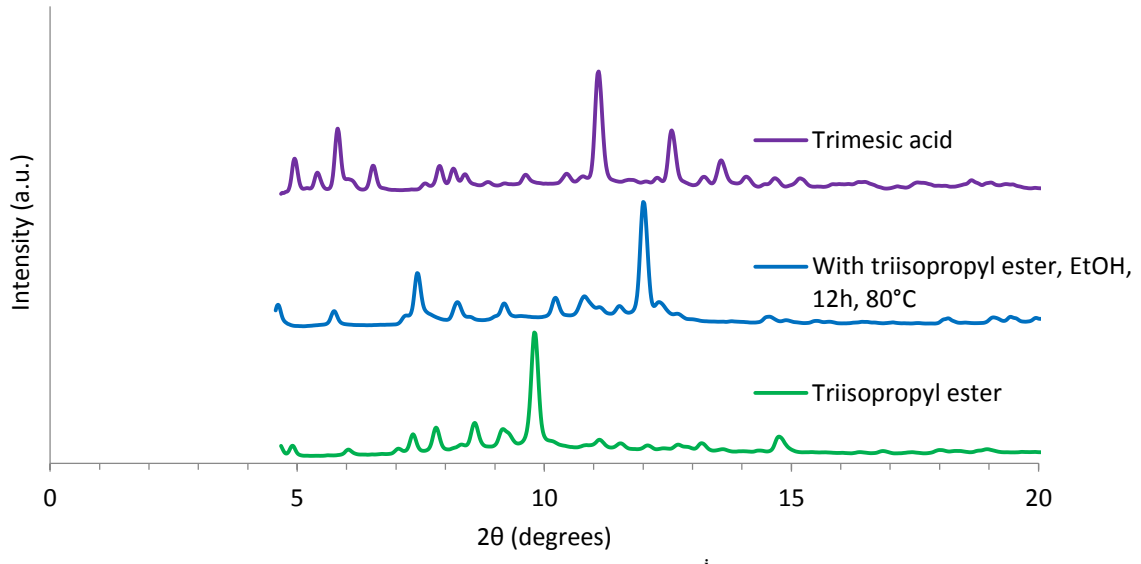

Figure 46. X-ray powder pattern of the product obtained by using $Ti(O^iPr)_4$ and the triisopropyl ester of H_3BTC as reagents, compared with the reference patterns of the reagents (experimental measurements).

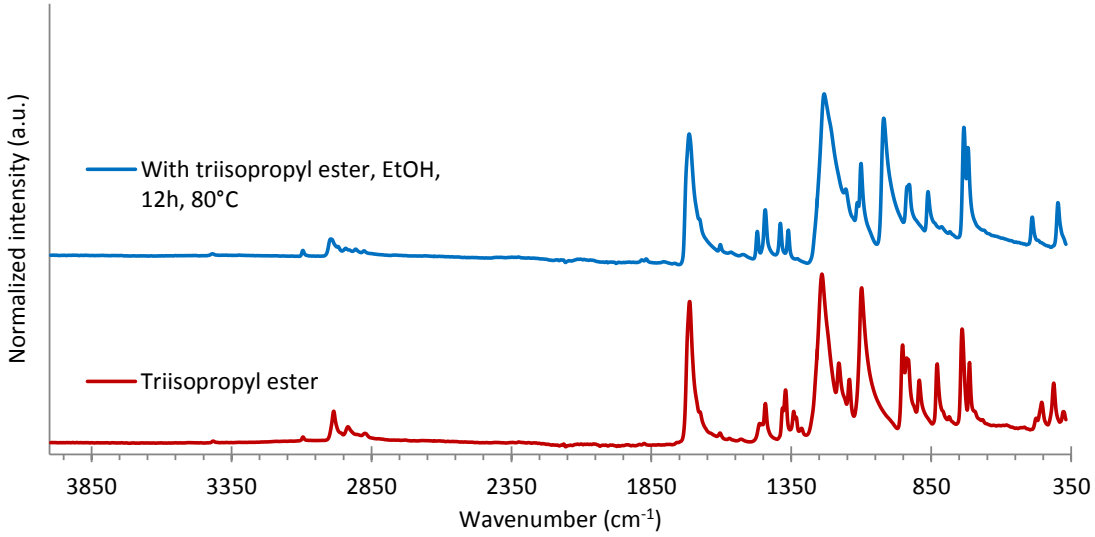

Figure 47. FTIR spectra of the product obtained from the reaction of $Ti(O^iPr)_4$ with the triisopropyl ester of H_3BTC, compared with a reference spectrum of the triisopropyl ester (experimental measurements).

2.2.6. Synthesis by mechanochemistry

The unsuccessful attempts to obtaine MIL-100-Ti^{IV} in solution led us to try mechanochemistry as the last approach. The Ti_6 cluster and H_3BTC were selected as precursors and were grinded by using a planetary ball-mill at 300 rpm for 6 cycles of 5 min, interrupted by 2 min breaks to avoid overheating and degradation. Two similar experiments were performed in parallel: one by dry grinding and the other with addition of 1 ml of ethanol before the milling (liquid-assisted grinding conditions). In both cases, the crude product and the one after washing with ethanol were analysed by PXRD.

Figure 48 shows the results for the dry ball milling, compared with the PXRD of H_3BTC, the cluster and a simulation of MIL-100-Ti. The as-synthesized product contains H_3BTC as the peak positions of both patterns match perfectly. The washed product does not contain H_3BTC anymore, as evidenced by the clear absence of peaks at 5.84° and 11.07°, among others. However, the diffraction peaks do not match with the ones of the simulated pattern of MIL-100-Ti. The analysis reveals that the product contains the initial, unreacted, Ti_6 cluster with a loss of crystallinity. Indeed, the positions of all the peaks of both patterns match very well.

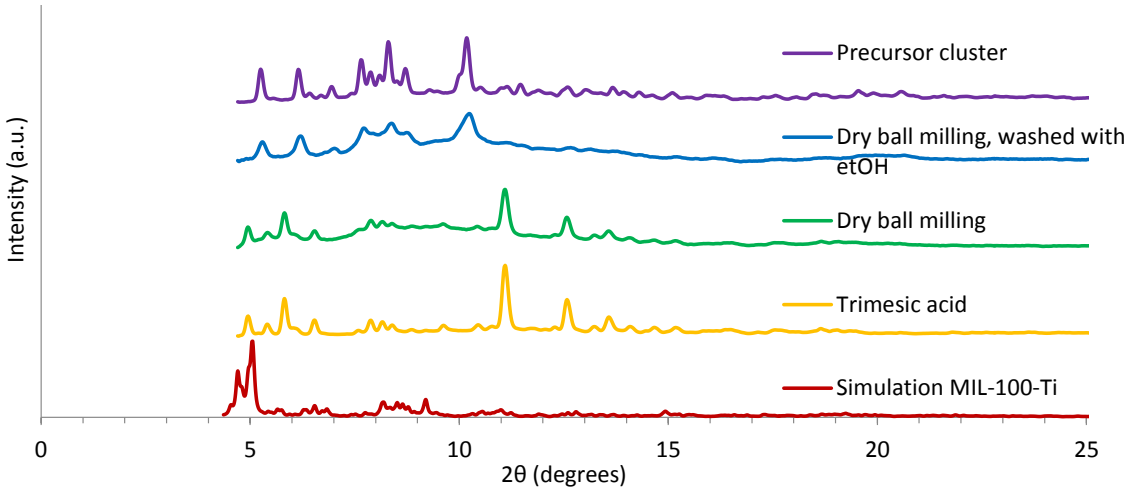

Figure 48. X-ray powder pattern of the crude and washed products obtained after dry ball milling, compared with H_3BTC and the cluster (both are experimental measurements) and a simulation of MIL-100-Ti (cif file[37]).

Concerning the liquid-assisted grinding, Figure 49 reveals that in the as-synthesized and washed products no H_3BTC is present under the same crystalline form as the one used for the synthesis as the peaks at 5.79° and 12.57° are absent in both cases. The PXRD pattern of the crude sample reveals that it contains the initial cluster, as all the peaks of this compound are present. After washing of the sample, the pure cluster is recovered, in highly crystalline form. Addition of ethanol did not yield MIL-100-Ti.

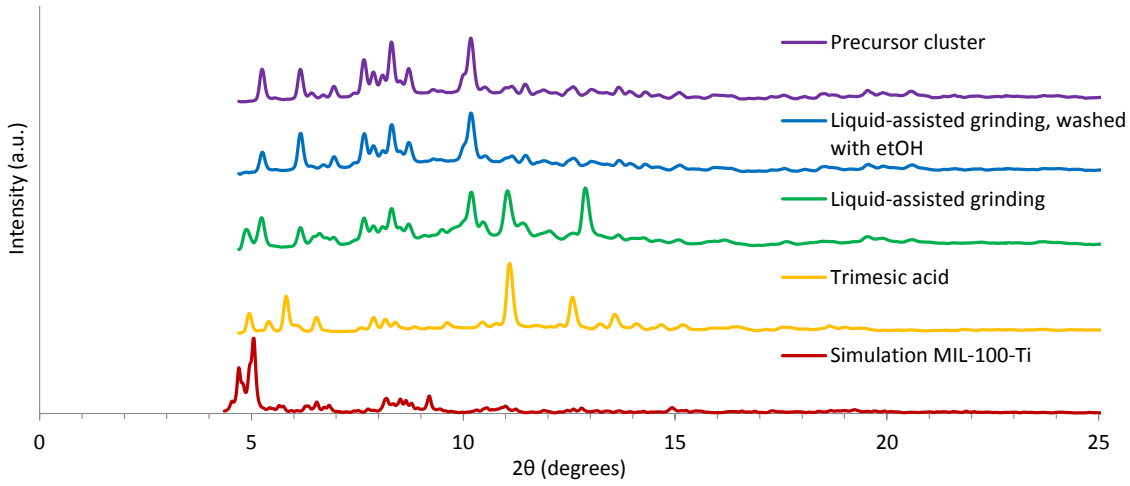

Figure 49. X-ray powder pattern of the crude and washed products obtained after the liquid-assisted grinding experiment, compared with H_3BTC (experimental measurement) and a simulation of MIL-100-Ti (cif file[37]).

Note that "Dry-ball milling" in Figure 48 gave an unexpected peak at 12.85°, indicating that a new crystalline phase was formed. The presence of ethanol may dissolve H_3BTC and the subsequent evaporation of ethanol may have led to the crystallization of trimesic acid as a solvate. Alternatively, a reaction between ethanol and the ligand may have

promoted a reaction such as an esterification. Whatever this crystalline phase might be, it is soluble in ethanol as shown by its disappearance after washing with this solvent.

Also, note that after washing the solids in both experiments, a difference in crystallinity is noticed for the recovered Ti_6 cluster. The product obtained under liquid-assisted conditions is much more crystalline that the one obtained by dry milling. Milling in the presence of ethanol may lubricate and consequently attenuate the loss of crystallinity. This is in line with reports that grinding introduces changes in crystalline compounds, such as defects, changes in particle size or even amorphization.[111]

2.3. MIL-100-(Al)$Ti^{III/IV}$ from $(TiCl_3)_3 \cdot AlCl_3$

2.3.1. Oil bath

Due to the failure to synthesize MIL-100-Ti by using Ti^{IV} precursors, we decided to try the synthesis of MIL-100 from a Ti^{III} source and explore the possibly to oxidise the final product under air to obtain MIL-100-Ti^{IV}, as was previously done for obtaining MIL-101-Ti^{IV} from MIL-101-Ti^{III}.[53] Since we had only limited quantities of an old stock of $TiCl_3$, and that we were unable to buy more as our suppliers discontinued the sale of solid $TiCl_3$, we decided to use $(TiCl_3)_3 \cdot AlCl_3$. Indeed, this compound can be obtained commercially and it is quite cheap. However, the synthesis should yield bimetallic MIL-100-(Al)Ti^{III} instead of monometallic MIL-100-Ti^{III}.

The synthesis was performed by starting from $(TiCl_3)_3 \cdot AlCl_3$ and H_3BTC in a DMF:ethanol mixture (10:1) under argon atmosphere at 120°C for a duration of 18h. The reaction conditions are inspired from[53,55].

As shown on the PXRD pattern in Figure 50, the product obtained at 120°C is not crystalline. However, a bump is present at the position expected for the main peaks of MIL-100, as evidenced by the comparison with the simulated pattern. From this, we concluded that either the obtained product is amorphous or, in the best case, it is composed MIL-100-(Al)Ti^{III} with very poor crystallinity, or nanoparticles thereof.

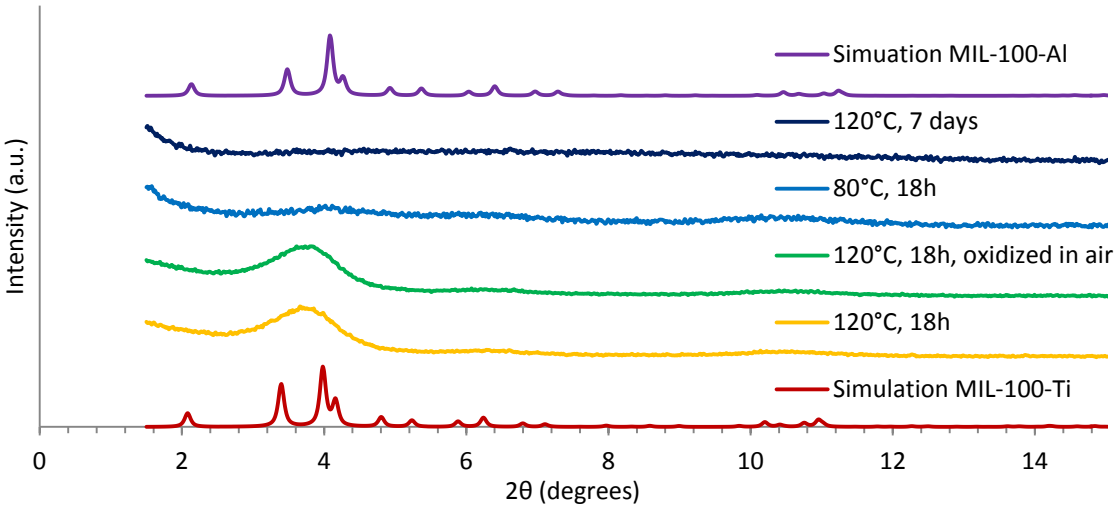

Figure 50. X-ray powder patterns of the products obtained from the reaction of $(TiCl_3)_3{\cdot}AlCl_3$ and H_3BTC as reagents at 120°C for 18h (before and after oxidation under air), at 80°C for 18h (as-synthesized product) and at 120°C for 7 days (as-synthesized product), compared with simulations of MIL-100-Al (cif file[27]) and MIL-100-Ti (cif file[37]).

The product was oxidized in air at room temperature to try to convert it to MIL-100-(Al)Ti^{IV}. During this oxidation, the colour of the solid changed from violet to yellow, evidencing the oxidation of Ti^{III} to Ti^{IV}. The PXRD pattern of the oxidized compound revealed the presence of the same bumpy feature at the position expected for the main peaks of MIL-100 (Figure 50), showing that the framework structure probably did not change during the oxidation process.

These results gave some hope concerning the possibility to obtain MIL-100-(Al)Ti but highlighted the need to optimize the synthesis to do so. The reaction temperature was set at lower temperature (80°C) in order to slow down the process, in the hope to yield a crystalline product. However, the completely flat powder pattern of the obtained product (Figure 50) shows that this experiment lead to an even worse result.

We thus concluded that a reaction temperature of 120°C is better than 80°C. Then, the influence of the reaction time was investigated. A new experiment was performed at 120°C for 7 days. However, a colour change from violet to yellow was observed after 4 days of reaction. This is probably due to and oxidation of Ti^{III} to Ti^{IV} in the product. This oxidation probably resulted from a failure to maintain air-tight conditions throughout the experiment. PXRD analysis (Figure 50) showed that in this case again an amorphous product was obtained. Therefore, the reaction time was maintained at 18h for further experiments.

2.3.2. Synthesis in the oven (120°C)

As the previous experiments showed that the reaction seems to work better at 120°C, the next experiments were performed at this temperature. The same procedure was applied, except that the mixture was placed in a closed glass bottle in the oven for 18h. The mixture was separated in two batches in order to test two different washing methods, the first one with DMF followed by THF and ether, and the second with water and ethanol. The crystallinity of the products obtained after both washings was evaluated by PXRD (see Figure 51).

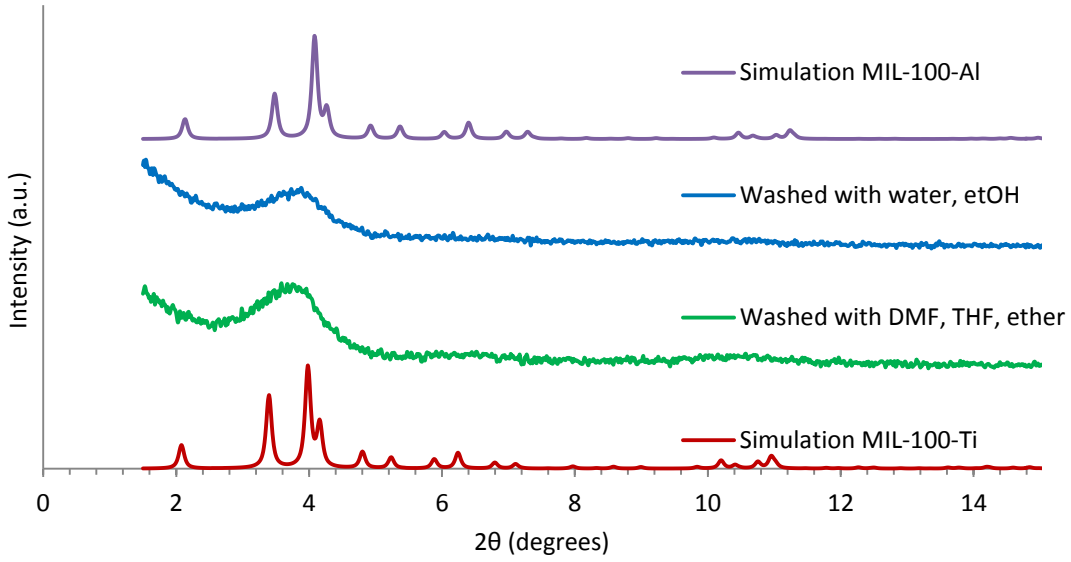

Figure 51. X-ray powder patterns of the products obtained by using $(TiCl_3)_3{\cdot}AlCl_3$ and H_3BTC as reagents at 120°C for 18h in a closed glass bottel in the oven, with two different washing methods, compared with a simulation of MIL-100-Al (cif file[27]) and a simulation of MIL-100-Ti (cif file[37]).

Similar patterns to the previous experiments were obtained: the products were not crystalline but bumpy features appeared at the positions were peaks are expected for MIL-100. We however noticed that the pattern of the compound washed with the first washing method (DMF, THF and ether) yielded a slightly more intense signal than the one of the product washed with water and ethanol.

2.3.3. Variating HCl concentrations

In a last attempt to obtain a crystalline product, the possibility to use HCl as modulator for the synthesis was investigated. This was done by performing the same reaction as previously but by adding different quantities (0.25, 0.5, 1 and 2 mL) of 37% HCl to the reaction mixture before heating in the oven. The products were collected by membrane filtration under argon, and the solids were analysed by PXRD (see Figure 52). All the samples

show the same bumpy features on their powder patterns as the previous experiments, and adding HCl to the medium did thus not allow to yield crystalline MIL-100.

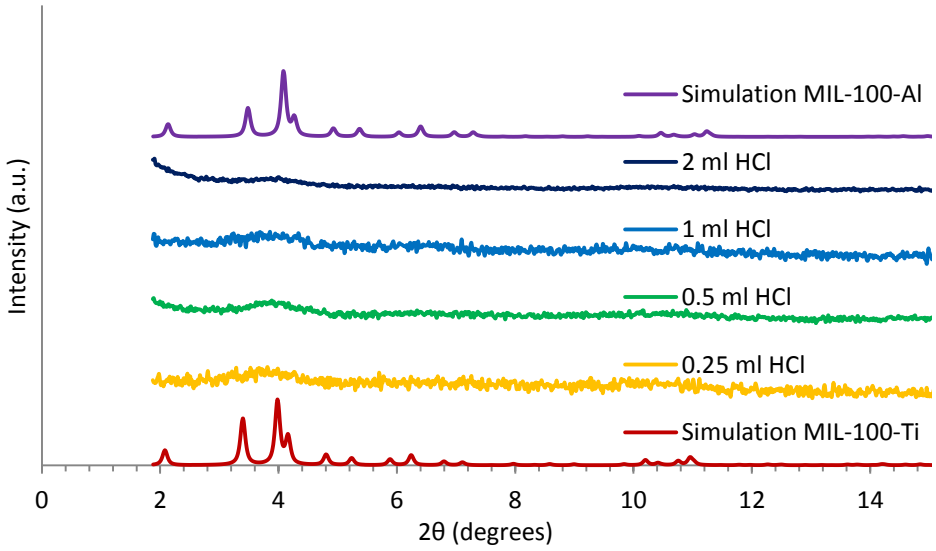

Figure 52. X-ray powder patterns of the products obtained by using $(TiCl_3)_3{\cdot}AlCl_3$ and H_3BTC as reagents at 120°C for 21h with four different amounts of HCl added, compared with simulations of MIL-100-Al (cif file[27]) and MIL-100-Ti (cif file[37]).

3. MIL-101

3.1. MIL-101-Ti

3.1.1. Synthesis from $TiCl_3$

Following the failures to synthesize MIL-100-Ti, we turned our attention to MIL-101-Ti. The synthesis of this MOF was carried out according to a published procedure.[53] In a first trial, the synthesis was tested with a small amount of titanium (III) chloride remaining from an old stock that we had in the lab from earlier projects. $TiCl_3$ and H_2BDC were heated at 120°C for 18h in DMF:ethanol 10:1 and filtered under argon atmosphere (Figure 53).

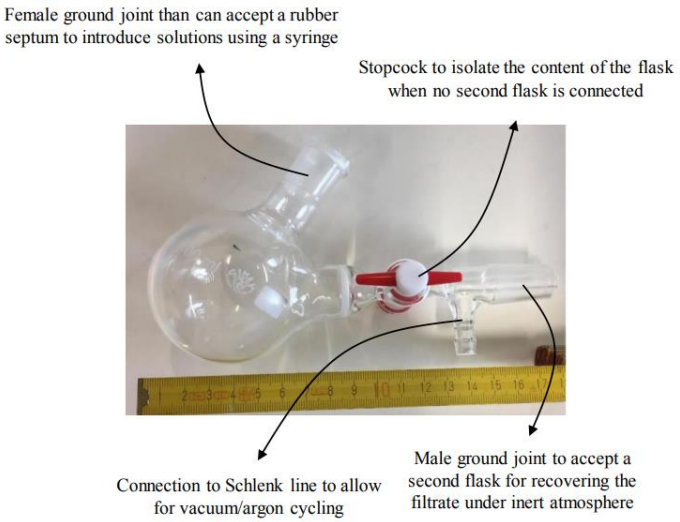

Figure 53. Photograph of a Schlenk flask (250 ml) equipped with a fritted disk to filtrate under argon atmosphere.

The obtained violet solid was analysed by PXRD and the results were compared with a simulation of MIL-101-Cr (see Figure 54). The isostructurality of both MOFs allows a suitable comparison basis to identify the structure. However, small differences in the radius of both metals can induce tiny differences in the crystallographic parameters, resulting in a slight peak shifting.

The experimental pattern shows neat diffraction peaks, indicating the formation of a crystalline product. Furthermore, the matching of peak positions between the sample and the simulation confirms the successful formation of MIL-101-Ti^{III}.

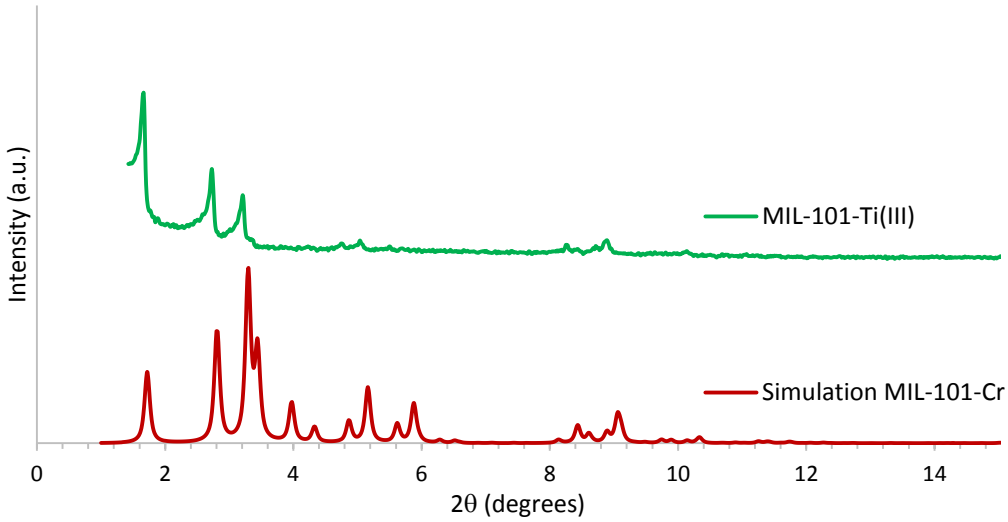

Figure 54. X-ray powder pattern of the product obtained by using $TiCl_3$ and H_2BTC as reagents at 120°C for 18h, compared with a simulation of MIL-101-Cr (cif file[41]).

The FTIR spectrum of the compound (Figure 55) correlates well with the reported spectrum (Figure 75 in the annexes). The BET and Langmuir surface areas calculated from

the nitrogen sorption isotherm (Figure 56) are 1416 and 1953 m²/g respectively. The reported values, however, are 2970 and 4440 m²/g respectively. The lower specific surface area of our MOF can be explained by the quality of the $TiCl_3$ used for the synthesis. Furthermore, additional washing of the MOF to get rid of unwanted guest molecules could increase it.

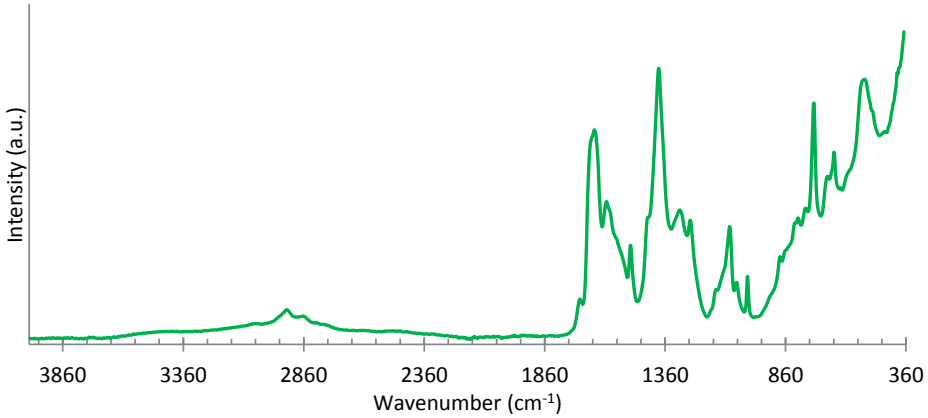

Figure 55. FTIR spectrum of as synthesized MIL-101-Ti.

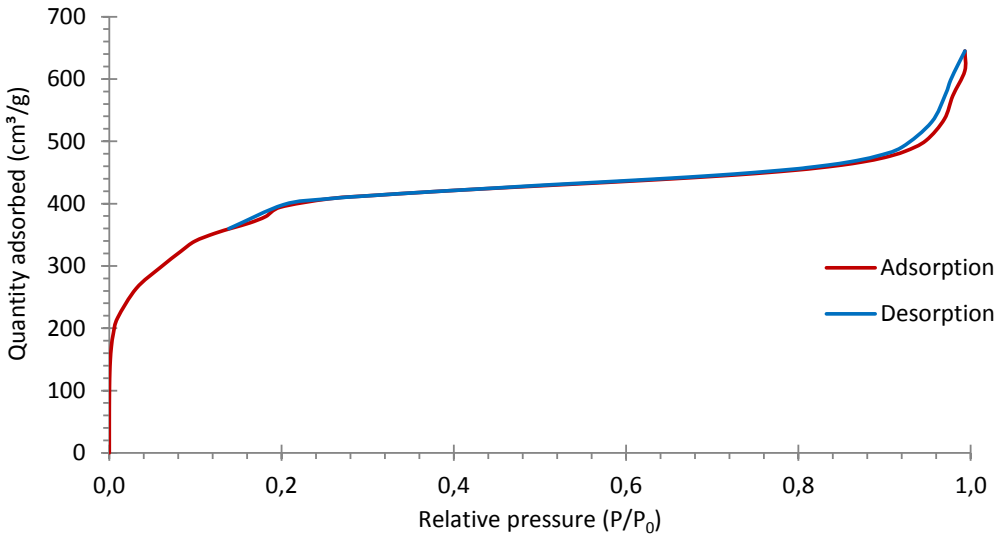

Figure 56. Nitrogen sorption isotherm of MIL-101-Ti^{III}.

3.1.2. Attempts to oxidize MIL-101-Ti^{III} into MIL-101-Ti^{IV}

In order to form MIL-101-Ti^{IV}, the synthesized MIL-101-Ti^{III} was oxidized in air at room temperature. FTIR analysis (Figure 57) shows that after oxidation of MIL-101-Ti, the

absorption band at 1098 cm^{-1} fades out. This correlates well with reported FTIR data (see Figure 76 in the annexes).

However, the PXRD analysis of the oxidized compound revealed that the structure decomposed, as the pattern shows a bumpy background with some peaks of an unknown crystalline phase but no peaks were left at the positions expected for MIL-101 (see Figure 58). The publication of Jarad A. Mason *et al.* reports that the framework can partially decompose due to the exothermic reaction with oxygen, and explains that performing the oxidation at lower temperature (-78°C) limits this phenomenon.[53] An attempt was done to oxidize the framework in air at -196°C by immersing the bottom of an open test tube containing the as synthesized MOF in a small Dewar container filled with some liquid nitrogen. However, in this case the reaction also led to decomposition of the product (results not shown). The product oxidized in air at 25°C was also characterized by TGA under air (Figure 59 + Figure 77 in the annexes). The decomposition starts at 414°C and the experimental mass loss at decomposition is 68.5%, which correlates with the theoretical value of 70% (assuming a residue of TiO_2).

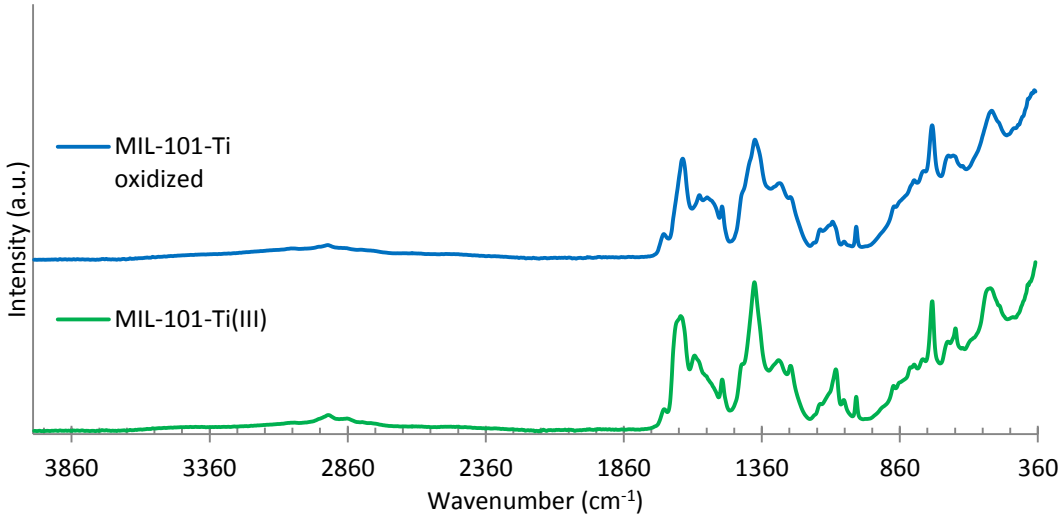

Figure 57. FTIR spectra of as synthesized MIL-101-Ti and after oxidation.

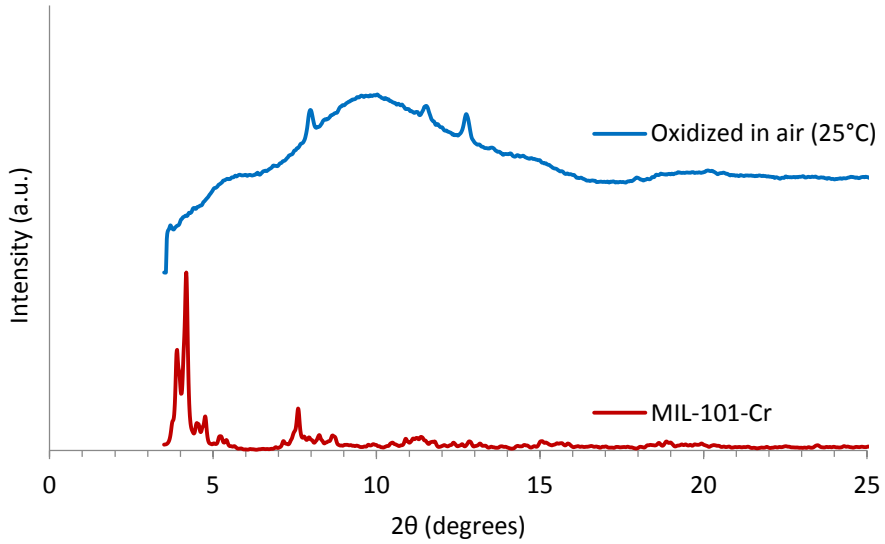

Figure 58. X-ray powder pattern of MIL-101-Ti after oxidation under air at 25°C, compared with a simulation of MIL-101-Cr (cif file[41]).

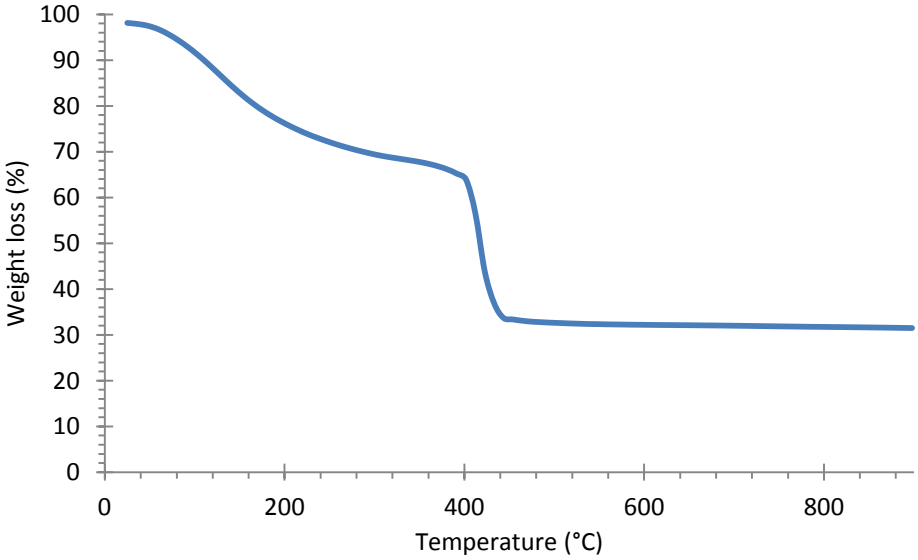

Figure 59. TGA under air of oxidized MIL-101-Ti.

3.2. MIL-101-Al

We wanted to figure out whether MIL-101-Al could form under the conditions used for synthesizing MIL-101-Ti^{III}. For this, the reaction conditions of the synthesis of MIL-101-Ti^{III} were adapted by replacing $TiCl_3$ by $AlCl_3$. The obtained solid was analysed by PXRD and turned out to be amorphous (see Figure 60). FTIR reveals the presence of

carboxylic acid (1417 cm^{-1}, 1638 cm^{-1}, broad signal at 2751 cm^{-1} and 2969 cm^{-1}), the ligands are thus not fully coordinated (see Figure 61).

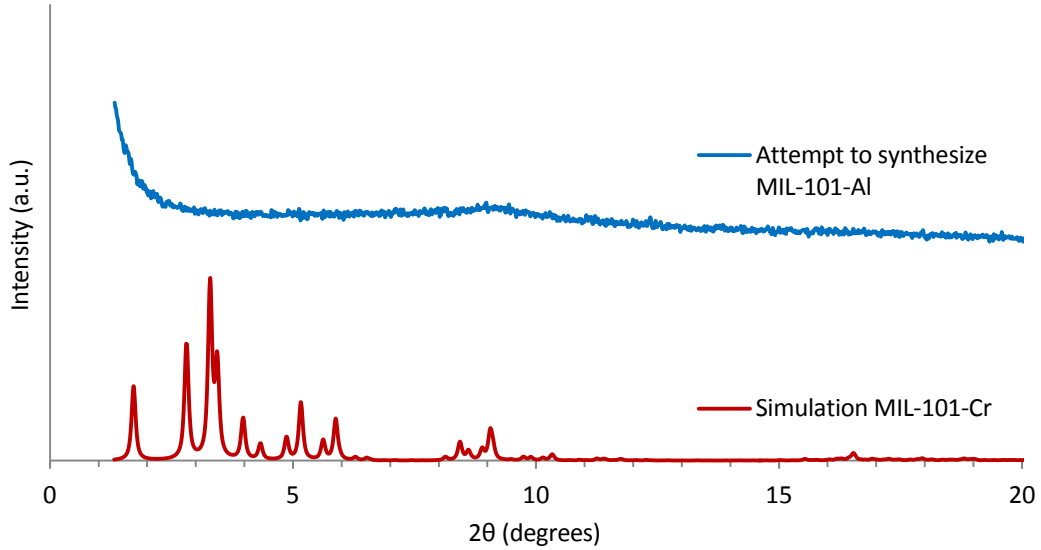

Figure 60. X-ray powder pattern of the product obtained by reacting $AlCl_3$ and H_2BDC at 120°C for 18h, compared with a simulation of MIL-101-Cr (cif file[41]).

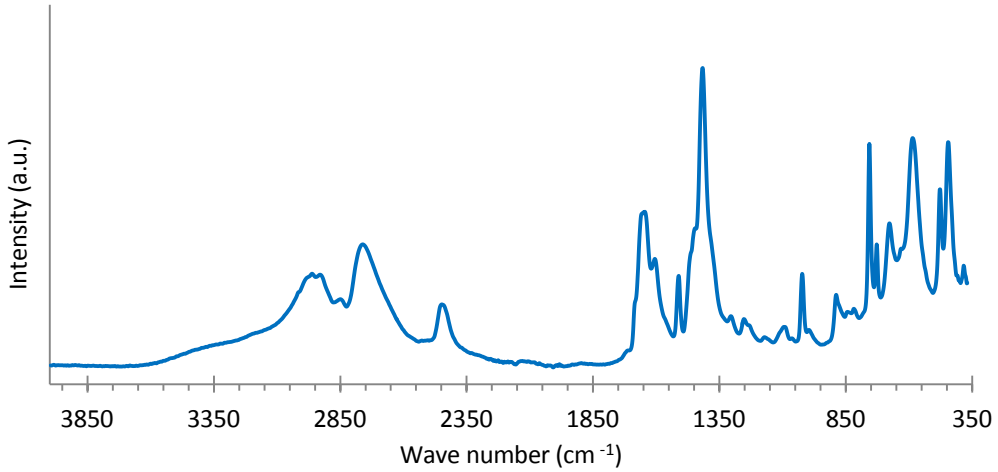

Figure 61. FTIR spectrum of the product obtained by reaction of $AlCl_3$ and H_2BDC at 120°C for 18h.

3.3. MIL-101-(Al)Ti^{IV} from $(TiCl_3)_3 \cdot AlCl_3$

The synthesis of MIL-101-Ti with high purity $TiCl_3$ was successful, but due to the limited amount of the available precursor it was unscalable for our needs. The idea to synthesize MIL-101 from a less expensive metal precursor is attractive. Therefore, $(TiCl_3)_3 \cdot AlCl_3$ was used for further synthesis as it is easy to obtain, on the contrary to $TiCl_3$.

Also the starting precursor containing both aluminium and titanium would yield a bimetallic MOF that keeps the advantages of the Ti^{IV}-MOF after oxidation, combined with the extreme light weight of Al.

Obtaining the bimetallic MOF was tried by applying the same synthetic procedure as for MIL-101-Ti^{III} but by replacing $TiCl_3$ with $(TiCl_3)_3 \cdot AlCl_3$. The product was separated by centrifugation and washed with DMF and THF. The obtained yellow solid was analysed by PXRD (see Figure 62). The pattern shows a very slight bump at 3.28°, which is the position expected for the main peaks of MIL-101, but due to the very poor signal, we concluded that the compound is largely amorphous and that the target product was not obtained.

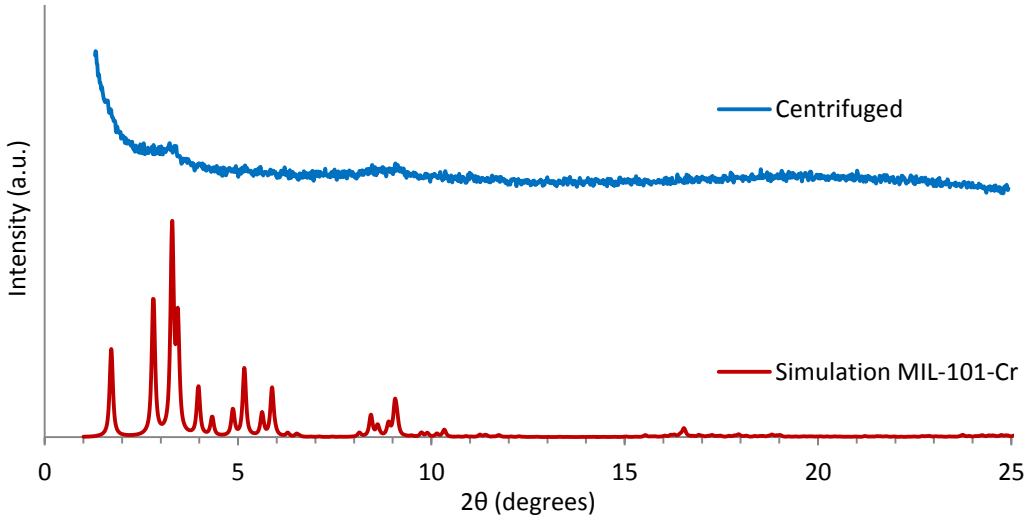

Figure 62. X-ray powder pattern of the product obtained by using $(TiCl_3)_3 \cdot AlCl_3$ and H_2BTC as reagents at 120°C for 21h, compared with a simulation of MIL-101-Cr (cif file[41]).

3.4. MIL-101-(Al)Ti^{III} from $(TiCl_3)_3 \cdot AlCl_3$

The amorphous phase obtained in the previous experiment could be due to the oxidation during the centrifugation process, which is carried out in air. To prevent the oxidation, a filtration system under argon atmosphere using a nylon membrane was constructed (see Figure 63, A). A specific filtration apparatus allows the fixation of the membrane to a filtration flask. A piece of tubing is connected to the argon supply of a Schlenk line on one side and to a normal funnel on the other side. The funnel is then placed upside-down above the filtration apparatus to keep the product under a constant argon flow.

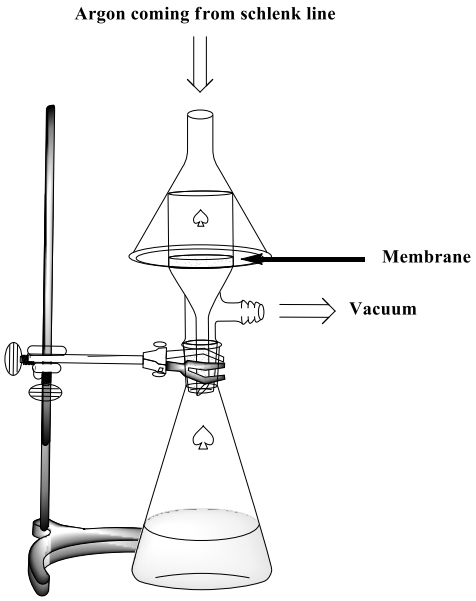

Figure 63. A: Schematic representation of the filtration system under argon.

The synthesis was performed again, with the same parameters as previously. The filtration protected by argon allowed to recover a violet solid this time, showing that Ti remained in its +III oxidation state after the synthesis. A small amount of the product was exposed to the air at room temperature to oxidize Ti^{III} to Ti^{IV} and the colour changed from violet to yellow. Figure 64 shows the PXRD patterns of the as synthesized product and after oxidation. The pattern of the obtained product however only presents a slight bump at 3.15°, the synthesis was not more successful by using filtration instead of centrifugation. However, we noticed that after oxidation the pattern became completely flat, which discouraged us to continue further trials with MIL-101-Ti as this MOF seems very fragile when exposed to air, which would hinder any further experiments.

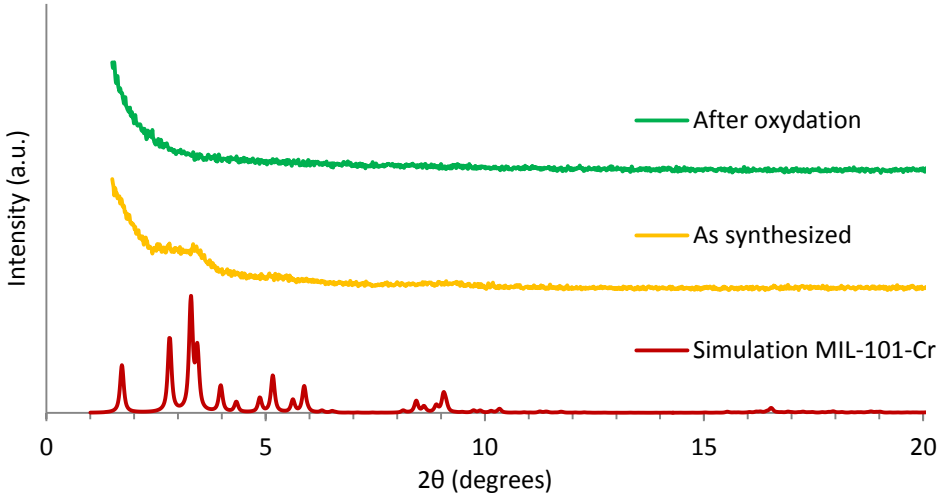

Figure 64. X-ray powder patterns of the products obtained with $(TiCl_3)_3{\cdot}AlCl_3$ and H_2BTC as reagents at 120°C for

17h before and after oxidation under air (but recuperated by filtration under argon protection), compared with a simulation of MIL-101-Cr (cif file[41]).

4. UiO-66-Zr

After the consecutive failures of the synthesis attempts of Al and/or Ti MIL-MOFs, our interest was turned to UiO-66-Zr. The complexity of the clusters and the smaller pores are the reasons why this MOF was not our first choice to explore. However, its synthesis is well-documented and procedures under mild conditions are described. The synthesis was performed by heating $ZrCl_4$ and H_2BDC in DMF with HCl at 80°C overnight.[112]

By this procedure, several grams of a white powder were recovered and the solid was analysed by PXRD (see Figure 65). The positions of the diffraction peaks on the obtained pattern match very well with the simulation. Furthermore, the product is highly crystalline, and even the smallest signals (e.g. at 13.92° and 20.80°) are easily observable. Small differences in relative intensities are noticeable, probably due to residual solvents. The FTIR spectrum correlates well with the literature (see Figure 66 and Figure 78 in annexes). To our great sadness, other characterisations could not be carried out and no functionalisation test could be performed due to the closure of the laboratory for Covid-19 pandemic.

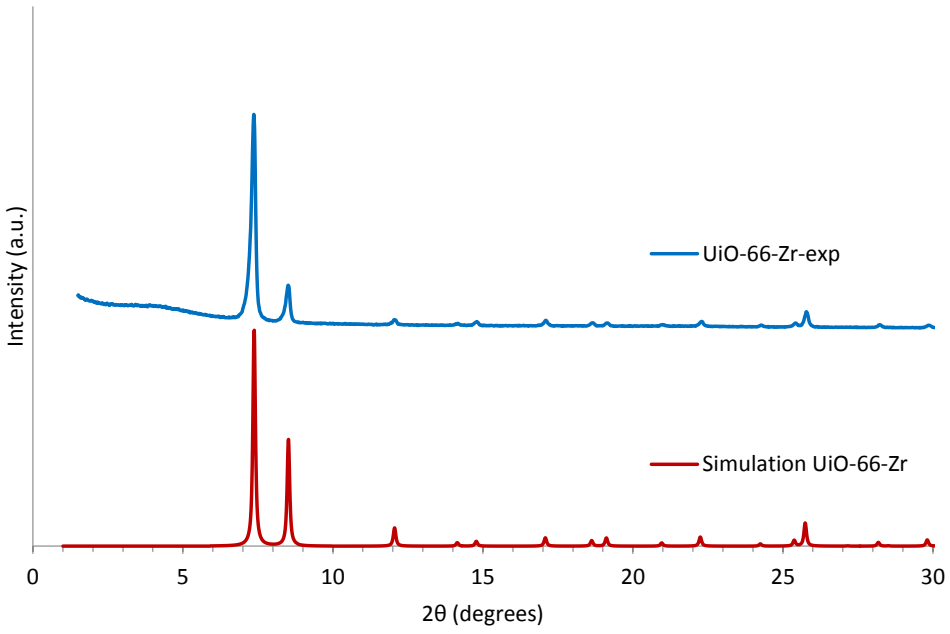

Figure 65. X-ray powder pattern of UiO-66-Zr, compared with a simulation of UiO-66-Zr (cif file[59]).

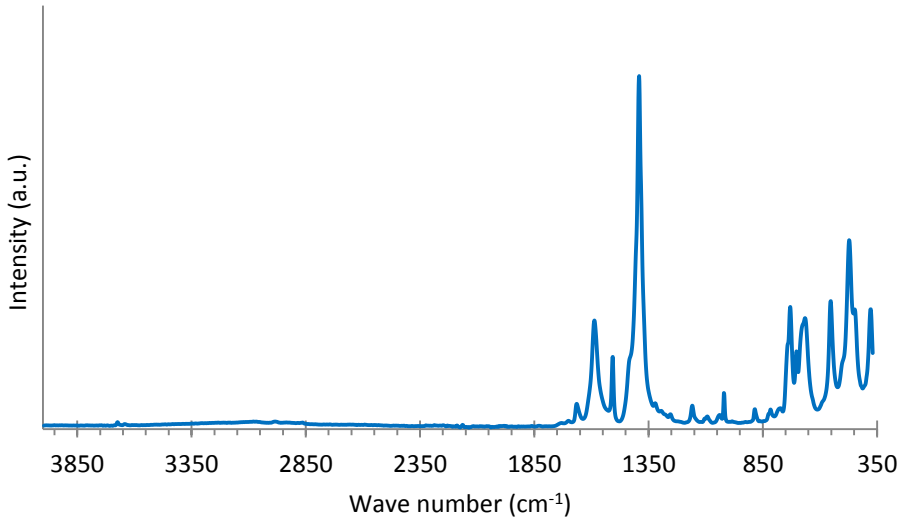

Figure 66. FTIR spectrum of UiO-66-Zr.

5. BODIPY derivative as fluorescent probe

The synthesis of the fluorescent BODIPY probe was reported in the literature.[113] It consists of three consecutive steps (see Scheme 1). First, the addition of thiophosgene to pyrrole produces a dipyrromethane bearing a thioketone function. Then, the obtained thioketone is methylated with methyl iodide to form the dipyrromethene. And finally, the dipyrromethene is deprotonated by triethylamine and subsequently complexed with $BF_3{\cdot}Et_2O$ to produce the target 8-thiomethyl BODIPY.

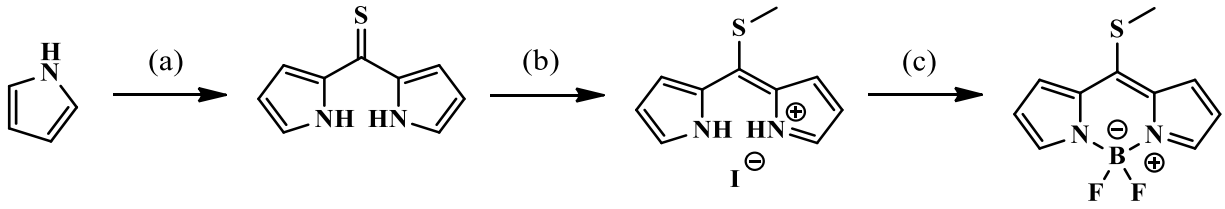

Dipyrromethane Dipyrromethene BODIPY

Scheme 1 a) (i) Thiophosgene (0.48 equiv.), Toluene, Et_2O, 25°C, 30 min. (ii) 10% MeOH in water, 25°C, 1h (b) CH_3I (18 equiv.), DCM, 25°C, 21h. (c) Et_3N (5.3 equiv.), $BF_3{\cdot}Et_2O$ (4.9 equiv.), DCM, 25°C, 24h. Adapted from [113].

Because the synthesis involves the use of thiophosgene, which is very toxic and volatile, and also because we are not familiar with this reaction, the synthesis was performed on a small scale. The desired fluorescent compound was successfully obtained but only in very small quantities, so the synthesis was performed again at a larger scale.

After purification by column chromatography on silica gel, a red solid was recovered. The purity was assessed by ^{1}HNMR and the spectrum corresponds with the literature (^{1}H NMR ($CDCl_3$, 300 MHz, 293K): δ 7.80 (2H, m), 7.42 (2H, m), 6.53-6.54 (2H, m), 2.91 (3H, s)). The yield is very poor, at around 5%. The purification steps (pad and chromatography on silica gel and extraction) between the reactions may induce the loss of product. A qualitative test was done by dissolving a small amount of BODIPY in CH_2Cl_2 in two different Erlenmeyer, and a drop of ethylenediamine was added to one of them. The examination under visible light does not show any difference, but under UV irradiation the result is clear: the Erlenmeyer with a mix BODIPY and ethylenediamine appears with a blue fluorescence, while the pure BODIPY in solution presents green fluorescence (see Figure 67 and Figure 68). The concept that we initially proposed has thus been validated.

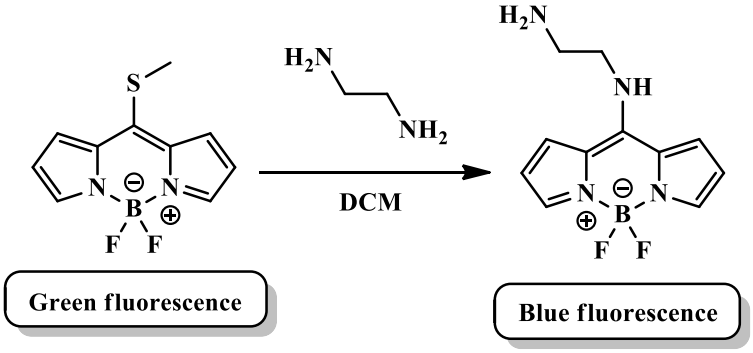

Figure 67. Reaction scheme of the BODIPY with ethylenediamine

A B

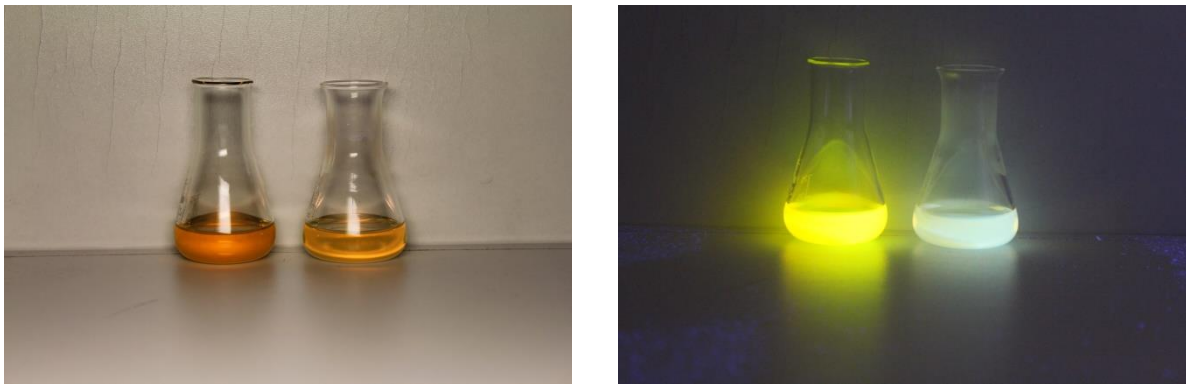

Figure 68. Photographs of the BODIPY probe in dichloromethane, before (left) and after (right) addition of a drop of ethylenediamine A: under visible light and B: under UV irradiation.

III. Conclusion and perspectives

1. Conclusion

The aim of the project was to synthesize stable metal-organic frameworks (MOFs) with potential open-metal sites and to functionalize them by anchoring ethylenediamine-like molecules. This would allow attaching free amine functions inside the porous network of the MOFs. Those materials post-functionalized through amine chemistry should find multiple uses in gas storage and catalysis.

We first explored the possibility of upscaling the synthesis MIL-100-Al through a procedure previously developed in our lab. The simple scale-up proved to be successful but was highly time consuming and used tremendous amounts of solvents to recover only a few grams of the compound. We thus performed some further experiments to evaluate the importance of synthesis parameters, and to explore the possibility of preparing more product in less time and by consuming less solvent. We found that addition of the modulator, HCl, during the reaction is crucial to obtain good-quality product and that increasing the temperature allowed to speed up the formation of MIL-100-Al. However, the reaction time was not optimal, as evidenced by the presence of a second MOF, MIL-96, in the product. We also noticed that increasing the concentrations of linker and metal source without modifying the quantities of modulators had a negative impact on the crystallinity of the obtained MOF.

We also explored the synthesis of the MIL-100-Ti^{IV} MOF through a reported procedure. The synthesis of the preformed cluster $[Ti_6O_6(4\text{-tbbz})_6(O^iPr)_6]$ was modified and allows the production of larger quantities with higher yields. However, we were not able to scale-up the MOF synthesis, neither to reproduce it under conditions similar to reported. Indeed, either unreacted reagents were recovered, or the reaction led to the formation of amorphous compounds or products with low crystallinity that were not the target MOF. We then explored the possibility to use $(TiCl_3)_3{\cdot}AlCl_3$ as Ti^{III} source to produce bimetallic MIL-100-(Al)Ti^{III}, with the aim to oxidize it in air to MIL-100-(Al)Ti^{IV}. However, all the attempts to produce this MOF also led to amorphous or poorly crystalline products. We determined that using HCl as modulator had no positive impact on the reaction and that lowering the temperature from 120°C to 80°C, increasing the reaction time, as well as washing the product with ethanol and water decreased its quality. In the best cases, we only

succeeded to obtain compounds having very poor crystallinity, which suggests that the MOF has formed with high amounts of defects and/or in the form of nanoparticles.

We tried to synthesize MIL-101-Ti^{III} by a reported procedure by using a small amount of $TiCl_3$ that was available in our lab. This MOF was successfully synthesized, as shown by the PXRD pattern and FTIR analysis of the obtained product. However, its surface area was significantly lower than the reported values. We attributed this to the poor quality of the used titanium(III) chloride. Because the supply of $TiCl_3$ was problematic, we investigated if $(TiCl_3)_3 \cdot AlCl_3$ was a suitable Ti^{III} precursor to make MIL-101-(Al)Ti^{III}. However, we only obtained compounds with virtually no crystallinity in all the tested synthetic conditions. We tried to oxidize the obtained MIL-101 compounds containing Ti^{III} in air, and observed that in all cases this led to complete collapse of the structures.

Finally, our attention turned to the synthesis of UiO-66-Zr, which is well documented. Much to our delight, we succeeded to obtain the MOF with high crystallinity and high yields from the first trial. However, the closure of the laboratory for Covid-19 pandemic prevented us from doing any further experiments and trials to functionalize this MOF.

In parallel of our experiments to obtain suitable MOFs, we found time to synthesize a fluorescent BODIPY probe that could be used to check the presence of available free amine functions within the grafted MOFs. The compound was obtained after a three-step synthesis in a rather poor yield (around 5%). However, it was obtained with a good purity, which was our priority. We performed a test under UV irradiation, which confirmed that the fluorescence colour changed efficiently upon contact with ethylenediamine.

2. Perspectives

We showed that the synthesis procedure of MIL-100-Al, which is quite tedious to perform at large scale under the conditions developed in our lab, can still be improved. Indeed, our results showed that MIL-100-Al could be obtained in less time when the reaction temperature is increased. However, during our trials, MIL-96-Al formed as a secondary phase, which indicates that the reaction time should be further decreased. Additional experiments in this direction should be carried out and the materials systematically characterized by PXRD as well as nitrogen sorption.

Nevertheless, the scaled-up sample that was synthesized in this work is currently being explored in our lab as a MOF to be functionalized with ethylenediamine. This study starts to show promising results, as NMR characterization confirmed the success of the grafting procedure and the presence of free amine sites. The obtained functionalized material should allow the capture of acidic gases such as CO_2. Further work should be performed by using derivatives of ethylenediamine (e.g. ethanolamine) and post-functionalization of the amine sites should be explored (e.g. to make supported homogeneous catalysts). In this perspective, the BODIPY probe that was synthesized in this work should enable assessing the availability of free amine functions for further reactions.

Concerning MIL-100-(Al)Ti^{III}, optimising its synthesis would be of utmost interest to enrich the knowledge about Ti-based MIL-100 structures, and more largely to get some insight in the chemistry of mixed Ti-Al MOFs. Therefore, additional experiments should be performed with the aim to yield a crystalline product. This could be achieved by increasing the reaction temperature, decreasing the reaction time or by changing the linker/metal ratio. If such a mixed MIL-100-(Al)Ti structure can be obtained, its properties should be investigated and tediously compared with the ones of its monometallic counterparts. Adding aluminium in the structure could for example increase its resistance towards air compared to the pure Ti^{III} MOF, since only the Ti atoms could be oxidised while the oxidation state of Al would not be affected.

Finally, the functionalization of the obtained UiO-66 sample with ethylenediamine and its derivatives should be performed, according to the initial goal of the project. If the functionalization attempts show that the molecules are too large to enter the pores, similar MOFs with longer linkers (and thus larger pore sizes), such as UiO-67 and UiO-68, could alternatively be synthesized and functionalized. Indeed, the syntheses of those MOFs are also well described in the literature and can even be achieved by the same procedure as the one we used to obtain UiO-66. The literature even describes methodologies to obtain single crystals of those MOFs. Such crystals could be used for functionalization tests to allow determining very precisely how the functionalisation takes place in the MOF by single crystal X-ray diffraction experiments. The possible applications of these functionalized MOFs are in gas storage and catalysis.

IV. Experimental part

1. Chemicals

The used isopropanol was technical grade. Zirconium(IV) chloride (98%, cont. 1-2% hafnium(IV) chloride), $Ti(O^{i}Pr)_4$ (> 97%) and $(TiCl_3)_3 \cdot AlCl_3$ ($TiCl_3$ 76.0%-78.5%) were purchased from Alfa Aesar. Boron trifluoride diethyletherate was purchased from Merck. H_3BTC (98%), thiophosgene (85%), iodomethane (99%, stabilized), terephthalic acid (> 99%), dry ether (99.5%, extra dry), pyrrole (99%), dry toluene (99.85%, extra dry), heptane (extra pure), triethylamine (99%) and sulphuric acid (96%) were purchased from Acros Organics. Denaturated ethanol (Technisolv, 99%), diethylether (GPR Rectapur), methanol (HiPerSolv, CHROMANORM), ACN (HiPerSolv, CHROMANORM), CH_2Cl_2 (HiPerSolv, CHROMANORM), dimethylformamide (HiPerSolv, CHROMANORM), THF (HiPerSolv, CHROMANORM), sodium hydroxide pellets, glacial acetic acid (> 99.7%) and hydrochloric acid (37%) were purchased from VWR Chemicals. Aluminium chloride (99.9%) 4-*tert*-butylbenzoic acid (4-tbbz-H, 99%), titanium (IV) chloride (99.9% trace metals basis) and titanium (III) chloride (99.999%) were purchased from Sigma-Aldrich.

Trimethyl-1,3,5-benzenetricarboxylate and triisopropyl-1,3,5-benzenetricarboxylate were previously obtained in the lab by the following procedure, and the stocks of the lab were used for the experiments presented in this Master Thesis. 10g of H_3BTC were dissolved in 100ml of the corresponding alcohol (either methanol or isopropanol), followed by addition of 1ml of sulphuric acid. The mixture was then refluxed overnight. After cooling down to room temperature, the sulphuric acid was neutralized by washing with a saturated aqueous solution of Na_2CO_3 (release of CO_2) and the product was extracted with diethylether. The organic phase was dried over Na_2SO_4 and the solvent was removed *in vacuo* to yield white crystals of the ester.

$Na_3BTC \cdot 3H_2O$ and MIL-100(Fe) were previously obtained in our lab by original published procedures[51] and the stocks of the lab were used for the experiments presented in this Master Thesis.

2. Instrumental

Low-resolution powder X-ray diffraction patterns were measured using a MAR345 diffractometer with X-rays generated by a Rigaku ultraX 18S X-ray generator (molybdenum anode, 0.71073 Å), with a monochromated beam (Xenocs FOX 3D mirror). The samples were prepared in glass capillaries (diameter: 0.7 mm). The raw data was integrated through the Fit2D software, using LaB_6 (measured in a 0.1 mm diameter capillary) as a reference sample.

High-resolution powder X-ray diffraction data were collected on a STOE STADI P Combi diffractometer using either MoKα radiation (50 kV, 40 mA) or CuKα radiation (40 kV, 40 mA) (graphite primary monochromator). The diffracted beam was recorded on a DECTRIS MYTHEN 1K strip detector. Samples were loaded in 0.7 mm diameter capillaries, aligned to the geometric centre of the diffractometer and measured in transmission, with independent 2theta movement.

ATR-FTIR spectra were recorded using a Bruker Alpha spectrometer equipped with a Platinum ATR module (diamond crystal) housed in an MBraun argon-filled glovebox. Samples were placed and pressed on the diamond sample holder without adding any additive (such as KBr). Spectra were recorded in the range of 4000 – 370 cm^{-1} with a resolution of 4 cm^{1}.

Nitrogen sorption measurements at 77 K were performed on a Micromeritics ASAP 2020 instrument. All samples were degassed at 200°C during 10h prior to analysis.

Ball-milling was performed with a Fritsch Pulverisette 7 premium line apparatus. The experiments were carried out in a stainless-steel milling bowls of 45 ml, and three stainless-steel balls of 10 mm were used in each bowls.

TGA/DSC measurements under air and nitrogen were recorded on a Mettler Toledo TGA/DSC 3+ STAR^e System. Gas flows of 100 ml/min and heating rates of 10 °C/min were used.

NMR spectra were recorded at room temperature (296 K) on a Bruker Avance II 300 spectrometer operating at 300.1 MHz for ^1H and 75.76 MHz for ^{13}C. Experiments were run under TopSpin program (3.2 version, Bruker) using a BBO or a BBFO {^1H,X} probeheads equipped with a z-gradient coil. Samples were dissolved in $CDCl_3$ (singlet, δ = 7.26 ppm).

Nylon membrane were purchased from Sigma Aldrich 1 x Nylon filter membranes, pore size 0.22 µm, diam. 47 mm, pack of 100 : Z290807-100EA

3. Syntheses

General notes on the syntheses:

1) Degassed solvents were obtained by bubbling argon through the solvents for approximately 30 minutes.
2) Reactions were performed under air atmosphere unless specifically mentioned.

*3.1. Attempt to obtain **MIL-100-Al***

Notice: the dissolution of $AlCl_3$ in water is exothermic, causes excessive and impressive fuming as well as release of HCl, and should be performed only under an efficient fumehood.

3.1.1. Large scale synthesis based on a procedure recently developed in our Lab (6 L scale)

To a solution of H_3BTC (31.5 g, 0.15 mol) in ethanol (3 L) with HCl (37%) (3.15 ml) was added a solution of $AlCl_3$ (17.30 g, 0.13 mol) in water (3 L) with DMF (34.95 ml). Then, the mixture was transferred in closed glass bottles (10 bottles of 500 ml capacity each containing 400 ml of the reaction mixture, and 1 bottle of 2.5 L capacity containing 2 L of the mixture) placed in an oven at 80°C for 6 days. The solid was separated by centrifugation (6000 rpm) and washed three times with water, and three times with ethanol. The obtained product was dried using a rotary evaporator and further dried under dynamic vacuum.

3.1.2. Small-scale synthesis without HCl

A first solution of H_3BTC (0.42 g, 2 mmol) in ethanol (40 ml) was added to a second solution of $AlCl_3$ (0.23 g, 1.7 mmol) in water (40 ml), containing some DMF (0.46 ml). Then, the mixture was transferred in a closed glass bottle (100 ml) and placed in an oven at 80°C for 6 days. The solid was separated by centrifugation and washed three times with water, and three times with ethanol. The obtained product was dried using a rotary evaporator and further dried under dynamic vacuum.

3.1.3. Variating the $AlCl_3$ and H_3BTC concentrations

A first solution of H_3BTC (1.69 g, 8 mmol) in ethanol (40 ml), containing some concentrated HCl (37%) (0.04 ml), was added to a second solution of $AlCl_3$ (0.92 g, 6.9 mmol) in water (40 ml), containing some DMF (0.46 ml). Then, the mixture was placed in a closed glass bottle (100 ml) and heated in an oven at 80°C for 6 days. The solid was separated by centrifugation and washed three times with water, and three times with ethanol. The obtained product was dried using a rotary evaporator and further dried under dynamic vacuum.

3.1.4. Increased reaction temperature (100°C) and reduced reaction time (41h)

To a solution of H_3BTC (2.1 g, 1 mmol) in ethanol (200 ml) with HCl (37%) (0.21 ml) was added a solution of $AlCl_3$ (1.15 g, 8.62 mmol) in water (200 ml) with DMF (2.33 ml). Then, the mixture was placed in an oven at 100°C for 41h in a closed glass bottle (500 ml). The solid was separated by centrifugation and washed three times with water, and three times with ethanol. The obtained product was dried using a rotary evaporator and further dried under dynamic vacuum.

*3.2. Synthesis of $[Ti_6O_6(4\text{-tbbz})_6(O^iPr)_6]$ (**Ti_6 cluster**)*

The synthesis of the Ti_6 cluster was carried out according to a published procedure.[51] In brief, 4-*tert*-butylbenzoic acid (4-tbbz-H) (8.03 eqs.) was first dissolved in a mixture of ^{i}PrOH:THF (3:1), followed by the addition of $Ti(O^iPr)_4$ (1 eq.). The obtained solution was stirred at first at 60°C for 24h and then further at 70°C for another 24h in a half full open Erlenmeyer flask under air atmosphere. The obtained crystals were filtered on a glass frit and washed using ^{i}PrOH. The obtained product was dried under vacuum at 100°C overnight to remove residual solvent. Different quantities were engaged to find a suitable way to produce a single large batch for further experiments (see Table 4 below).

Table 4. Study of the variation of reactant quantities to scale up the synthesis of $[Ti_6O_6(4\text{-tbbz})_6(O^iPr)_6]$.

Sample	A	B	C	D
Reactant				
$Ti(O^iPr)_4$	0.35 ml 1.19 mmol	1.8 ml 6.02 mmol	1.8 ml 6.02 mmol	3.5 ml 11.9 mmol
4-tbbz-H	1.70 g 9.55 mmol	8.51 g 47.7 mmol	8.51 g 47.7 mmol	17.01 g 95.55 mmol
^iPrOH:THF (3:1)	30 ml	150 ml	150 ml	75 ml
Yield (%)	86	97	Quantitative	Quantitative

*3.3. Attempts to obtain **MIL-100-Ti^{IV}** from Ti_6 cluster*

The first three following syntheses were performed according to a procedure described in the literature.[36]

3.3.1. In Teflon bomb

Ti_6 (0.145 g, 80.5 µmol) and H_3BTC (0.5 g, 2.38 mmol) were added to 60 ml of a ACN:THF (3:1) mixture in an Erlenmeyer flask, followed by sonication to obtain a homogeneous suspension. Then, glacial acetic acid was added (5 ml, 87.36 mmol) and the mixture was heated in an oven at 160°C for 40h in a teflon bomb (250 ml). The solid was separated by centrifugation and washed three times with ethanol. The obtained product was dried using a rotary evaporator, followed by further drying under dynamic vacuum.

3.3.2. In stainless steel autoclave

Ti_6 (0.433 g, 0.24 mmol) and H_3BTC (1.5 g, 7.14 mmol) were added to 180 ml of a ACN:THF (3:1) mixture in an Erlenmeyer flask, followed by sonication to obtain a homogeneous suspension. Then, glacial acetic acid was added (15 ml, 262.1 mmol) and the mixture was transferred to a stainless-steel teflon lined autoclave (300 ml) and heated with a heating mantle at 160°C for 44h without stirring. The solid was separated by centrifugation and washed three times with ethanol. The obtained product was dried using a rotary evaporator and further dried under dynamic vacuum.

3.3.3. In glass vial

Ti_6 (7.4 mg, 4.11 µmol) and H_3BTC (25.2 mg, 0.12 mmol) were added to 3 ml of a ACN:THF (3:1) mixture in a vial, followed by sonication to obtain an homogeneous suspension. Then, glacial acetic acid was added (0.25 ml, 4.37 mmol) and the mixture was heated in an oven at 160°C for 2h in a 4 ml screw capped glass vial. Due to excess pressure, the solvents were volatized and a dry solid was obtained. The solid was separated by centrifugation and washed three times with water and three times with ethanol. The obtained product was dried using a rotary evaporator and further dried under dynamic vacuum.

3.3.4. In aqueous solution using $Na_3BTC{\cdot}3H_2O$ at room temperature

Ti_6 (1 g, 0.55 mmol) was added to a solution of $Na_3BTC{\cdot}3H_2O$ (0.92 g, 2.8 mmol) in 80 ml of water. The suspension was then stirred at room temperature (25°C) for 24h in an Erlenmeyer flask (250 ml) using a magnetic stirrer. The solid was separated by centrifugation and washed three times with water and three times with ethanol. The obtained product was dried using a rotary evaporator and further dried under dynamic vacuum.

3.3.5. In aqueous solution using $Na_3BTC{\cdot}3H_2O$ at 80°C

Ti_6 (1 g, 0.55 mmol) was added to a solution of $Na_3BTC{\cdot}3H_2O$ (0.92 g, 2.8 mmol) in 80 ml of water and the resulting mixture was sonicated to obtain a homogeneous suspension. Then, the mixture was heated at 80°C for 63h in an open Erlenmeyer flask (250 ml) using an oil bath. The solid was separated by centrifugation and washed three times with water and three times with ethanol. The obtained product was dried using a rotary evaporator and further dried under dynamic vacuum.

*3.4. Attempt to obtain **MIL-100-Ti^{IV}** by metal exchange from MIL-100-Fe*

MIL-100-Fe (55.7 mg) was first activated by heating overnight at 205°C under vacuum in a three-neck flask equipped with a condenser, a rubber septum and a glass stopcock connected to a Schlenk line, and subsequently cooled down to room temperature under vacuum. Then, THF (25 ml) was added through a rubber septum (when the flask was still under vacuum), and the flask was backfilled with argon, followed by the addition of $TiCl_4$ (0.55 ml, 5 mmol). The mixture was refluxed for 63h using an oil bath. The solid product was separated by centrifugation and washed three times with THF. The obtained product was dried using a rotary evaporator and further dried under dynamic vacuum.

*3.5. Attempts to obtain **MIL-100-Ti^{IV}** from Ti(O^iPr)$_4$*

3.5.1. From H_3BTC in ethanol (-78°C)

A solution of H_3BTC (0.5 g, 2.38 mmol) in 25 ml of ethanol in an Erlenmeyer flask (100 ml) was cooled down to -78°C (dry ice/acetone bath). Then, a solution of Ti(O^iPr)$_4$ (0.7 ml, 2.4 mmol) in 25 ml of ethanol was added dropwise under air. The mixture was subsequently allowed to reach room temperature, leading to the formation of a white gel. After 12h, the solid was separated by centrifugation and washed three times with ethanol. The obtained product was dried using a rotary evaporator and further dried under dynamic vacuum.

3.5.2. From trimethyl 1,3,5-benzenetricarboxylate

To a mixture of trimethyl 1,3,5-benzenetricarboxylate (0.5 g, 1.99 mmol) in 10 ml of formic acid in an Erlenmeyer flask (25 ml) Ti(O^iPr)$_4$ (1.1 ml, 3.7 mmol) was added under air. Then, the mixture was stirred for 16h at 70°C using a magnetic stirrer hotplate and an oil bath. The solid was separated by centrifugation and washed three times with methanol. The obtained product was dried using a rotary evaporator and further dried under dynamic vacuum.

3.5.3. From triisopropyl 1,3,5-benzenetricarboxylate

Ti(O^iPr)$_4$ (1.1 ml, 3.7 mmol) was added to a solution of triisopropyl 1,3,5-benzenetricarboxylate (0.5 g, 1.49 mmol) in 25 ml of ethanol in an Erlenmeyer flask (50 ml) under air. Then, the mixture was stirred for 12h at 80°C using a magnetic stirrer hotplate and an oil bath. The solid was separated by centrifugation and washed three times with ethanol. The obtained product was dried using a rotary evaporator and further dried under dynamic vacuum.

*3.6. Attempt to obtain **MIL-100-Ti^{IV}** by mechanochemistry*

3.6.1. Dry ball-milling

A mixture of H_3BTC (0.41 g, 1.95 mmol) and Ti_6 (0.59 g, 0.33 mmol) was ground in a 45 ml stainless-steel grinding bowl containing three stainless-steel balls (10 mm diameter) using a planetary ball-mill. The rotation speed was set at 300 rpm, and the mixture was milled

during 6 cycles of 5 min, using 2 min breaks to avoid overheating. The solid was collected, dissolved in ethanol, centrifuged and washed three times with ethanol. The obtained product was dried under vacuum.

3.6.2. Liquid-assisted grinding

A mixture of H_3BTC (0.41 g, 1.95 mmol) and Ti_6 (0.59 g, 0.33 mmol) was ground in a 45 ml stainless-steel grinding bowl containing three stainless-steel balls (10 mm diameter) after prior addition of 1 ml of ethanol (just before closing the lid of the grinding bowl) using a planetary ball-mill. The rotation speed was set at 300 rpm, and the mixture was milled during 6 cycles of 5 min, using 2 min breaks. The solid was separated by centrifugation and washed three times with ethanol. The obtained product was dried under vacuum.

*3.7. Attempts to obtain **MIL-100-(Al)Ti$^{III/IV}$** from $(TiCl_3)_3{\cdot}AlCl_3$*

3.7.1. In oil bath

In a 250 ml three-neck flask equipped with a condenser, H_3BTC (1.68 g, 8 mmol) was dissolved in 80 ml of degassed DMF:ethanol (10:1) under argon atmosphere. Then, $(TiCl_3)_3{\cdot}AlCl_3$ (1.5 g, 2.5 mmol) was introduced in a separate 100 ml flask under argon atmosphere (in a glovebox) and 85 ml of degassed DMF:ethanol (10:1) was added (outside the glovebox) to dissolve the solid. Then, this solution was added to the three-neck flask. The obtained light blue solution was heated under stirring for 18h at 80°C or 120°C for 18h to 7 days (see Table 5 below) using an oil bath. After that, the violet product was filtered on a nylon membrane (pore size 0.22 µm) under argon atmosphere and washed with degassed DMF, THF and ether. The solid was dried under vacuum. A small amount of the product was oxidized in the air at room temperature. The colour changed from violet (Ti^{III}) to yellow (Ti^{IV}).

Table 5. Study of variations of the temperature and the reaction time on the reaction.

Sample	120°C-18h	80°C-18h	120°C-7d
Parameters			
T(°C)	120	80	120
Reaction time	18h	18h	7 days

3.7.2. Synthesis in the oven (120°C)

In a 250 ml flask, H_3BTC (1.68 g, 8 mmol) was dissolved in 80 ml of degassed DMF:ethanol (10:1) under argon atmosphere. Then, $(TiCl_3)_3 \cdot AlCl_3$ (1.50 g, 2.52 mmol) was introduced in a separate 100 ml flask under argon atmosphere (glovebox) and the solid was dissolved by adding 85 ml of degassed DMF:ethanol (10:1) (outside the glovebox). The obtained solution was then added to the content of the 250 ml flask. The obtained mixture was transferred in a 250 ml closed glass bottle (under a flux of argon) and heated in the oven for 18h at 120°C. The obtained mixture was separated in two batches which were filtered on a nylon membrane (pore size 0.22 µm) under argon atmosphere. Each batch was washed with different solvents:

- ✓ Batch 1: DMF (degassed) → THF (degassed) → ether (degassed)
- ✓ Batch 2: Water → Ethanol

Both solids were dried under vacuum.

3.7.3. Variating the HCl concentration

In a 500 ml flask, H_3BTC (3.37 g, 16.04 mmol) was dissolved in 150 ml of a degassed DMF:ethanol mixture (10:1) under argon atmosphere. Then, another 500 ml flask was charged with $(TiCl_3)_3 \cdot AlCl_3$ (2.99 g, 5.02 mmol) in a glovebox. The flask was then removed from the glovebox and 180 ml of a degassed DMF:ethanol mixture (10:1) was added *via cannula* to dissolve the solid, and the resulting solution was then added *via cannula* to the other 500 ml flask. 66 ml aliquots of this Ti/Al/H_3BTC solution were transferred (under a flux of argon) into 100 ml screw-capped glass bottles containing a variable amount of concentrated HCl (37%) (see Table 6 below). The closed bottles were heated in the oven for 21h at 120°C. After that, the products were filtered on a nylon membrane (pore size 0.22 µm) under argon atmosphere and washed with degassed DMF, THF and ether. The solids were dried under vacuum. A small amount of each product was oxidized in the air at room temperature. The colour changed from violet (Ti^{III}) to yellow (Ti^{IV}).

Table 6. Study of the variation of the HCl concentration on the reaction.

Sample	0.25 ml HCl	0.5 ml HCl	1 ml HCl	2 ml HCl
Reactants				
Ti/Al/H_3BTC solution	66 ml	66 ml	66 ml	66 ml
HCl (37%)	0.25 ml	0.5 ml	1 ml	2 ml

*3.8. Synthesis of **MIL-101-Ti^{III}** from $TiCl_3$*

The synthesis was performed according to a procedure described in the literature.[50] In brief, a Schlenk flask (250 ml) equipped with a fritted disk was charged with H_2BDC (0.34 g, 2.04 mmol) and $TiCl_3$ (0.40 g, 2.59 mmol) and sealed with a rubber septum under argon atmosphere (glovebox). Then (outside the glovebox), degassed DMF (150 ml) and ethanol (15 ml) were added. The mixture was heated and stirred at 120°C for 18h using a magnetic stirrer hotplate and an oil bath. The obtained violet solid was decanted, filtered and washed with degassed DMF (225 ml) and degassed THF (50 ml). Finally, the product was dried under vacuum.

*3.9. Attempt to oxidize MIL-101-Ti^{III} into **MIL-101-Ti^{IV}***

In order to oxidize MIL-101-Ti$^{\mathbf{III}}$ in MIL-101-Ti$^{\mathbf{IV}}$, two aliquots of the MOF were placed in an open test tube, which was exposed to air overnight, either:

- ✓ at room temperature, or;
- ✓ plunged in a Dewar filled with liquid N_2

During both oxidations, the colour changed from violet (Ti^{III}) to beige (Ti^{IV}).

*3.10. Attempt to obtain **MIL-101-Al^{III}** from $AlCl_3$*

A flask (250 ml) under argon atmosphere was charged with H_2BDC (0.34 g, 2.04 mmol) and $AlCl_3$ (0.33 g, 2.47 mmol). Then, degassed DMF (150 ml) and ethanol (15 ml) were added. The mixture was heated and stirred at 120°C for 18h using a magnetic stirrer hotplate and an oil bath. The resulting mixture was filtered and washed three times with ethanol. Finally, the two product was dried under vacuum.

*3.11. Attempts to obtain **MIL-101-(Al)Ti^{IV}** from $(TiCl_3)_3 \cdot AlCl_3$*

A Schlenk flask (250 ml) equipped with a fritted disk was charged with H_2BDC (0.34 g, 2.04 mmol) and $(TiCl_3)_3 \cdot AlCl_3$ (0.38 g, 0.64 mmol) under argon atmosphere (glovebox) and closed with a rubber septum. Then (outside the glovebox), degassed DMF (150 ml) and ethanol (15 ml) were added through the rubber septum. The violet mixture was heated and stirred at 120°C for 21h (without condenser). The mixture was centrifuged and washed with DMF and THF. During this procedure, the colour of the compounds changed from violet (Ti^{III}) to yellow (Ti^{IV}).

*3.12. Attempts to obtain **MIL-101-(Al)Ti^{III}** from $(TiCl_3)_3 \cdot AlCl_3$*

In a 250 ml three-neck flask equipped with a condenser and rubber septa, H_2BDC (0.34 g, 2.04 mmol) was dissolved in 100 ml of a DMF:ethanol (10:1) mixture. The solution was subsequently degassed under argon atmosphere. Then, a 100 ml one-neck round-bottom flask was charged with $(TiCl_3)_3 \cdot AlCl_3$ (0.38 g, 0.64 mmol) in a glovebox and was stoppered with a rubber septum. The flask was then removed from the glovebox and connected to the argon supply of a Schlenk line *via* a connected needle that was introduced through the septum. 65 ml of a degassed DMF:ethanol (10:1) mixture were then added and the solid dissolved. The obtained solution was added to the mixture in the three-neck flask using a syringe. The obtained light blue solution was heated and stirred for 17h at 120°C using a magnetic stirrer hotplate and an oil bath. After that, the solid was filtered under argon atmosphere using a nylon membrane (pore size 0.22 µm) and washed with degassed DMF and THF. Once all the solvents were passed through the membrane, an argon flux was passed over the product until it was dry enough to be transferred in a flask equipped with a stopcock connected to a Schlenk line. The product was further dried under vacuum and then stored in a glovebox. A small amount of the product was exposed to the air at room temperature to oxidize Ti^{III} to Ti^{IV}. The colour changed from violet (Ti^{III}) to yellow (Ti^{IV}).

*3.13. Synthesis of **UiO-66-Zr***

The synthesis was performed according to a procedure described in the literature.[108] In brief, $ZrCl_4$ (2.14 g, 9.18 mmol) was dissolved in DMF (85 ml) and HCl (37%) (17 ml) in a glass bottle (500ml) using an ultrasonic bath for 20 min. Then, H_2BDC (2.08 g, 12.52 mmol) followed by DMF (169 ml) were added and the mixture was placed in an ultrasonic bath for another 20 min. The closed glass bottle (500 ml) was heated in the oven at 80°C overnight.

The obtained solid was filtered using a nylon membrane (pore size 0.22 µm) and washed with DMF. The solid was then collected and washed with water (3 times) and ethanol (3 times) by centrifugation. The synthesis was performed two times in parallel. In the end, the two batches were mixed together.

*3.14. Synthesis of the **BODIPY** probe*

The synthesis was performed based on a previously described procedure, [109] according to the reactions of Scheme 2.

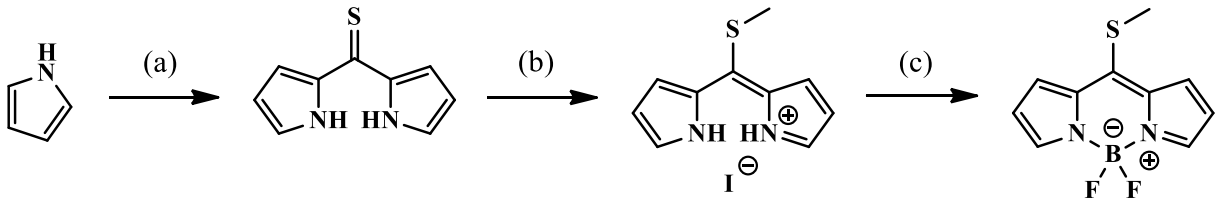

Dipyrromethane Dipyrromethene BODIPY

Scheme 2 a) (i) Pyrrole (1 equiv.), Thiophosgene (0.48 equiv.), Toluene, Et_2O, 25°C, 30 min. (ii) 10% MeOH in water, 25°C, 1h (b) CH_3I (18 equiv.), DCM, 25°C, 21h. (c) Et_3N (5.3 equiv.), $BF_3{\cdot}Et_2O$ (4.9 equiv.), DCM, 25°C, 24h. Adapted from [109]

<u>Notice</u>: Thiophosgene causes skin irritation and is toxic if inhaled; the experiment should be performed only under efficient fumehood and with protective gloves, protective clothes and eyes protection.

Methyl iodide is toxic if inhaled and has a potential carcinogenicity; the experiment should be performed only under efficient fumehood and with protective gloves, protective clothes and eyes protection.

3.14.1. Synthesis of dipyrromethane

Dry ether and pyrrole (see quantities in the Table 7 below) were introduced in a flamed 250 ml flask under argon atmosphere. Dry toluene and thiophosgene (see quantities in the Table 7 below) were added in another flamed 500 ml flask under argon atmosphere. Then, the solution of pyrrole was added dropwise to the thiophosgene solution, at 0°C (ice bath). The mixture was stirred further for 30 min after addition. To quench the reaction, a solution of methanol in water (10% Volume) with NaOH (10% Molar) (see quantities in the Table 7 below) was added and the resulting solution was stirred for 1h. Solvents were removed under

reduced pressure. The gummy crude product was dissolved in a minimum amount of CH_2Cl_2 and evaporated *in vacuo* to obtain a solid (solid deposit). The solid was deposited on a pad of silica gel and eluted using a heptane:CH_2Cl_2 mixture (1:3) containing 1% of triethylamine (the collection was stopped once the bright orange colour started to fade out). The product was recovered as red crystals after evaporation *in vacuo*.

The synthesis was performed on a small and a large scale (see Table 7 below). The large scale synthesis was realized at the same time in two separate batches and the final products collected in a single batch for further experiments to avoid manipulation of a too large amount of thiophosgene.

Table 7 Quantities engaged for the synthesis at a small scale and a large scale for the synthesis of BODIPY 1

Sample	Small scale	Large scale (done 2 times)
Reactant		
Pyrrole	1.05 ml, 15.2 mmol	(2 x) 4.2 ml, 60.71 mmol
Thiophosgene	0.58 ml, 7.50 mmol	(2 x) 2.3 ml, 30.0 mmol
Dry ether	20 ml	(2 x) 90 ml
Dry toluene	20 ml	(2 x) 80 ml
H_2O/MeOH/NaOH	25 ml	(2 x) 100 ml

3.14.2. Synthesis of dipyrromethene

The dipyrromethane was dissolved in CH_2Cl_2 under argon atmosphere (see Table 8 below for the amounts). Then, methyl iodide (see Table 8 below for the amount) was added and the mixture was stirred at room temperature for a given amount of time (Table 8). Solvents were removed using a rotary evaporator under reduced pressure. The obtained products were used as obtained without purification and further analysis.

Table 8 Quantities engaged for the synthesis at a small scale and a large scale

Sample	Small scale	Large scale
Reactant		
Dipyrromethane	0.285 g	0.45g
MeI	1.8 ml, 29.17 mmol	2.9 ml, 47.0 mmol
CH_2Cl_2	5 ml	7.4 ml
Time	21h	26h

3.14.3. Synthesis of BODIPY

The dipyrromethene was dissolved in CH_2Cl_2 (see Table 9 below for the amounts) under argon atmosphere. Then, triethylamine (see Table 9) was added and the mixture was stirred at room temperature for 40 min. Subsequently, $BF_3{\cdot}Et_2O$ (see Table 9) was added and the mixture was stirred for 24h at room temperature. Solvents were removed with a rotary evaporator under reduced pressure.

The synthesis was performed first on a small scale and then on a large scale (see Table 9). The purification was different for both batches:

- ✓ Small scale: The product was first chromatographed on silica gel (eluent= heptane:CH_2Cl_2:triethylamine = 100:10:1.1 → 100:100:2 → 50:100:1.5) and then washed by extraction with toluene and water;
- ✓ Large-scale: The product was first washed by extraction with toluene and water, then chromatographed on silica gel (eluent= heptane:CH_2Cl_2:triethylamine = 100:10:1.1 → 100:100:2 → 50:100:1.5).

Table 9. Quantities engaged for the synthesis at a small scale and a large scale.

Sample	Small scale	Large scale
Reactant		
Dipyrromethene	0.51 g	0.88 g
CH_2Cl_2	45 ml	19 ml
NEt_3	1.2 ml, 8.89 mmol	2 ml, 14.81 mmol
$BF_3{\cdot}Et_2O$	0.95 ml, 7.70 mmol	1.63 ml, 13.21 mmol

V. Bibliography

1. Li, J. R. *et al.* Carbon dioxide capture-related gas adsorption and separation in metal-organic frameworks. *Coord. Chem. Rev.* **255**, 1791–1823 (2011).

2. Zhao, S. N., Song, X. Z., Song, S. Y. & Zhang, H. jie. Highly efficient heterogeneous catalytic materials derived from metal-organic framework supports/precursors. *Coord. Chem. Rev.* **337**, 80–96 (2017).

3. Zhang, X. *et al. Metal–Organic Frameworks (MOFs) and MOF-Derived Materials for Energy Storage and Conversion*. *Electrochemical Energy Reviews* vol. 2 (Springer Singapore, 2019).

4. Wu, D. *et al.* Design and preparation of porous polymers. *Chem. Rev.* **112**, 3959–4015 (2012).

5. Zhang, S. *et al.* Porous Organic Frameworks: Advanced Materials in Analytical Chemistry. *Adv. Sci.* **5**, (2018).

6. Batten, S. R. *et al.* Terminology of metal–organic frameworks and coordination polymers (IUPAC Recommendations 2013). *Pure Appl. Chem.* **85**, 1715–1724 (2013).

7. Kitagawa, S. & Matsuda, R. Chemistry of coordination space of porous coordination polymers. *Coord. Chem. Rev.* **251**, 2490–2509 (2007).

8. Horike, S., Shimomura, S. & Kitagawa, S. Soft porous crystals. *Nat. Chem.* **1**, 695–704 (2009).

9. Chen, J. & Li, Y. The Road to MOF-Related Functional Materials and Beyond: Desire, Design, Decoration, and Development. *Chem. Rec.* **16**, 1456–1476 (2016).

10. Lee, J. H., Jeoung, S., Chung, Y. G. & Moon, H. R. Elucidation of flexible metal-organic frameworks: Research progresses and recent developments. *Coord. Chem. Rev.* **389**, 161–188 (2019).

11. Herbst, A. & Janiak, C. MOF catalysts in biomass upgrading towards value-added fine chemicals. *CrystEngComm* **19**, 4092–4117 (2017).

12. J. Rouquerol *et al.* Recommandations for the characterization of porous solids. *Pure Appl. Chem* **66**, 1739–1758 (1994).

13. Yuan, S. *et al.* Stable Metal–Organic Frameworks: Design, Synthesis, and Applications. *Adv. Mater.* **30**, 1–35 (2018).

14. Rubin, H. N. & Reynolds, M. M. Functionalization of Metal-Organic Frameworks To Achieve Controllable Wettability. *Inorg. Chem.* **56**, 5266–5274 (2017).

15. Thommes, M. *et al.* Physisorption of gases, with special reference to the evaluation of surface area and pore size distribution (IUPAC Technical Report). *Pure Appl. Chem.* **87**, 1051–1069 (2015).

16. Furukawa, H., Cordova, K. E., O'Keeffe, M. & Yaghi, O. M. The chemistry and applications of metal-organic frameworks. *Science (80-.).* **341**, (2013).

17. Urquhart, J. World's first commercial MOF keeps fruit fresh. https://www.chemistryworld.com/news/worlds-first-commercial-mof-keeps-fruit-fresh/1017469.article (2016).

18. Lee, Y. R., Kim, J. & Ahn, W. S. Synthesis of metal-organic frameworks: A mini review. *Korean J. Chem. Eng.* **30**, 1667–1680 (2013).

19. Ouyang, W., Santiago, A. R. P., Cerdán-Gómez, K. & Luque, R. Nanoparticles within functional frameworks and their applications in photo(electro)catalysis. *Photoactive Inorg. Nanoparticles Surf. Compos. Nanosyst. Funct.* 109–138 (2019) doi:10.1016/B978-0-12-814531-9.00005-1.

20. Haynes, W. M. *Abundance of elements in the Earth's crust and in the sea*. (CRC Handbook of Chemistry and Physics, 2016).

21. Loiseau, T., Volkringer, C., Haouas, M., Taulelle, F. & Férey, G. Crystal chemistry of aluminium carboxylates: From molecular species towards porous infinite three-dimensional networks. *Comptes Rendus Chim.* **18**, 1350–1369 (2015).

22. Takeno, N. Atlas of Eh-pH diagrams Intercomparison of thermodynamic databases. *Natl. Inst. Adv. Ind. Sci. Technol. Tokyo* 285 (2005).

23. Helmboldt, O. *et al.* Aluminum Compounds, Inorganic. *Ullmann's Encycl. Ind. Chem.*

2, 569–584 (2012).

24. Giovine, R. *et al.* NMR crystallography to probe the breathing effect of the MIL-53(Al) metal-organic framework using solid-state NMR measurements of 13C-27Al distances. *Acta Crystallogr. Sect. C Struct. Chem.* **73**, 176–183 (2017).

25. Loiseau, T. *et al.* MIL-96, a Porous Aluminum Trimesate 3D Structure Constructed from a Hexagonal Network of 18-Membered Rings and µ3-Oxo-Centered Trinuclear Units. *J. Am. Chem. Soc.* **128**, 10223–10230 (2006).

26. Volkringer, C. *et al.* A microdiffraction set-up for nanoporous metal-organic-framework-type solids. *Nat. Mater.* **6**, 760–764 (2007).

27. Volkringer, C. *et al.* Synthesis, single-crystal X-ray microdiffraction, and NMR characterizations of the giant pore metal-organic framework aluminum trimesate MIL-100. *Chem. Mater.* **21**, 5695–5697 (2009).

28. Serra-Crespo, P., Ramos-Fernandez, E. V., Gascon, J. & Kapteijn, F. Synthesis and characterization of an amino functionalized MIL-101(Al): Separation and catalytic properties. *Chem. Mater.* **23**, 2565–2572 (2011).

29. Séraphin, L. Production du titane. *Encyclopædia Universalis [en ligne]* http://www.universalis.fr/encyclopedie/titane/.

30. Greenwood, N. N. & Earnshaw, A. *Chemistry of the Elements*. (Butterworth-Heinemann, 1997).

31. Bradley, D. C., Ram C. Mehrotra & Rothwell, I. P. *Alkoxo and Aryloxo Derivatives of Metals*. (Academic Press, 2001).

32. Sibum, H. *et al.* Titanium, Titanium Alloys, and Titanium Compounds. Ullmann's Encyclopedia of Industrial Chemistry. *Ullmann's Encycl. Ind. Chem.* **37**, 1–35 (2017).

33. Acevedo-Peña, P., Vazquez-Arenas, J., Cabrera-Sierra, R., Lartundo-Rojas, L. & González, I. Ti Anodization in Alkaline Electrolyte: The Relationship between Transport of Defects, Film Hydration and Composition. *J. Electrochem. Soc.* **160**, C277–C284 (2013).

34. Kent, J. A., Bommoraju, T. V. & Barnicki, S. D. *Handbook of Industrial Chemistry*

and Biotechnology. (Springer International Publishing, 2017).

35. Nielsen, R. H. & Wilfing, G. Zirconium and Zirconium Compounds. *Ullmann's Encycl. Ind. Chem.* **39**, 753–778 (2012).

36. Nguyen, H. L. The chemistry of titanium-based metal-organic frameworks. *New J. Chem.* **41**, 14030–14043 (2017).

37. Castells-Gil, J. *et al.* De novo synthesis of mesoporous photoactive titanium(iv)-organic frameworks with MIL-100 topology. *Chem. Sci.* **10**, 4313–4321 (2019).

38. Férey, G. Gérard Férey. https://www.gerard-ferey.org/ (2016).

39. Eddaoudi, M., Sava, D. F., Eubank, J. F., Adil, K. & Guillerm, V. Zeolite-like metal-organic frameworks (ZMOFs): Design, synthesis, and properties. *Chem. Soc. Rev.* **44**, 228–249 (2015).

40. Férey, G. *et al.* A hybrid solid with giant pores prepared by a combination of targeted chemistry, simulation, and powder diffraction. *Angew. Chemie - Int. Ed.* **43**, 6296–6301 (2004).

41. Lebedev, O. I., Millange, F., Serre, C., Van Tendeloo, G. & Férey, G. First direct imaging of giant pores of the metal-organic framework MIL-101. *Chem. Mater.* **17**, 6525–6527 (2005).

42. D'Amore, M., Civalleri, B., Bush, I. J., Albanese, E. & Ferrabone, M. Elucidating the Interaction of CO2 in the Giant Metal-Organic Framework MIL-100 through Large-Scale Periodic Ab Initio Modeling. *J. Phys. Chem. C* **123**, 28677–28687 (2019).

43. Mowat, J. P. S. *et al.* Synthesis, characterisation and adsorption properties of microporous scandium carboxylates with rigid and flexible frameworks. *Microporous Mesoporous Mater.* **142**, 322–333 (2011).

44. Lieb, A. *et al.* MIL-100(V) - A mesoporous vanadium metal organic framework with accessible metal sites. *Microporous Mesoporous Mater.* **157**, 18–23 (2012).

45. Biswas, S. *et al.* Vanadium analogues of nonfunctionalized and amino-functionalized MOFs with MIL-101 topology - Synthesis, characterization, and gas sorption properties. *Eur. J. Inorg. Chem.* 2481–2486 (2012) doi:10.1002/ejic.201200106.

46. Reinsch, H. & Stock, N. Formation and characterisation of Mn-MIL-100. *CrystEngComm* **15**, 544–550 (2013).

47. Zhu, J., Li, P. Z., Guo, W., Zhao, Y. & Zou, R. Titanium-based metal–organic frameworks for photocatalytic applications. *Coord. Chem. Rev.* **359**, 80–101 (2018).

48. Hupp, J. T. & Poeppelmeler, K. R. Chemistry: Better living through nanopore chemistry. *Science (80-.).* **309**, 2008–2009 (2005).

49. Seoane, B. *et al.* Metal organic framework synthesis in the presence of surfactants: Towards hierarchical MOFs? *CrystEngComm* **17**, 1693–1700 (2015).

50. Yang, J., Wang, J., Deng, S. & Li, J. Improved synthesis of trigone trimer cluster metal organic framework MIL-100Al by a later entry of methyl groups. *Chem. Commun.* **52**, 725–728 (2016).

51. Steenhaut, T., Hermans, S. & Filinchuk, Y. Green synthesis of a large series of bimetallic MIL-100(Fe,M) MOFs. *New J. Chem.* **44**, 3847–3855 (2020).

52. Mali, G. *et al.* Unraveling the Arrangement of Al and Fe within the Framework Explains the Magnetism of Mixed-Metal MIL-100(Al,Fe). *J. Phys. Chem. Lett.* **10**, 1464–1470 (2019).

53. Mason, J. A., Darago, L. E., Lukens, W. W. & Long, J. R. Synthesis and O2 Reactivity of a Titanium(III) Metal-Organic Framework. *Inorg. Chem.* **54**, 10096–10104 (2015).

54. Hong, K., Bak, W. & Chun, H. Robust molecular crystals of titanium(IV)-oxo-carboxylate clusters showing water stability and CO2 sorption capability. *Inorg. Chem.* **53**, 7288–7293 (2014).

55. Antonio, A. M., Rosenthal, J. & Bloch, E. D. Electrochemically Mediated Syntheses of Titanium(III)-Based Metal-Organic Frameworks. *J. Am. Chem. Soc.* **141**, 11383–11387 (2019).

56. Padial, N. M. *et al.* Heterometallic Titanium-Organic Frameworks by Metal-Induced Dynamic Topological Transformations. *J. Am. Chem. Soc.* **142**, 6638–6648 (2020).

57. Winarta, J. *et al.* A Decade of UiO-66 Research: A Historic Review of Dynamic Structure, Synthesis Mechanisms, and Characterization Techniques of an Archetypal

Metal-Organic Framework. *Cryst. Growth Des.* **20**, 1347–1362 (2020).

58. Hall, J. N. & Bollini, P. Structure, characterization, and catalytic properties of open-metal sites in metal organic frameworks. *React. Chem. Eng.* **4**, 207–222 (2018).

59. Øien, S. *et al.* Detailed structure analysis of atomic positions and defects in zirconium metal-organic frameworks. *Cryst. Growth Des.* **14**, 5370–5372 (2014).

60. Falaise, C. *et al.* Three-dimensional MOF-type architectures with tetravalent uranium hexanuclear motifs (U6O8). *Chem. - A Eur. J.* **19**, 5324–5331 (2013).

61. Falaise, C., Charles, J. S., Volkringer, C. & Loiseau, T. Thorium terephthalates coordination polymers synthesized in solvothermal DMF/H2O system. *Inorg. Chem.* **54**, 2235–2242 (2015).

62. Martin, N. P. *et al.* Synthesis and structural characterization of the first neptunium based metal-organic frameworks incorporating {Np6O8} hexanuclear clusters. *Chem. Commun.* **54**, 6979–6982 (2018).

63. Hastings, A. *et al.* Advancement of Actinide Metal–Organic Framework Chemistry via Synthesis of Pu-UiO-66. *J. Am. Chem. Soc.* **142**, 9393–9371 (2020).

64. Rogge, S. M. J. *et al.* Charting the Metal-Dependent High-Pressure Stability of Bimetallic UiO-66 Materials. *ACS Mater. Lett.* **2**, 438–445 (2020).

65. Kim, M., Cahill, J. F., Fei, H., Prather, K. A. & Cohen, S. M. Postsynthetic Ligand and Cation Exchange in Robust Metal-Organic Frameworks. *J. Am. Chem. Soc.* **134**, 18082–18088 (2012).

66. Hon Lau, C., Babarao, R. & Hill, M. R. A route to drastic increase of CO2 uptake in Zr metal organic framework UiO-66. *Chem. Commun.* **49**, 3634–3636 (2013).

67. Hendrickx, K. *et al.* Exploring Lanthanide Doping in UiO-66: A Combined Experimental and Computational Study of the Electronic Structure. *Inorg. Chem.* **57**, 5463–5474 (2018).

68. Bae, Y. S., Farha, O. K., Hupp, J. T. & Snurr, R. Q. Enhancement of CO2/N2 selectivity in a metal-organic framework by cavity modification. *J. Mater. Chem.* **19**, 2131–2134 (2009).

69. Nowacka, A., Briantais, P., Prestipino, C. & Llabrés I Xamena, F. X. Facile 'green' Aqueous Synthesis of Mono- And Bimetallic Trimesate Metal-Organic Frameworks. *Cryst. Growth Des.* **19**, 4981–4989 (2019).

70. Fei, H. *et al.* Reusable oxidation catalysis using metal-monocatecholato species in a robust metal-organic framework. *J. Am. Chem. Soc.* **136**, 4965–4973 (2014).

71. Cheong, V. F. & Moh, P. Y. Recent advancement in metal–organic framework: synthesis, activation, functionalisation, and bulk production. *Mater. Sci. Technol. (United Kingdom)* **34**, 1025–1045 (2018).

72. Wu, S., Chen, L., Yin, B. & Li, Y. 'Click' post-functionalization of a metal-organic framework for engineering active single-site heterogeneous Ru(III) catalysts. *Chem. Commun.* **51**, 9884–9887 (2015).

73. Nguyen, H. G. T., Weston, M. H., Farha, O. K., Hupp, J. T. & Nguyen, S. T. A catalytically active vanadyl(catecholate)-decorated metal organic framework via post-synthesis modifications. *CrystEngComm* **14**, 4115–4118 (2012).

74. Hwang, Y. K. *et al.* Amine grafting on coordinatively unsaturated metal centers of MOFs: Consequences for catalysis and metal encapsulation. *Angew. Chemie - Int. Ed.* **47**, 4144–4148 (2008).

75. Haque, E. *et al.* Adsorptive removal of methyl orange from aqueous solution with metal-organic frameworks, porous chromium-benzenedicarboxylates. *J. Hazard. Mater.* **181**, 535–542 (2010).

76. Luo, X., Ding, L. & Luo, J. Adsorptive removal of Pb(II) ions from aqueous samples with amino-functionalization of metal-organic frameworks MIL-101(Cr). *J. Chem. Eng. Data* **60**, 1732–1743 (2015).

77. Lee, Y. R., Yu, K., Ravi, S. & Ahn, W. S. Selective Adsorption of Rare Earth Elements over Functionalized Cr-MIL-101. *ACS Appl. Mater. Interfaces* **10**, 23918–23927 (2018).

78. Xie, Y., Fang, Z., Li, L., Yang, H. & Liu, T. F. Creating Chemisorption Sites for Enhanced CO2 Photoreduction Activity through Alkylamine Modification of MIL-101-Cr. *ACS Appl. Mater. Interfaces* **11**, 27017–27023 (2019).

79. Liu, L., Tai, X. & Zhou, X. Au3+/Au0 supported on Chromium(III) terephthalate metal organic framework (MIL-101) as an efficient heterogeneous catalystfor three-component coupling synthesis of propargylamines. *Materials (Basel).* **10**, (2017).

80. Bhadra, B. N., Ahmed, I. & Jhung, S. H. Remarkable adsorbent for phenol removal from fuel: Functionalized metal-organic framework. *Fuel* **174**, 43–48 (2016).

81. Lin, Y., Kong, C. & Chen, L. Amine-functionalized metal-organic frameworks: Structure, synthesis and applications. *RSC Adv.* **6**, 32598–32614 (2016).

82. Hasan, Z., Choi, E. J. & Jhung, S. H. Adsorption of naproxen and clofibric acid over a metal–organic framework MIL-101 functionalized with acidic and basic groups. *Chem. Eng. J.* **219**, 537–544 (2013).

83. Ahmed, I., Hasan, Z., Khan, N. A. & Jhung, S. H. Adsorptive denitrogenation of model fuels with porous metal-organic frameworks (MOFs): Effect of acidity and basicity of MOFs. *Appl. Catal. B Environ.* **129**, 123–129 (2013).

84. Lee, W. R. *et al.* Diamine-functionalized metal-organic framework: Exceptionally high CO 2 capacities from ambient air and flue gas, ultrafast CO2 uptake rate, and adsorption mechanism. *Energy Environ. Sci.* **7**, 744–751 (2014).

85. Wang, N., Mundstock, A., Liu, Y., Huang, A. & Caro, J. Amine-modified Mg-MOF-74/CPO-27-Mg membrane with enhanced H2/CO2 separation. *Chem. Eng. Sci.* **124**, 27–36 (2015).

86. Yeon, J. S. *et al.* Homodiamine-functionalized metal-organic frameworks with a MOF-74-type extended structure for superior selectivity of CO2 over N2. *J. Mater. Chem. A* **3**, 19177–19185 (2015).

87. Andirova, D., Lei, Y., Zhao, X. & Choi, S. Functionalization of Metal-Organic Frameworks for Enhanced Stability under Humid Carbon Dioxide Capture Conditions. *ChemSusChem* **8**, 3405–3409 (2015).

88. Pentyala, V., Davydovskaya, P., Ade, M., Pohle, R. & Urban, G. Carbon dioxide gas detection by open metal site metal organic frameworks and surface functionalized metal organic frameworks. *Sensors Actuators, B Chem.* **225**, 363–368 (2016).

89. Jo, H. *et al.* Fine-Tuning of the Carbon Dioxide Capture Capability of Diamine-Grafted

Metal–Organic Framework Adsorbents Through Amine Functionalization. *ChemSusChem* **10**, 541–550 (2017).

90. Zhong, R. *et al.* A solvent ‘squeezing’ strategy to graft ethylenediamine on Cu3(BTC)2 for highly efficient CO2/CO separation. *Chem. Eng. Sci.* **184**, 85–92 (2018).

91. Yuan, H. *et al.* On-Chip Tailorability of Capacitive Gas Sensors Integrated with Metal–Organic Framework Films. *Angew. Chemie - Int. Ed.* **58**, 14089–14094 (2019).

92. Ahmed, I., Lee, Y. R., Yu, K., Bhattacharjee, S. & Ahn, W. S. Gd 3+ Adsorption over Carboxylic- and Amino-Group Dual-Functionalized UiO-66. *Ind. Eng. Chem. Res.* **58**, 2324–2332 (2019).

93. Zhou, Z., Wu, C. & Zhang, B. ZIF-67 Membranes Synthesized on α-Al2O3-Plate-Supported Cobalt Nanosheets with Amine Modification for Enhanced H2/CO2 Permselectivity. *Ind. Eng. Chem. Res.* **59**, 3182–3188 (2020).

94. Asghar, A. *et al.* Ethylenediamine loading into a manganese-based metal-organic framework enhances water stability and carbon dioxide uptake of the framework. *R. Soc. Open Sci.* **7**, (2020).

95. Tella, A. C. *et al.* Synthesis and characterization of amino and cyano-functionalized zinc-terephthalate metal–organic frameworks for loading of piroxicam drug. *Chem. Pap.* **74**, 2287–2296 (2020).

96. Zhang, X. lei *et al.* Ammoniated MOF-74(Zn) derivatives as luminescent sensor for highly selective detection of tetrabromobisphenol A. *Ecotoxicol. Environ. Saf.* **187**, 109821 (2020).

97. Molavi, H., Moghimi, H. & Taheri, R. A. Zr-Based MOFs with High Drug Loading for Adsorption Removal of Anti-Cancer Drugs: A Potential Drug Storage. *Appl. Organomet. Chem.* **34**, 4–9 (2020).

98. Gu, X., Lu, Z. H., Jiang, H. L., Akita, T. & Xu, Q. Synergistic catalysis of metal-organic framework-immobilized au-pd nanoparticles in dehydrogenation of formic acid for chemical hydrogen storage. *J. Am. Chem. Soc.* **133**, 11822–11825 (2011).

99. Chen, G., Wu, S., Liu, H., Jiang, H. & Li, Y. Palladium supported on an acidic metal-organic framework as an efficient catalyst in selective aerobic oxidation of alcohols.

Green Chem. **15**, 230–235 (2013).

100. Xu, S. *et al.* Dynamic kinetic resolution of amines by using palladium nanoparticles confined inside the cages of amine-modified MIL-101 and lipase. *J. Catal.* **363**, 9–17 (2018).

101. Alamgholiloo, H. *et al.* Formation and stabilization of colloidal ultra-small palladium nanoparticles on diamine-modified Cr-MIL-101: Synergic boost to hydrogen production from formic acid. *J. Colloid Interface Sci.* **567**, 126–135 (2020).

102. McDonald, T. M. *et al.* Capture of carbon dioxide from air and flue gas in the alkylamine-appended metal-organic framework mmen-Mg 2(dobpdc). *J. Am. Chem. Soc.* **134**, 7056–7065 (2012).

103. Zhang, H., Yang, L.-M. & Ganz, E. Adsorption Properties and Microscopic Mechanism of CO 2 Capture in 1,1-Dimethyl-1,2-ethylenediamine-Grafted Metal–Organic Frameworks . *ACS Appl. Mater. Interfaces* **12**, 18533–18540 (2020).

104. Sepehrmansouri, H. *et al.* Multilinker phosphorous acid anchored En/MIL-100(Cr) as a novel nanoporous catalyst for the synthesis of new N-heterocyclic pyrimido[4,5-b]quinolines. *Mol. Catal.* **481**, 1–17 (2020).

105. Liu, F. *et al.* Highly recyclable cysteamine-modified acid-resistant MOFs for enhancing Hg (II) removal from water. *Environ. Technol. (United Kingdom)* 1–30 (2019) doi:10.1080/09593330.2019.1598504.

106. Mortazavi, S. S., Abbasi, A., Masteri-Farahani, M. & Farzaneh, F. Sulfonic Acid Functionalized MIL-101(Cr) Metal-Organic Framework for Catalytic Production of Acetals. *ChemistrySelect* **4**, 7495–7501 (2019).

107. Molea, A., Popescu, V. & Rowson, N. A. The Obtaining of Nanostructured Nitrogen Doped Titanium Dioxide Powders in Presence of Triethanolamine. *Energy* 273–280 (2010).

108. Rezaee, M., Mousavi Khoie, S. M. & Liu, K. H. The role of brookite in mechanical activation of anatase-to-rutile transformation of nanocrystalline TiO2: An XRD and Raman spectroscopy investigation. *CrystEngComm* **13**, 5055–5061 (2011).

109. Manxzer, L. E., Deaton, J., Sharp, P. & Schrock, R. R. Tetrahydrofuran Complexes of

Selected Early Transition Metals. *Inorg. Synth.* 135–140 (1982) doi:10.1002/9780470132524.ch31.

110. Horcajada, P. *et al.* Synthesis and catalytic properties of MIL-100(Fe), an iron(III) carboxylate with large pores. *Chem. Commun.* **100**, 2820–2822 (2007).

111. Boldyrev, V. V. Mechanochemistry and mechanical activation of solids. *Russ. Chem. Rev.* **75**, 177–189 (2006).

112. Katz, M. J. *et al.* A facile synthesis of UiO-66, UiO-67 and their derivatives. *Chem. Commun.* **49**, 9449–9451 (2013).

113. Kim, D., Yamamoto, K. & Ahn, K. H. A BODIPY-based reactive probe for ratiometric fluorescence sensing of mercury ions. *Tetrahedron* **68**, 5279–5282 (2012).

114. Assi, H., Mouchaham, G., Steunou, N., Devic, T. & Serre, C. Titanium coordination compounds: From discrete metal complexes to metal-organic frameworks. *Chem. Soc. Rev.* **46**, 3431–3452 (2017).

VI. Annexes

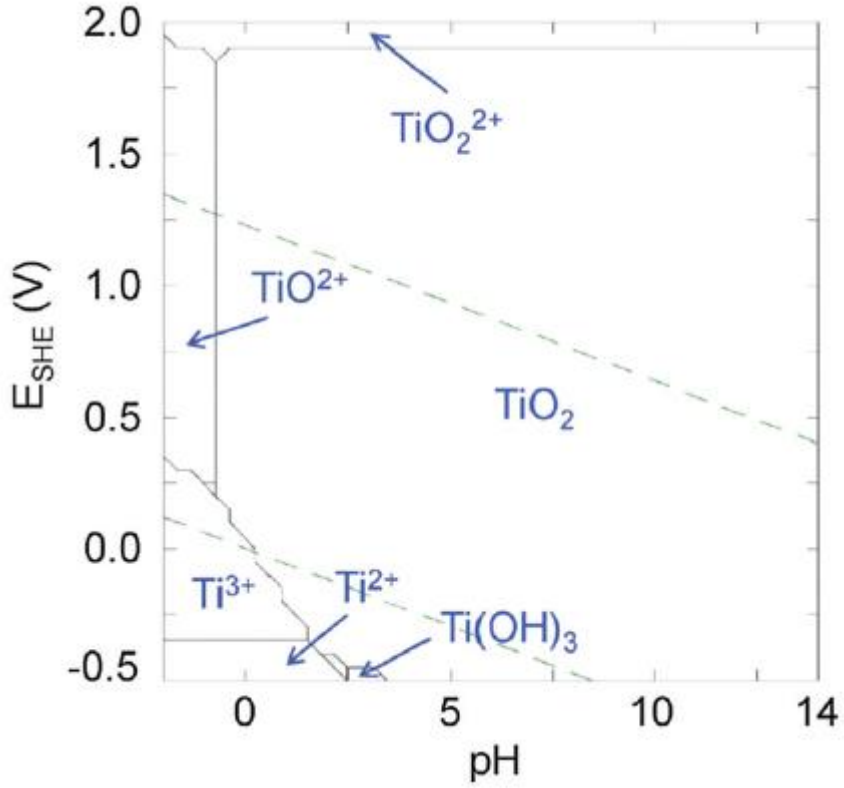

Figure 69. Pourbaix diagram of titanium calculated for $[Ti^{4+}] = 10^{-3}$mol L^{-1} at 25°C using the Hydra and Medusa softwares. Green sahed lines: O_2/H_2O and H_2O/H_2 redox couples, taken from[114]

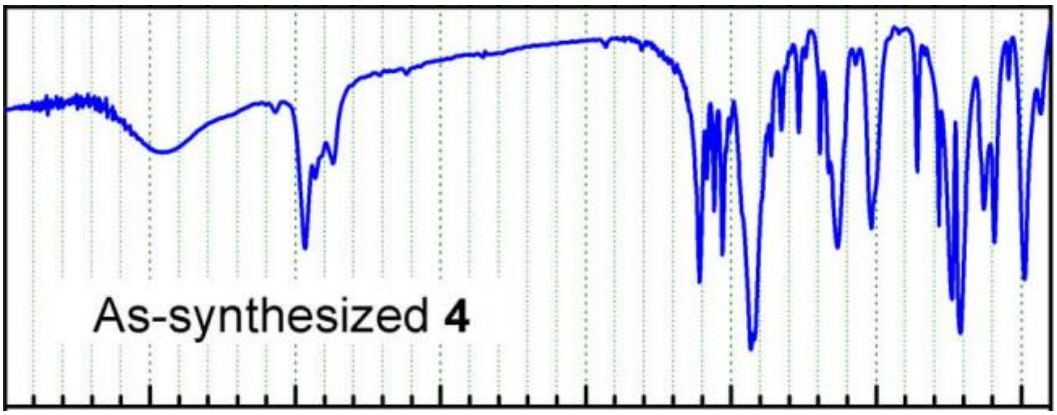

Figure 70. FTIR spectrum of the $[Ti_6O_6(4\text{-tbbz})_6(O^iPr)_6]$ cluster, taken from[54]

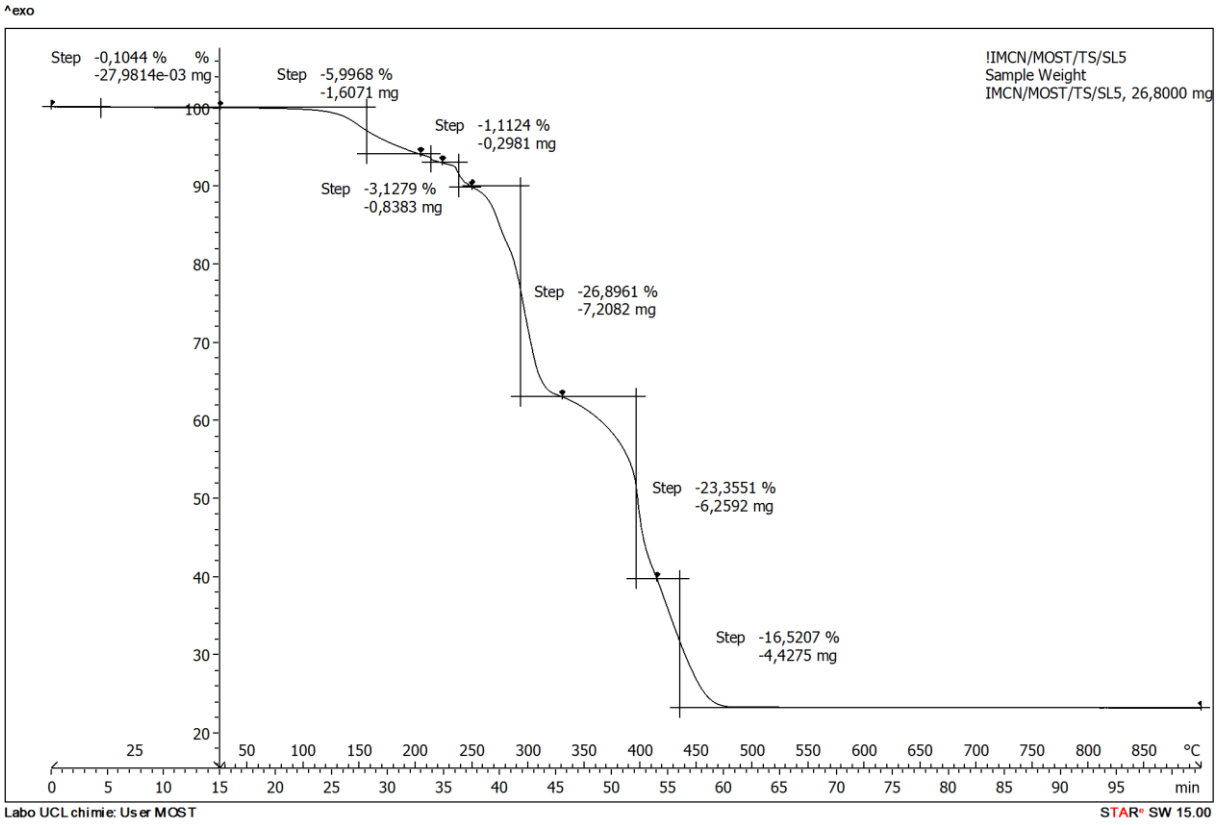

Figure 71. TGA of the $[Ti_6O_6(4\text{-tbbz})_6(O^iPr)_6]$ cluster sample D

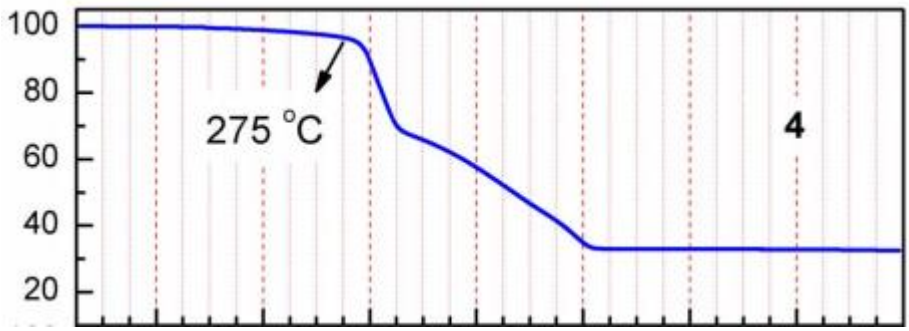

Figure 72. TGA of the $[Ti_6O_6(4\text{-tbbz})_6(O^iPr)_6]$ cluster, taken from[54]

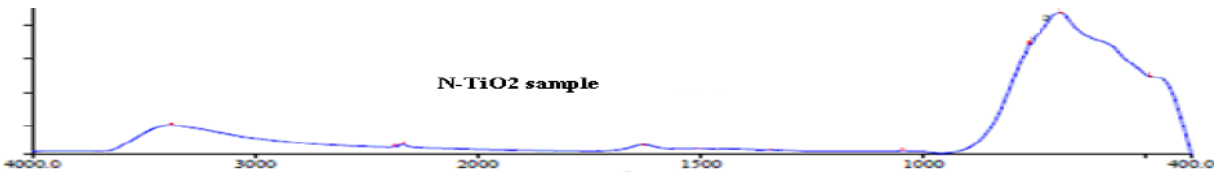

Figure 73. FTIR spectrum of TiO_2 nanoparticles, modified from[107]

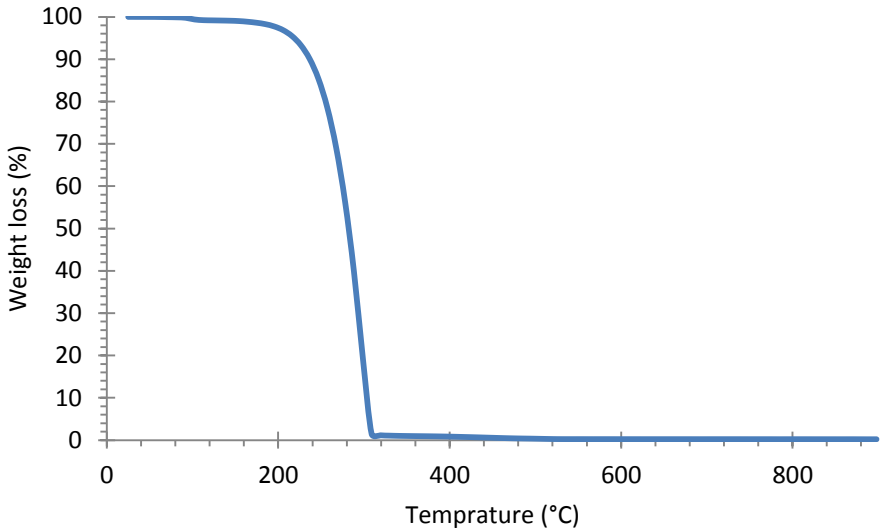

Figure 74. TGA under air of the product obtain with $Ti(O^iPr)_4$ and triisopropyl ester as reagent

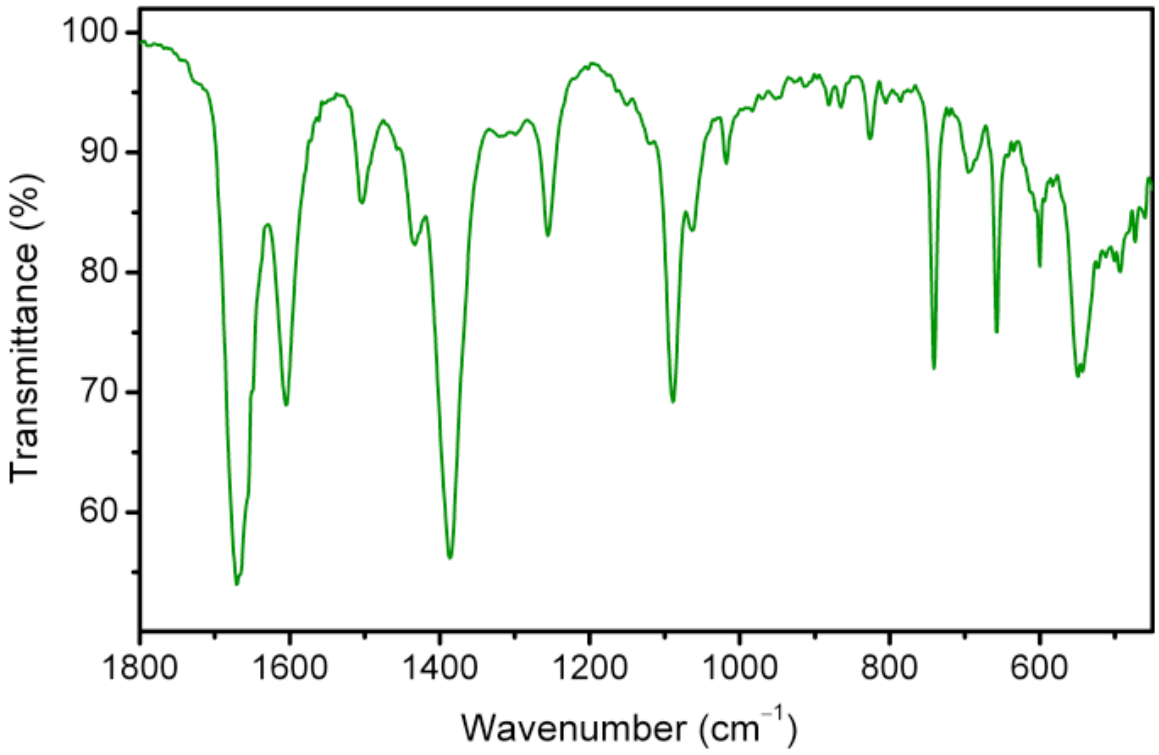

Figure 75. FTIR spectrum of MIL-101-Ti as synthesized, taken from[53]

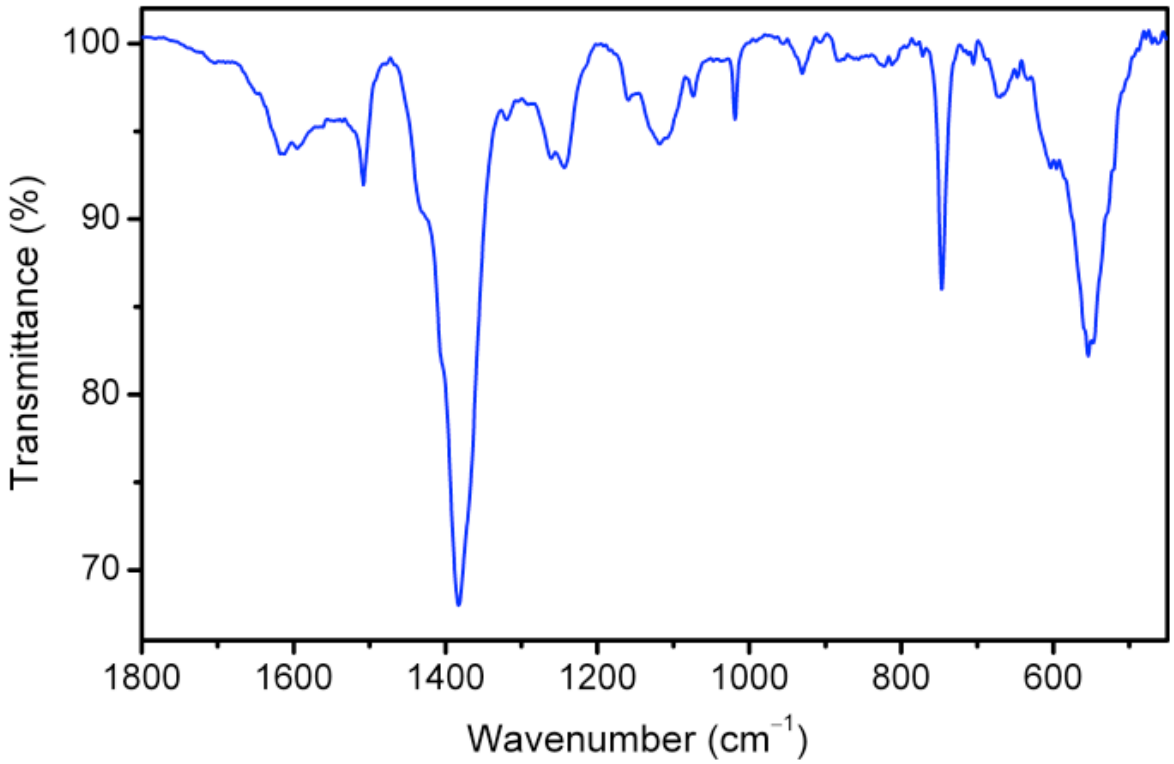

Figure 76. FTIR spectrum of MIL-101-Ti after oxidation at -78°C, taken from[53]

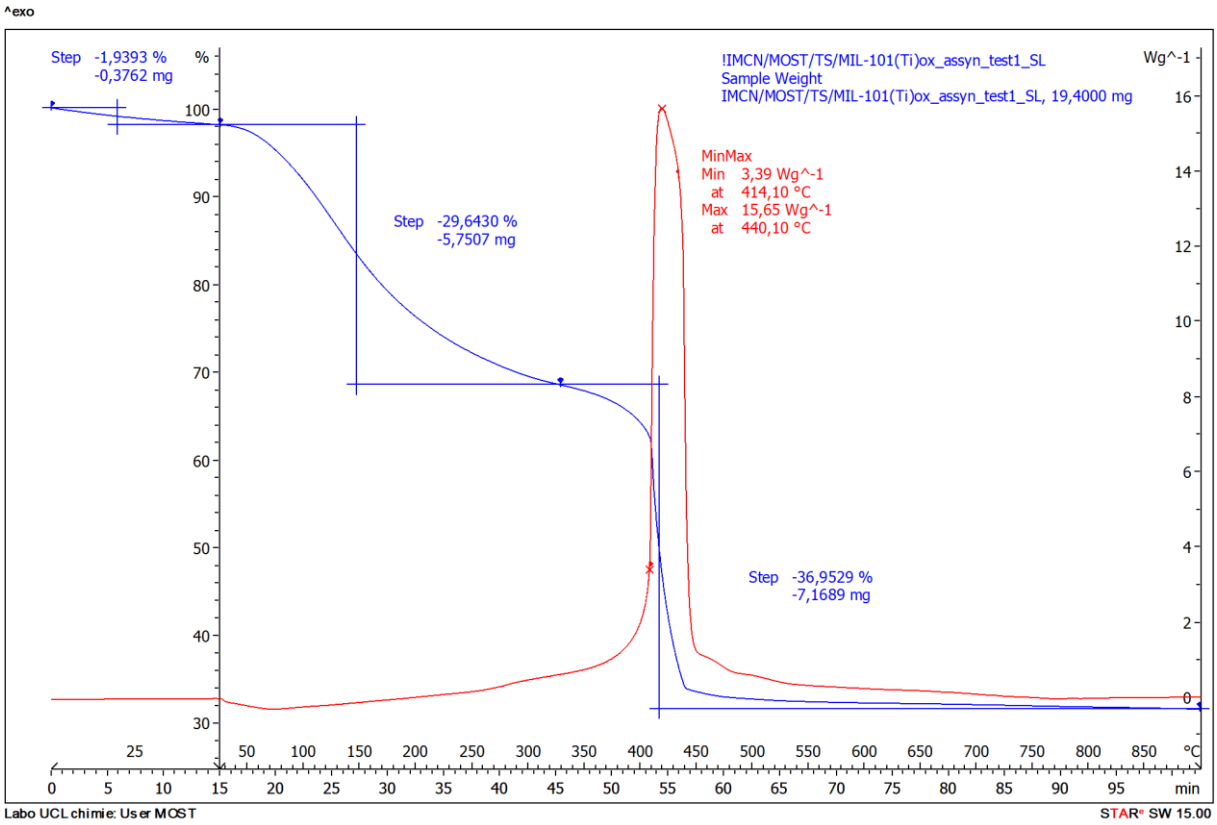

Figure 77. TGA under air of MIL-101-Ti

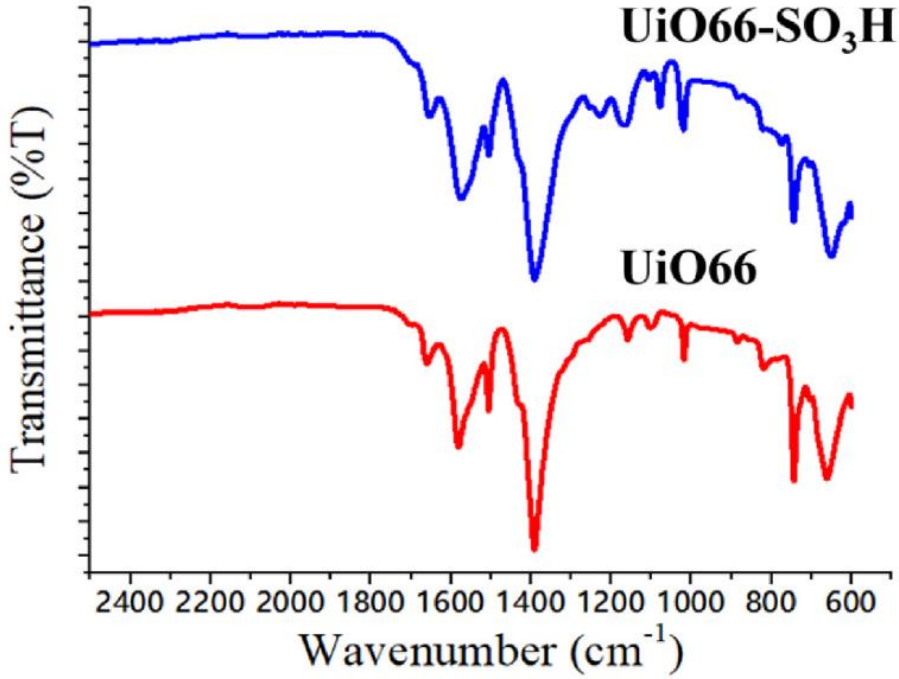

Figure 78. FTIR spectrum of UiO-66, taken from[114]

UNIVERSITÉ CATHOLIQUE DE LOUVAIN
Faculté des sciences
Place des sciences, 2 bte L6.06.01, 1348 Louvain-la-Neuve, Belgique | **www.uclouvain.be/sc**